

## Chlorite in sandstones

R. H. Worden<sup>1\*</sup>, J. Griffiths<sup>1,2</sup>, L. J. Wooldridge<sup>1,2</sup>, J. E. P. Utle<sup>1</sup>, A. Y. Lawan<sup>1,4</sup>, D. D. Muhammed<sup>1</sup>, N. Simon<sup>1</sup>, P. J. Armitage<sup>1,3</sup>

1. Department of Earth, Ocean and Ecological Sciences, University of Liverpool, Liverpool, L69 3GP, UK
2. BP Exploration, Chertsey Road, Sunbury-on-Thames, Middlesex, TW16 7LN, UK
3. BP Upstream Technology, Chertsey Road, Sunbury-on-Thames, Middlesex, TW16 7LN, UK
4. Department of Geology, Bayero University, Kano State, Nigeria.

\* contact author - email: r.worden@liv.ac.uk, phone 00441517945184, mobile 00447791722581

### Abstract

Chlorite, an Fe- and Mg-rich aluminosilicate clay, may be either detrital or authigenic in sandstones. Detrital chlorite includes mineral grains, components of lithic grain, matrix and detrital grain coats. Authigenic chlorite may be grain-coating, pore-filling or grain-replacing. Chlorite can be observed and quantified by a range of laboratory techniques including light optical and scanning electron microscopy and X-ray diffraction; the presence of chlorite in sandstone can be identified by the careful integration of signals from downhole logs. Grain-coating chlorite is the only type of chlorite that can help sandstone reservoir quality since it inhibits quartz cementation in deeply buried sandstones. Grain coats are up to about 10  $\mu\text{m}$  thick and typically isopachous on all grain surfaces; they result from rapid indiscriminate nucleation at high levels of chlorite supersaturation in the pore waters and then growth of appropriately oriented nuclei as ultra-thin, roughly equant crystals. Chlorite can have many possible origins, but it is likely that grain-coating chlorite results from closed system diagenesis at the bed scale. Chlorite sources include transformation of detrital Fe-rich berthierine, transformation of Mg-rich smectite, reaction of kaolinite with sources of Fe and breakdown of volcanic grains. The specific origin of chlorite controls its composition, with marine sandstones having a berthierine source and continental sandstones having a smectite source. Incorporation of precursor clays required for chlorite growth can be achieved by a variety of processes; these most commonly occur in marginal marine environments possibly explaining why Fe-rich chlorite coats are most commonly found in marginal marine sandstones.

### Keywords

Chlorite; sandstone; cement; grain-coating; pore-filling; quartz-inhibition; estuary; delta; reservoir quality; wireline log; siderite; pyrite; burial diagenesis; mesodiagenesis; eodiagenesis; sedimentary environment, petrophysics

### Introduction: the significance of chlorite in sandstones

At temperatures > 80 to 100°C sandstones with grain coats can have relatively high porosity compared to sandstones without grain coats because grain coats typically inhibit the growth of pore-filling syntaxial quartz overgrowths in sandstones (Cecil and Heald, 1971; Heald and Larese, 1974). Sandstones with clay mineral coats (and specifically chlorite grain coats) are of interest and are the focus of this work although microquartz grain coats have also caused some interest as they too inhibit syntaxial quartz overgrowths (Aase et al., 1996; Cazier et al., 1995; Warren and Pulham, 2001). The term “clay mineral” strictly refers to a family of hydrous phyllosilicates that represent a large collection of compositions although the

common rock-forming clay minerals are typically aluminosilicates. In contrast, the term “clay” or “clay grade” refers to particles that are < 2 µm (Wentworth, 1922). Thus, clay grade materials are not necessarily clay minerals; conversely clay minerals are not necessarily clay grade.

Chlorite is a specific type of clay mineral that typically contains abundant iron and magnesium (Deer et al., 2013b). The clay minerals of the chlorite group are well known in low temperature, prograde metamorphic rocks, in retrograde alteration products of ferroan metamorphic minerals, as a low temperature alteration product of biotite in acid igneous rocks and as a hydrothermal alteration product (Deer et al., 2013a). However, some texts and basic sources of geological and mineralogical information (King, 2019) neglect to mention that chlorite is an important constituent of many sedimentary and diagenetic systems. Chlorite is a common weathering product transported from continents out into the oceans (Gingele et al., 2001); chlorite is most abundant in high-latitude ocean sediments due to reduced chemical weathering in the hinterland (Rateev et al., 2008). Chlorite is an important constituent of fine-grained marine sediments and sedimentary rocks. Significantly, chlorite can also be an important clay mineral in coarse-grained clastic sediment such as sandstones. Chlorite has been of interest to petroleum geologists for well over 50 years, since it was realised that deeply-buried sandstones that contain coats of chlorite on sand grains have unusually high porosity and permeability compared to non-chlorite-coated sandstones (Heald and Anderegg, 1960; Pittman and Lumsden, 1968).

### **Positive and negative effects of chlorite on sandstone reservoir quality: grain-coating versus pore-filling chlorite**

If chlorite coats are absent, and there are no other natural mechanisms to inhibit quartz cement, e.g. early oil emplacement (Marchand et al., 2000; Worden et al., 2018b; Worden et al., 1998), microquartz grain coats (French and Worden, 2013; French et al., 2012; Worden et al., 2012) or early development of overpressure (Osborne and Swarbrick, 1999; Stricker and Jones, 2018; Stricker et al., 2016), then abundant quartz cement grows in deeply-buried sandstones. Quartz cement is typically considered to be a kinetically controlled process that initiates at temperatures > 80 to 100°C, with quartz precipitation rate typically assumed to be the rate-limiting step (Lander et al., 2008; Walderhaug, 1994a; Walderhaug et al., 2000). Well-sorted sandstones that lack detrital clay-size matrix (i.e., clean sandstones), typically a target during oil and gas exploration, become extensively cemented by quartz during deep burial (> 80 to 100°C) and thus risk having low porosity and permeability (Fig. 1). Against the expectation of those who assume that the cleanest (i.e., most clay-free) sandstones have the best reservoir quality, a small amount (a few volume percent) of clay, in the form of chlorite grain coats, can lead to far superior reservoir quality than totally clay-free sandstones (Bloch et al., 2002).

It has been known for more than 50 years that chlorite grain coats inhibit the growth of quartz cement in deeply-buried (i.e., increasingly warm) sandstones (Heald and Anderegg, 1960; Heald and Larese, 1974; Pittman and Lumsden, 1968). When chlorite grain coats are well-developed, then porosity can be much higher than expected for sandstones buried to > 3,000 m and heated to > 80 to 100°C due to the inhibition of the normally endemic quartz cement (Ehrenberg, 1993). Chlorite grain coats thus lead to anomalously elevated intergranular porosity, but permeability also tends to be relatively high for the depth of burial because pore throats, as well as pores, tend to remain open (Fig. 1). However, a note of caution needs to be recorded; not all chlorite in sandstones is grain-coating. Chlorite can also be pore-filling (Table 1). Forms of chlorite other than grain-coating chlorite tends to be bad for reservoir quality because they both fill pores and cause narrowing of pore-throats. Pore-filling chlorite is typically microporous leading to rocks with a relatively low bulk density (and thus relatively high porosity) but low permeability (Fig. 1).

To summarise, not all chlorite is benign for sandstone reservoir quality; the physical position and overall volume of chlorite in the pore network is paramount.

## What is chlorite?

The crystal structure and chemistry of chlorite, and related Fe-rich clays, are important since they have major impacts on the sedimentology and geochemistry of chlorite growth, the kinetics of chlorite nucleation and growth and the petrophysical properties of chlorite-bearing sandstones.

### Crystal structure

Clay minerals typically have two-dimensional, tetrahedrally-coordinated Si-O layers that either face or sandwich two-dimensional, octahedrally-coordinated Al-O, Fe-O or Mg-O layers (Moore and Reynolds Jr., 1997). The octahedral layers are abbreviated to “O”; the tetrahedral layers are abbreviated to “T”. The simplest clay minerals have a T-O, or 1:1 structure; more complex clay minerals have a T-O-T, or 2:1, structure (Fig. 2). The two-dimensional T-O-T layers are loosely bonded to facing T-O-T layers by hydroxyl (-OH) units to charge balance the crystal structure. The distance between the repeating units (the T-O or T-O-T sheets) plays a large role in controlling the crystal structure of the clay mineral and thus in defining the magnitude of the Miller indices of the normally dominant (001) interlayer spacing (Fig. 2).

The chlorite group of minerals are hydrous phyllosilicates with a repeating T-O-T structure that also has an extra octahedrally-coordinated Al-O, Fe-O or Mg-O two-dimensional layer. The chlorite group are thus known as T-O-T-O or 2:1:1, clay minerals (Fig. 2). The extra octahedrally-coordinated layers present in chlorite are loosely bonded to the facing T-O-T layers by yet more hydroxyl units resulting in, compared to illite and kaolinite, the unusually high quantity of hydroxyl groups per unit cell of chlorite. Chlorite thus has a relatively large quantity of hydrogen atoms per unit cell compared to practically all other common rocks forming minerals; this gives chlorite an unusually high neutron log signal (see later section: Effects of chlorite on log responses). Chlorite has a large repeating unit cell in the c-axis to the extra octahedral sheet compared, for example, to illite or other 2:1 clay minerals; chlorite's  $d_{(001)}$  value is about 14Å (Fig. 2).

Berthierine has a similar overall composition to chamositic chlorite but has a simpler crystal structure with tetrahedrally-coordinated Si-O two-dimensional layers that face octahedrally-coordinated Al-O, Fe-O or Mg-O two-dimensional layers (Hillier and Velde, 1992; Hornibrook and Longstaffe, 1996). Berthierine thus is a 1:1 clay and has a T-O structure with a commensurately smaller repeating unit cell in the c axis, its  $d_{(001)}$  is about 7Å.

### Mineral chemistry of chlorite and related minerals

Chlorite has a generalized chemical composition of  $(X,Y)_{4-6}(Si,Al)_4O_{10}(OH,O)_8$ . The X and Y in the formula represent divalent or trivalent ions in the octahedrally-coordinated layers, which commonly might include:  $Fe^{2+}$ ,  $Fe^{3+}$ , Mg or Al. In this paper, aluminium occupying an octahedral site will be labelled  $Al^{VI}$  while aluminium occupying a tetravalent site will be labelled  $Al^{IV}$ .

As can be seen in the generalized chemical formula, chlorite has a wide range of compositional variations due to the effect of the three main chemical substitutions (Fig. 3): (i)  $Fe^{2+}$  substituting for Mg, (ii)  $2Al^{IV}$  substituting for Si(Mg, $Fe^{2+}$ ), also known as the Tschermak substitution, and (iii) di/trioctahedral  $3(Mg, Fe^{2+})$  substituting for  $\square + 2Al^{VI}$  (where  $\square$  represents an octahedral vacancy). Some of these substitutions are known, theoretically at least, to be sensitive to pressure and temperature conditions at the time of the growth of chlorite (Bourdelle et al., 2013; Decaritat et al., 1993), as well as to the bulk composition of the rock and to the physico-chemical properties of the environment such as the chemistry of the ambient fluid. There have been attempts to develop geothermometers and geobarometers based on chlorite composition in metamorphic rocks (Bourdelle et al., 2013; Decaritat et al., 1993) but such an approach is

unlikely to work in sedimentary rocks due to: (i) the combination of detrital chlorite from unweathered lithic fragments from all, or any, rock types in the hinterland, chlorite formed in soil during weathering in the hinterland, plus chlorite resulting from early diagenetic processes and true diagenetic chlorite, (ii) the probable lack of chemical (i.e., thermodynamic) equilibrium between the sedimentary rock and the ambient fluid during chlorite growth in the host sediment, and (iii) the possible heterogeneity of fluid composition within typically compartmentalised sedimentary systems. Chlorite composition in sandstones, and other sedimentary rocks, is of interest (see later section: Is authigenic chlorite Fe-rich?), but it is not necessarily subject to the same rules as chlorite in metamorphic rocks that have attained equilibrium across large volumes of rock.

Different names have been given to different compositional types of chlorite (Fig. 3). Chlorite typically contains no potassium in the interlayer sites and is thus clearly compositionally different to illitic or common smectitic clays. If analyses of chlorite report measurable potassium, this is most likely to represent a small quantity of a contaminating second mineral, such as illite or muscovite. Note that detrital chlorite derived from higher temperature rocks is routinely associated with potassium-bearing micas, thus explaining potassium reported in chlorite analyses (Worden et al., 2018c). A similar explanation probably accounts for any calcium reported during the analysis of chlorite with Ca being present as contaminant calcite, some have used the presence of Ca to suggest that chlorite replaced precursor Ca-smectite (Humphreys et al., 1994). In theory, chlorite contains none of the common radioactive element, potassium, uranium or thorium (K, U, Th), and thus should lead to no response from bulk or spectral gamma logs (see later section: Effects of chlorite on log responses). There may be small quantities of entrained minerals that contain K, U or Th but these are not innate to chlorite; K-U-Th measurements from spectral gamma ray logs should not, despite convention (Quirein et al., 1982), be used for chlorite identification.

## **Physical types of chlorite in sandstones**

### **Detrital chlorite**

Detrital chlorite can occur in clastic sediments as discrete laminae, as chlorite-rich lithics, as silt- and clay-grade matrix and as detrital grain coats (Table 1) (Griffiths et al., 2019b; Griffiths et al., 2019c).

Chlorite, like just about all other minerals, can occur as a detrital mineral in sandstones. Being a hydrous mineral, typical of low grade metamorphism (Yardley, 1989) and low temperature hydrothermal alteration, it is not amongst the most reactive of minerals to be fed into a sedimentary system. Compared to, for example, olivine or anorthite, chlorite is relatively slow to undergo weathering and alteration in hinterlands (Hartmann et al., 2013), soils and during transport and is therefore a common detrital mineral in sedimentary systems.

Detrital chlorite can be present within fine-grained clastic sediments as either silt- or mud-grade material. In petrophysical terms, beds of chlorite-rich matrix are called “laminar chlorite” (Table 1) (Griffiths et al., 2019b).

Detrital chlorite can be present in sands and sandstones in a wide variety of physical forms including monomineralic grains (individual chlorite crystals), as part of complex polymineralic lithic grains or even as part of a fine grained (clay- or silt-grade) matrix. Sand grains generated in a hinterland, i.e., external to the sedimentary environment, are called allogenic grains (Table 1); common chlorite-bearing allogenic lithics include metamorphic, typically phyllite or schist, rock fragments (Fig. 4), or igneous grains that have been hydrothermally altered to chlorite before being fed into the sediment supply. Note that volcanic rock fragments have long been proposed as a way of delivering the key ingredients for

authigenic chlorite (Anjos et al., 2003; Berger et al., 2009; Grigsby, 2001). In petrophysical terms, grains that are rich in chlorite represent “structural chlorite” (Table 1). Chlorite-rich grains are relatively ductile and thus more susceptible to deformation during compaction (Worden et al., 2000). Deformed chlorite-rich grains are not always easy to discern from depositional matrix and a general term of pseudo-matrix is commonly used (Table 1).

Fe-clay minerals, with a composition like chlorite, can also occur within autogenic grains (i.e., grains created within the sedimentary environment: Table 1). Fe-oids are a relatively common type of autogenic grain found in ancient sedimentary systems. Fe-oids are composed of concentric layers of Fe-rich clay, typically with minor quantities of other clays such as illite. The onion-like ooid layering can be discerned by small variations in the amounts of subordinate illite (Fig. 5 and 6A). Although Fe-oids are not ubiquitous within chlorite-coated sandstones, they are common as a minor component in most, or many, estuarine-deltaic chlorite-coated sandstones (Ehrenberg, 1993; Gould et al., 2010).

Chlorite can also enter a sandstone attached to sand grain surfaces as part of a detrital grain coat (Griffiths et al., 2018b; Wooldridge et al., 2019a) (Table 1). Modern detrital-clay coats consist of a diverse mixture of phyllosilicates (e.g. chlorite, illite, kaolinite, berthierine, smectite, and other Fe-clay minerals) that are bound to framework sand grain surfaces (Daneshvar, 2011; Dowey et al., 2017; Ehrenberg, 1993) (Fig. 7). Detrital-clay coats are composed of aggregates of clay minerals, clay- and silt-sized lithics, organic matter and bioclasts (e.g. diatoms) which form discontinuous accumulations attached to sand grain surfaces (Dowey et al., 2017; Wooldridge et al., 2017b). Detrital chlorite-bearing clay coats have been shown to adhere to sand grain surfaces in modern sedimentary environments due to the presence of biofilms that, at least in some cases, derived from the normal life activities of diatoms and other forms of macro- and micro-biota (Needham et al., 2005; Wooldridge et al., 2017a).

### Authigenic chlorite

Authigenic chlorite can occur in clastic sediments as grain-replacing chlorite, as a replacement product of detrital or earlier authigenic clay minerals, as coats on sand grains that may be thin or thick or even as pore-filling clay (Table 1).

Grain replacing chlorite occurs when a detrital grain undergoes partial or total authigenic replacement by chlorite (Fig. 4). For replacement by chlorite to occur, the detrital grain typically must be Fe-Mg-Al-rich; minerals such as biotite (Morad and Aldahan, 1986), hornblende and other amphiboles, garnet and tourmaline will all be susceptible to replacement by authigenic chlorite. Mafic and intermediate igneous rock fragments are also susceptible to replacement by chlorite as they are typically pyroxene and plagioclase-rich. Biotite and chlorite have similar crystal structures so that the replacive chlorite grows directly on the detrital biotite allowing easy identification of the alteration process. Where chlorite nucleates or grows away from the altered primary mineral, or if the primary mineral has been entirely replaced then recognition of the primary mineral source of the authigenic chlorite may be impossible by petrographic means.

Clay-replacing chlorite occurs when detrital or early diagenetic clay minerals are replaced by chlorite. For example, kaolinite has been reported to be replaced by chlorite during mesodiagenesis (Burton et al., 1987). Detrital Fe-rich clay minerals such as odinite, phyllite-V (Odin, 1990) or berthierine all undergo alteration to chlorite during heating and burial; such reactions may be effectively isochemical involving no loss or gain of other chemical species (Worden and Morad, 2003).

Diagenetic coats of chlorite may develop on grain coats during burial (Table 1) (Figs. 4 to 8). Diagenetic coats may be the result of alteration of minerals present in detrital clay coats; these are known as diagenetic-recrystallized clay coats (Table 1) (Wooldridge et al., 2019a). Diagenetic-recrystallized clay

coats are governed by the primary depositional fabric of the sediment as the clay coat originally formed in the primary depositional environment. Alternatively, chlorite coats may be the result of alteration of non-coating primary minerals; these are known as diagenetic-authigenic clay coats and are provenance-controlled (Wooldridge et al., 2019a). Chlorite coats are often uniformly thick; these are known as isopachous coats (Figs. 4 to 8).

Pore-lining chlorite is the same thing as grain-coating chlorite (Table 1) but from the perspective of the pore instead of the grain. This unfortunate proliferation of jargon probably resulted from the mode of observation and the purpose of the study; those using Secondary Electron Imaging (SEI) seem to use the term pore-lining chlorite. Those using thin sections to study sandstone mineralogy and petrography observe a thin layer of chlorite sitting on the surfaces of sand grains and are likely to use the term grain-coating.

Pore throats are classed as macro ( $> 2 \mu\text{m}$ ), meso ( $0.5$  to  $2 \mu\text{m}$ ) or micro ( $< 0.5 \mu\text{m}$ ) (Pittman, 1992). Finer-grained sandstones tend to have smaller pore throats than coarser-grained sandstones (Beard and Weyl, 1973; Bryant et al., 1993) so that thick chlorite grain coats ( $> 10 \mu\text{m}$ ) will tend to close up pore throats and restrict fluid flow through pores in the finest grained sandstones but be less detrimental to reservoir quality in medium to coarse-grained sandstones.

Authigenic chlorite can also be present as pore-filling material (Berger et al., 2009) (Fig. 4) but it may be unclear how the pore-filling volume of chlorite originated. Such material is typically referred to as pseudo-matrix (Worden et al., 2000). Some pore-filling chlorite possibly originated as thick grain coats that grew so extensively that they blocked pore throats and filled pores (Armitage et al., 2013; Armitage et al., 2010) (Fig. 6). Other types of pore-filling chlorite probably originated as chlorite-rich grains, e.g., Fe-ooids (Fig. 5) or possibly allogenic lithic grains rich in Fe, Mg and Al, such as volcanic (Anjos et al., 2003), or metamorphic rock fragments (Fig. 4) that underwent ductile compaction during burial (Worden et al., 2000). Pore-filling chlorite is highly detrimental to reservoir quality (Armitage et al., 2013; Armitage et al., 2010; Cao et al., 2018) (Fig. 1) so that a deeply-buried sandstone simply being described as chlorite-bearing does not guarantee good porosity and permeability through the inhibition of quartz cement since abundant chlorite is likely to be highly detrimental to reservoir quality.

## Methods for chlorite investigation

### Light optical characteristics of chlorite

Large volumes of pore-filling, lithic-grain-bearing or Fe-ooidal chlorite in sandstones can typically be detected by the characteristic pleochroic (i.e., the variable intensity of the colour in transmitted light upon rotation) green colour (Fig. 6A). Chlorite is also characterised by the anomalous birefringence (Berlin blue) in cross-polarised light (Deer et al., 2013b). Chlorite tends to be a duller shade of green than glauconite, which tends to have a yellowish-green colour and does not have anomalous birefringence.

Thin coats of chlorite on sand grain surfaces, as opposed to lithic grains or pore-filling chlorite, can be challenging to identify. However, chlorite coats can usually be differentiated from illite (which has bright birefringence colours) and kaolinite which is colourless and has low (white to pale yellow) birefringence colours. Under favourable circumstances, the overall appearance of chlorite coats can be diagnostic, with (i) the grain-fringing clay mineral being pale-green in transmitted light and with anomalous birefringence in polarised light (Deer et al., 2013b), (ii) the coat is composed of crystals that are approximately perpendicular to the grain surface, and (iii) the outer margins of the coat typically appear made up of small bladed crystals (as opposed to wispy, elongated fibres as found in illite coats, see inset in Fig. 4B).

Chlorite coats do not look solid in transmitted light microscopy; based on the diffuse nature of chlorite grain coats, most petrographers would assume that they are microporous.

### X-ray diffraction analysis of chlorite

Chlorite can be usefully studied using X-ray diffraction (XRD) techniques (Hillier, 2003; Moore and Reynolds Jr., 1997). These rely on the identification of planes within a crystal lattice by noting the occurrence of diffracted primary X-rays as the incidence angle is systematically decreased. XRD can be used on mineral mixtures (rocks, sediments, etc.) to identify and quantify proportions of minerals, including chlorite. XRD can also be used to help define details of the composition (i.e. Fe/Mg ratio) of some minerals, including chlorite, because peak height ratios and positions can vary as a function of composition. For chlorite, the most simple indicator of composition, using XRD data, is the ratio of odd to even (00l) diffraction peaks, e.g. (001)/(002) (Fig. 2) (Hillier, 2003; Moore and Reynolds Jr., 1997).

### Electron microscope studies of chlorite

Chlorite grain coats are best studied using either secondary electron imaging (SEI), backscattered electron microscopy (BSEM) or energy dispersive spectroscopy (EDS) mapping (Figs 4 and 5). The finely crystalline nature of chlorite grain coats is clearly visible in secondary electron images (Fig. 8). Chlorite grain coats tend to blanket detrital grains with isopachous layers. Chlorite is typically absent at grain-grain contacts leaving a scar visible in Secondary Electron Images (SEI) where overlying grains were removed during sample preparation (Fig. 8A). Chlorite crystals tend to be perpendicular to the sand grain surface and seem to be randomly oriented with the chlorite's C-axis (001 plane) free to adopt any rotational angle on the surface (Fig. 8B). Chlorite indiscriminately coats quartz, K-feldspar, plagioclase and any lithic grains.

BSEM images taken using polished thin sections of chlorite-cemented sandstones (Fig. 7A-C) give further details of the indiscriminate nature of the chlorite coat and its routine absence at grain-grain contacts (Fig. 7B). The crystals within chlorite grains can sit directly on detrital quartz grains or they can grow out of poorly-structured, detrital clay-coating material (Fig. 6A); authigenic chlorite growing on top of detrital grain coats is relatively common. Detrital clay coats in chlorite-cemented sandstones tend to be highly enriched in chlorite that has a much smaller crystal size (sub 1  $\mu\text{m}$ ) than the authigenic chlorite coat (4 to 6  $\mu\text{m}$  long). BSEM imaging is also useful for studying chlorite-rich clasts such as Fe-ooids (Taylor et al., 2002). Fe-ooids typically have a nucleus (any sort of detrital grain) and have concentric layers of chlorite-dominated clay; the layering visible in Fe-ooids is typically the result of small quantities of illite (1 to 5 %) being present in the concentric layers. Chlorite-dominated Fe-ooids can be coated with authigenic chlorite and show evidence of both: (i) ductile deformation and delamination of the layers and (ii) some degree of dissolution and replacement and the development of microporosity (Fig. 7C).

Chlorite, and other Fe-rich clays such as berthierine, have been studied using Transmission Electron Microscopy (TEM), which can resolve details of the crystal lattice and crystallography. It is not used routinely by petrographers or petrophysicists because chlorite decomposes under the intense beam conditions required of TEM examination and there are other, simpler, techniques that can address routine questions. Nevertheless, a TEM-study usefully showed nanocrystalline quartz cement growing between the roots of grain-perpendicular chlorite plates; quartz could not continue to grow due to the space limits imposed by the chlorite, the chlorite was visibly embedded into the cemented quartz grain to the depth of the grain-quartz cement boundary (Durand et al., 2003).

The composition of chlorite can be directly determined using energy dispersive or wavelength dispersive spectroscopy of secondary X-rays in electron microscopes or dedicated electron microprobes (Curtis et al., 1984). This approach is needed if the chemistry of the chlorite is in question.

Compositional imaging using Scanning Electron Microscopy-Energy Dispersive Spectrometry (SEM-EDS) analysis (Armitage et al., 2010) utilises characteristic X-rays to build up an image of a rock by rastering an electron beam over a surface, collecting enough X-rays at each point to facilitate unique identification of the mineral. During SEM-EDS imaging, one or 2  $\mu\text{m}$  spacing between data collection points is usually employed for high resolution images e.g., capturing chlorite grain coats, whereas 20  $\mu\text{m}$  spacing between data collection points can be employed to calculate the bulk mineralogy across the entire thin section. These mineral definitions are assembled in a list that is effectively an archived mineral library. Each mineral is assigned a colour, and these data points are combined to form a contiguous false colour image of the sample (Figs. 4 and 5). In addition to the images, the sum of each occurrence of a mineral is tabulated so that minerals and groups of minerals may be quantified (giving volume percentage proportions). The Fe-Mg ratio of any physical type of chlorite can be determined using an SEM-EDS method developed at the University of Liverpool by Worden et al. (2018c). This approach has major advantages over other techniques, for example, conventional microprobe analysis as it gives spatially resolved data for large areas of a polished section as opposed to a few spot-points. The approach also uniquely reveals whether different types or morphologies of chlorite have different compositions (Fig. 7B).

### Micro-CT studies of chlorite in sandstones

3D images of the spatial arrangements of grain, cements, pore and throats can be generated from micro-CT images. Micro-CT is a relatively new technique to be applied to diagenetically altered rocks that can produce high-resolution 3D images of rocks, via X-ray tomography of whole rock samples (Munawar et al., 2018). Initial attempts to use micro-CT to image chlorite-rich grains (Markussen et al., 2019) and even chlorite grain coats (Golab et al., 2015) in core plugs have shown promise but the technique is not yet a routine tool in the study of diagenetic cement distribution in sandstones.

### Is authigenic chlorite Fe-rich?

A compilation of more than 200 microprobe analyses of authigenic chlorite, collated from studies worldwide (Table 2), has been plotted to reveal the distribution of  $\text{Fe}/(\text{Fe}+\text{Mg})$  values (Fig. 9). It is apparent that authigenic chlorite is not necessarily highly enriched in iron but there are modes that do represent highly iron-enriched compositions.

The same data compilation has also been plotted to reveal the range of  $\text{Fe}/(\text{Fe}+\text{Mg})$  values as a function of the environment of deposition (Fig. 10A). There is a significant variation from relatively low  $\text{Fe}/(\text{Fe}+\text{Mg})$  chlorite in continental sediments through to high  $\text{Fe}/(\text{Fe}+\text{Mg})$  in marginal marine sediments.

As previously concluded by Hillier (1994), there are likely to be different explanations for the origin of chlorite in different sedimentary environments. The low  $\text{Fe}/(\text{Fe}+\text{Mg})$  chlorite in continental sediments probably originated as detrital Mg-rich clay, such as palygorskite, or Mg-rich trioctahedral smectites such as saponite. The high  $\text{Fe}/(\text{Fe}+\text{Mg})$  chlorite in estuarine sediments possibly originated as berthierine given that this juvenile  $7\text{\AA}$  clay is also highly Fe-enriched (Fig. 10B). The chlorite in the turbidite examples probably originated as lithic grains (e.g. volcanic grains) (Bloch et al., 2002; Yezerski and Shumaker, 2017) which can have a wide range of Fe-Mg ratios. However, accumulated clay coated grains produced in a marginal marine setting and then re-transported but variably preserved in high density flows has been proposed as the origin of clay-coated sand grains for some turbidite sandstones.

There are no simple relationships between  $\text{Fe}/(\text{Fe}+\text{Mg})$  values and the quantities of aluminium in octahedral or tetrahedral sites within chlorite. However, there is a tendency for chlorite from shallow and marginal marine sedimentary environments to have more tetrahedral aluminium and less octahedral



aluminium than chlorite from fluvial and alluvial sedimentary environments (Figs. 10C and E). This might be a function of the types of compounds that become chlorite (e.g., smectite versus berthierine, and see later section: Chlorite generating mesogenetic reactions in sandstones) but caution is needed because the aluminium composition of chlorite within the tetrahedral and octahedral sites can be a function of temperature and pressure as well as primary composition of the supplying minerals (Bourdelle et al., 2013). It seems that there are no simple conclusions to be made from the aluminium in octahedral or tetrahedral sites within berthierine (Figs. 10D and F).

## **Diagenetic chlorite: open or closed system diagenesis**

Based on the electron microprobe data compiled from sources in Table 2, chlorite and berthierine in sandstones display a wide range of compositions; diabanite, brunsvigite, ripidolite, chamosite and thuringite are relatively common; interestingly, true clinocllore is apparently not found in any sedimentary environments (Fig. 11).

Where do the raw ingredients for authigenic chlorite come from? Chlorite is dominated by oxides of iron, magnesium, aluminium and silicon. A fundamental question is whether chlorite in sandstones is the originates from primary depositional processes, whereby its key ingredients were present in the sediment at the time of deposition (closed system diagenesis), or whether the key ingredients have been fluxed into the sandstone during burial and diagenesis (open system diagenesis). In the subsequent section, the fundamental question which underpins our understanding of chlorite in sandstones is addressed: Is authigenic chlorite in sandstones the result of open or closed system diagenesis, or does it have a mixed origin?

Aluminium and silicon, although sparingly soluble in sedimentary formation waters, are ubiquitous in clastic sediments because they are present in fine fraction clay minerals and coarse fraction detrital micas and feldspars. Iron also has low solubility in formation waters, as indicated by the typically low, to below detection, concentrations in sedimentary formation waters (Warren and Smalley, 1994). In contrast, magnesium is relatively soluble in formation waters, typically present at the thousands of ppm concentration. Formation water chemistry data that report both dissolved iron and magnesium from UK oil and gas fields have been compiled (Warren and Smalley, 1994; Worden et al., 2006a). The absolute and relative concentrations of dissolved iron and magnesium are compared in Figure 12. The median concentration of iron for all stratigraphic intervals is 0.000077 mol/L. The median concentration of magnesium is 0.01544 mol/L. Magnesium is approximately 200 times more concentrated than dissolved iron in UK formation waters.

Many models of sandstone diagenesis have invoked large-scale water flow systems as the main controls on reservoir quality (Benbaccar et al., 1995; Brosse et al., 2003; Burley, 1993; Giles et al., 2000; Mullis and Haszeldine, 1995; Sanjuan et al., 2003); such models assumed relatively open geochemical systems. Some studies invoked a vital role for organic acids derived from source rocks enhancing the concentration of scarcely soluble Al, Si and possibly Fe (Barth and Riis, 1992; Harrison and Thyne, 1992). More recent models have recognized the limited complexing ability of organic acids and their scarcity in formation waters and now tend to assume a relatively closed system for sandstone diagenesis (Lander and Walderhaug, 1999).

Observations from cemented veins routinely show limited penetration of the cementing fluid from the vein into the matrix, suggesting that mass-import of material cannot be a process that affects the bulk properties of a porous rock unit (Worden et al., 2018a). The degree of openness of a diagenetic system is likely to be partly a function of the aqueous solubility of a given species in a sandstone with Al, Si, Fe and Ti being largely immobile (and thus part of a closed system) at the bed scale while CO<sub>2</sub> is demonstrably

part of an open diagenetic system in sandstones given percentage level concentrations of CO<sub>2</sub> in many gas fields and dissolved CO<sub>2</sub> in oil fields. Interestingly, there are detailed, large-scale studies of diagenetic systems that seem to require loss or gain of species such as calcium and magnesium (Consonni et al., 2018; Poteet et al., 2018) and potassium (Gier et al., 2018) to explain the distribution of minerals in reservoirs.

Fundamental proof of the openness of CO<sub>2</sub> in diagenetic systems comes from (i) pyrolysis experiments that show that CO<sub>2</sub> is generated from source rocks in large volumes (Andresen et al., 1994) and (ii) the  $\delta^{13}\text{C}$  values of carbonate cements reflecting external input in many systems (Macaulay et al., 2000). Carbonate rocks probably require open system diagenesis of magnesium during dolomitization (Jiang et al., 2014) and are also probably susceptible to influxes of CO<sub>2</sub> during kerogen maturation (Worden and Heasley, 2000).

Magnesium is a diagenetically interesting element as it is relatively soluble and is commonly found at concentrations of thousands of parts per million in sedimentary formation waters (Hanor and McIntosh, 2007; Warren and Smalley, 1994) (Fig. 12). Moreover, dolomitization is common in carbonates, and dolomite and ankerite cements are common mesogenetic (i.e. burial diagenetic) cements in many sandstones suggesting that magnesium is a relatively mobile element during mesodiagenesis. Magnesium diagenesis cannot therefore be assumed to be isochemical; the presence of magnesium in chlorite may be at least partly a result of mass flux into any sandstone. In direct contrast, iron is typically found at far lower concentrations in sedimentary formation waters than magnesium; Figure 12 shows that magnesium has two hundred times the median concentration of iron in UK oil field formation waters (Warren and Smalley, 1994; Worden, 2018). Model reactions between alumino-silicate minerals (e.g. kaolinite, muscovite and K-feldspar) and either dissolved magnesium or dissolved iron have been assessed for the relative number of pore volumes required to convert the initial aluminosilicates into either Mg- or Fe-chlorite (Table 3). Given a median North Sea formation water iron concentration of 0.000077 mol/L and a rock with 4% kaolinite and 20% porosity, it would require > 130,000 pore volumes of water to convert kaolinite into Fe-chlorite. Given a median North Sea formation water magnesium concentration of 0.01544 mol/L and a rock with 4% kaolinite and 20% porosity, it would require 652 pore volumes of water to convert kaolinite into Mg-chlorite (Table 3). This suggests that a vast and unlikely scale of flux (Bjørlykke and Egeberg, 1993) of Fe-bearing water during burial diagenesis would be required to cause the non-isochemical growth of Fe-chlorite at the expense of pre-existing aluminosilicates minerals. Similar calculations for the conversion of muscovite and kaolinite into chlorite show similar unreasonably great number of pore volumes are required for non-isochemical Fe-chlorite growth. In contrast, growth of Mg-chlorite due to non-isochemical processes requires a much lower number of pore volumes of water flux. Note that early diagenetic flux of Fe has been proposed in some flowing groundwater systems (Chan et al., 2000; Parry et al., 2004). However, this does not counter the arguments made here for broadly isochemical mesogenetic systems, with respect to Fe at the bed-scale, because long-lived and large scale meteoric-water driven flow of geochemically active groundwater is well understood whereas it is not easy to understand how >130,000 pore volumes of typical Fe-bearing formation water could flux through each pore volume to cause Fe-chlorite growth at the expense of Al-silicate minerals. In summary, the presence of iron in the detrital sediment is a key control on the presence of chlorite in sandstones, especially where the chlorite is highly iron-enriched. To reiterate this key point, appropriate hinterland geology (sediment provenance) that can supply abundant iron is a primary requirement for the accumulation of sandstones that contain chlorite.

The question of open versus closed diagenetic systems (Worden, 2018) is probably too simplistic for chlorite cement in sandstone reservoirs. Al, Si and Fe are probably part of a largely closed geochemical system at the cm- to dm-scale (i.e. bed-scale) (Worden et al., 2018a). In contrast, the common occurrence of dolomitization and late diagenetic dolomite cement in sandstones suggests that Mg is part

of a more open geochemical system on the scale of hundreds of metres, perhaps even to kilometres. Thus chlorite may have hybrid characteristics with Fe-rich chlorite effectively limited to beds that contained abundant Fe (plus Al and Si) at the time of deposition but it is not impossible that the Fe/Mg ratio of authigenic chlorite may be affected by a net flux of Mg into a sandstone during diagenesis (Hillier et al., 1996).

Therefore, a key issue for the presence of chlorite in a sandstone is how the iron was delivered, i.e., in what mineral form, to the point of final sediment accumulation. This issue is best dealt with by considering different size fractions of sediment.

### Coarse fraction minerals

In theory, any minerals in the hinterland can become part of the coarse sediment fraction and be deposited along with the ubiquitous quartz and feldspar. However, weathering tends to geochemically change high temperature primary igneous and metamorphic minerals such as olivine, pyroxene, garnet and amphiboles into lower temperature minerals such as Fe-oxides and Fe-clay minerals. Lower temperature, hydrothermally altered igneous and metamorphic rocks tend to contain minerals such as chlorite and biotite which may be more resistant to weathering as they are less distant from thermodynamic equilibrium than olivine, etc. In summary, lithic grains can contain any minerals found in the hinterland but chlorite- and biotite-bearing lithics are relatively more chemically-stable and thus more likely to survive and be deposited with sand than olivine-, pyroxene- or amphibole-bearing lithics.

Heavy minerals are a separate class of, often monomineralic, sand grains that have proved useful for provenance studies (Morton and Hallsworth, 1999). Iron-bearing heavy minerals include amphibole, epidote, garnet, ilmenite, staurolite, and haematite (Table 5) (Flemal, 1969; Walderhaug and Porten, 2007). The concentration of many heavy minerals in sandstone decreases during burial and diagenesis with amphibole, epidote, staurolite and garnet all showing clear signs of diagenetic replacement during burial to the mesogenetic realm (Walderhaug and Porten, 2007). The iron liberated from the alteration of these heavy minerals must be incorporated into diagenetic minerals; it is possible that a small amount of chlorite may result from the alteration of small detrital quantities of Fe-rich heavy minerals.

The hydraulic conditions in the hinterland, and perhaps more importantly, at the site of deposition, is the paramount control that concentrates iron minerals in the sand fraction. The exact grain size fraction that contains the maximum quantity of iron minerals needs to be known before it is possible to make predictions about the preferential site of deposition of iron-enriched sediment (Griffiths et al., 2019a; Griffiths et al., 2018b; Griffiths et al., 2019c).

### Fine fraction minerals

Following weathering of bedrock in the sediment's hinterland, the resulting Fe-oxides and Fe-clay minerals (Table 4) will get transported, along with the coarse fraction, down the catchment, typically during flood events but also, at lower concentrations, during a river's normal base flow. The fine fraction generated in the hinterland contains clay minerals and oxides as function of the intensity of the weathering regime. Warmer and higher humidity climates, shallow gradients and large hinterlands will all tend to lead to more advanced stages of weathering than cold, arid, steep gradient and small hinterlands (Hill et al., 2000; McKinley et al., 2003). Thus, smectite and detrital chlorite at the point of deposition tend to be the hallmark of limited chemical weathering, whereas Fe-oxides and hydroxides at the point of deposition tend to be the hallmark of extreme weathering (Chamley, 1989; Rateev et al., 2008).

Fine and coarse sediment fractions are naturally separated by hydrodynamic processes during transport; fine grained materials tend to be passed out, eventually, into ocean basins whereas coarse fraction sediment is trapped at continental margins, although turbidite systems can deliver sand grade material out on to the abyssal plain. Fine fraction sediment, including Fe-oxides, Fe-clays and even silt-grade lithic fragments are thus theoretically separated from the coarse-grained, quartz-dominated fraction. Fine and coarse fraction sediment can be recombined, overcoming the initial hydraulic separation, by a variety of processes such as: (i) soft-sediment deformation, (ii) bioturbation (Taylor and Goldring, 1993), and (iii) infiltration (Matlack et al., 1989) so that these mechanisms may introduce Fe-oxides and Fe-clays into otherwise Fe-deficient sediment. Fine fractions can also be combined with coarse fraction sediment by the presence of biofilms that adhere fine fraction sediment onto sand grains (Jones, 2017; Wooldridge et al., 2017a; Wooldridge et al., 2018). Biofilms are thus another way of introducing Fe-oxides and Fe-clays into otherwise Fe-deficient, coarse-grained sediment.

### **Dissolved iron: Fe-speciation and concentration in rivers versus the sea**

Some iron is transported in a truly dissolved form in rivers although ferric iron, the stable form of iron at the Earth's surface, has very low aqueous solubility. Much iron is transported from hinterlands into depositional sedimentary systems in the form of organic complexes, such as Fe-humic complexes (Sholkovitz, 1976). The practical definition of "dissolved iron" is that the material passes through 0.45  $\mu\text{m}$  filters; the term dissolved iron thus practically includes dissolved and organically-complexed iron as well as ultra-fine-grained particulates such as clay minerals and Fe-oxides (Barrie et al., 2015; Boyle et al., 1977; Eckert and Sholkovitz, 1976; Sholkovitz, 1976; Sholkovitz, 1978; Sholkovitz et al., 1978). Organically-complexed iron probably originates in soil, and evolves during fluvial transport (Konhauser and Urrutia, 1999), under the action of biologically active weathering in a low salinity environment, typical of hinterlands and rivers.

Rivers can contain > 25  $\mu\text{m/L}$  dissolved iron (Berner and Berner, 2012; Boyle et al., 1977). Seawater, at open-ocean salinity, and mid latitude temperature, typically contains approximately 0.0003  $\mu\text{m/L}$  dissolved iron (Liu and Millero, 2002) so that the iron concentration of river water is nearly 80,000 higher than that of seawater (Fig. 13). The implication of this is that the vast majority of fluvially-transported, organic-complexed iron does not make it out into the ocean. The Fe-humic complexes become destabilised in the presence of seawater when rivers enter estuaries or deltas and create Fe-rich flocs (the process is known as flocculation) that get deposited in the delta or estuary (Fig. 13). The vast majority of the fluvially-transported dissolved and organically-complexed iron gets deposited within the river water-seawater mixing zone (Boyle et al., 1977; Eckert and Sholkovitz, 1976; Sholkovitz, 1976; Sholkovitz, 1978; Sholkovitz et al., 1978). A consequence of this loss of fluvial iron, due to river water-seawater mixing, is that one of the key ingredients of chlorite (iron) is localised at the site where rivers meet the sea within estuaries (and deltas) (Ehrenberg, 1993). This may partly explain why many chlorite-bearing sandstones were deposited in estuaries and deltas (Dowey et al., 2012). Of course, it is possible that the deposited organically-complexed iron is moved further down the sediment system, by storm events, so that the near coastal marine system may also become enriched in these flocculated and deposited Fe-minerals (Odin, 1990).

## **Overview of the sedimentary context of chlorite-bearing sandstones**

### **Provenance issues**

Simply stated, the vast majority of chlorite-cemented sandstones were deposited in marginal marine environments and are relatively Fe-rich (Fig. 10A) (Dowey et al., 2012). Thus, a critical control on the development of chlorite in sandstones is the primary depositional environment and the drainage of iron-

enriched rocks in the hinterland. It is not possible to generate chlorite-enriched sandstones if the hinterland to the sedimentary basin is depleted in Fe-enriched rocks.

Table 5, and a subset of the data plotted in Figure 14, represent a snapshot of the compositions of some of the most important end-member rock types (and their metamorphic equivalents) that occur in the hinterlands to sedimentary basins. The data have been presented in terms of absolute oxide % concentrations and molar ratios relative to iron. Clearly some hinterlands can be rather deficient in iron which probably means that such rocks will be unlikely to produce sandstones that are relatively rich in chlorite.

Table 6 and Figure 15 represent the compositions of different types of sandstone as defined by mineral proportions. Table 6 was developed using assumed mineral compositions listed in Table 7. The emphasis in Table 6 and Figure 14 is the presence and abundance of the various iron minerals found in sandstones (chlorite, biotite, siderite, pyrite and ilmenite, in this case). Relatively Fe-rich sandstones can contain 5 to 15% chlorite, but equally they can contain siderite, pyrite or other Fe-rich minerals (Fig. 15). The presence of chlorite requires the sandstone to be moderately Fe-rich but note that this type of Fe-rich sediment does not necessarily lead to the occurrence of chlorite, it could create siderite- or pyrite-bearing sandstone instead.

## Climate issues

Climate plays a role in controlling the presence of chlorite in modern sediment and ancient sandstones in terms of weathering within the hinterland and its influence on the physical environmental conditions at the site of sediment deposition (Meunier, 2005; Rateev et al., 2008; Velde, 1985).

Weathering influences the physical form of iron in the sedimentary system. Low degrees of weathering in the hinterland can result from one or more of: (i) low temperature, (ii) low humidity, (iii) steep gradient resulting in rapid sediment transport, (iv) short distance between hinterland and site of deposition (McKinley et al., 2003). Low degrees of weathering result in the sediment supply containing the Fe-minerals that are present in the bedrocks in the hinterland and a low degree of the creation of clay minerals and Fe-oxides and -hydroxides. High degrees of weathering result in the alteration of the Fe-minerals that are present in the bedrocks in the hinterland and replacement by low temperature clay minerals and Fe-oxides and -hydroxides. Low degrees of weathering commonly result in the deposition of Fe-rich lithic fragments and Fe-rich monomineralic sand grains (e.g. detrital biotite, chlorite, ilmenite, garnet, etc.). Moderate degrees of weathering commonly result in the deposition of Fe-clays (e.g. smectite) and Fe-rich oxides and hydroxides (Fritz and Toth, 1997; Toth and Fritz, 1997). More advanced weathering therefore tends to push Fe into the finest size fractions in a clastic sediment supply and results in the creation of Fe-free clays, such as kaolinite, and Fe-rich oxides and hydroxides.

Limited weathering due to low temperature, low humidity and rapid transport resulting from steep hinterland gradients (e.g., synrift alluvial-fan sediments deposited at high-latitudes) leads to sediment being relatively enriched in primary minerals found in the bedrocks in the hinterland resulting in possible sediment enrichment in metamorphic and igneous Fe-minerals, possibly including detrital chlorite with the composition controlled by the composition of chlorite in the hinterland bedrocks. Conversely, advanced weathering due to high temperature, high humidity and slow transport resulting from shallow hinterland gradients (e.g., post-rift low-density turbidite sediments deposited at low-latitudes) leads to sediment being relatively enriched in secondary alteration products including low temperature Fe-clay minerals and Fe-oxides and hydroxides which may react during subsequent burial to create Fe-enriched chlorite.

## Post depositional processes and eodiagenesis

Eodiagenesis represents the collection of processes that occur immediately after the sediment has been deposited and therefore is influenced by the depositional environment (Worden and Burley, 2003). Eodiagenesis also occurs before sediment is buried sufficiently either to: (i) isolate it from Earth surface conditions, or (ii) heat it up to temperatures at which mineral reactions have the kinetic drive to start changing the disequilibrium collection of deposited minerals into a more stable mineralogy (Worden et al., 2018a). Eodiagenesis involves: redox processes, animal-sediment interaction, microbial processes, dissolution of reactive minerals and growth of relatively more stable new minerals, grain rearrangement during initial compaction, and even the growth of deformation bands in friable sediment (Griffiths et al., 2018a; Worden and Morad, 2003).

## Redox, bioturbation and micro-fauna and -flora considerations

Oxidation-reduction processes (“redox”), typically bacterially-mediated, are common in marine and marginal marine sediments. There is a well-studied series of reactions involving the reduction of nitrate, manganese, iron and sulphate that lead to predictable processes and products (Berner, 1980), including the development a black-sand layer in marine and marginal marine sediment (Fig. 16A). This is the result of bacterial sulphate and Fe reduction creating a layer of blackened FeS-enriched sand that would become pyrite-rich if the sediment was buried into the mesogenetic realm. The growth of FeS is reversible soon after formation, as shown by the localised re-oxidation of the black sand into white sand (Fig. 16A) in the vicinity of worm irrigation burrows that extend from the sediment surface to below the black sand redox boundary.

Burrowing animals have multiple roles in the generation of a sediment’s pore scale character. Bioturbation is one of the main ways that hydrodynamically separated clay and silt fraction of bedded sediments are recombined with sand-grade material (Fig. 16B and C). Thus, if clean sand is mixed with clay and silt fraction materials that were the host for the results of flocculation of formerly organically-complexed fluvial iron, then the sand may have the key ingredients for Fe-clay growth during diagenesis. For example, if there is abundant Fe-oxide or -hydroxide in the fine fraction and there is abundant feldspars in the discrete coarse fraction, and if the sand-grade feldspars continue to undergo weathering and alteration soon after burial, creating aluminosilicate clay minerals, then the neoformed Al-Si clays plus the newly admixed Fe-oxide and -hydroxide may produce Fe-clay minerals, such as berthierine, that then go on to produce chlorite during mesodiagenesis. Faecal pellets result from sediment ingestion and excretion by animals and either result in the creation of clay coats adhered to sand grains (Needham et al., 2005) or the conversion of previously suspended clay into silt or sand grain size aggregates (Pryor, 1975). Both processes are mechanism for introducing clay into coarser grained sediment.

If there is repeated flushing of the sediment by water that is enriched in bacterial sulphate reduction-derived aqueous sulphide then all available iron minerals, including all precursor minerals for chlorite, may be converted in Fe-sulphide minerals thus mitigating the chance of the host sandstone being chlorite-bearing during subsequent burial. Three scenarios are possible to prevent excess bacterial sulphate reduction: (i) rapid burial of sediment out of the active redox zone, thus cutting off the supply of aqueous sulphide, (ii) interstitial waters being depleted in aqueous sulphate, for example due to the dominance of fresh water at the site of deposition, as found in proximal estuarine, as opposed to open marine, conditions (Fig. 17), (iii) lack of bacteria or organic nutrients in the sediment thus minimising bacterial sulphate reduction and cutting off the supply of aqueous sulphide. The converse of these scenarios will lead to growth of bacterial FeS and reduce the chance of the occurrence of chlorite in the sandstones (Fig 17).

Micro-fauna and flora are so small that they do not lead to a record of their life activities via bioturbation. However, diatoms are now known to be key, at least in some sedimentary environments, for the creation of detrital grain coats (Fig. 18) (Wooldridge et al., 2017a; Wooldridge et al., 2018). It is likely that the biological realm, including bacteria and algae, plays a major role in the formation of a sediment's Fe-mineral suite.

## Infiltration

In soil science terms, eluviation is the transport of material from upper layers of soil to lower levels by downward movement of water through soil horizons, and accumulation of this material at lower levels is called illuviation (Buurman et al., 1998). Infiltration has been routinely invoked as way of incorporating fine grained clays and clay minerals into previously well-sorted and clay-deficient sands (Matlack et al., 1989). Some have attributed coatings of oriented clay in coarse sediments to a process of infiltration of muddy river water or muddy overland flow (Moraes and De Ros, 1992). If surface water carries fine suspended sediment and percolates through a porous, unsaturated zone, such as a vadose zone of an unconsolidated, typically low salinity aquifer, especially where there is a fluctuating groundwater table, or into intertidal granular sediments at low tide in estuaries or deltas, then the fine suspended sediment may be retained within the granular matrix. The matrix acts as a filter and traps the fine suspended sediment; this is known as mechanical infiltration (De Ros and Scherer, 2012; Herringshaw and McIlroy, 2013; Matlack et al., 1989; Moraes and De Ros, 1990). Infiltration is therefore potentially one way to add fine sediment to previously clean, clay-free sediment and this may be an important way of adding Mg-rich clay chlorite-precursor minerals into aeolian Rotliegend Formation (Hillier et al., 1996) and dry-land river Skaggerak Formation sediments (Stricker and Jones, 2018). Infiltration can only happen when clay-rich water percolates into permeable but unsaturated (typically granular) sediment and is thus of importance to granular sediment with a water table (i.e., deltaic or estuarine clastic sediments at low tide or fluvial clastic sediment above the vadose zone). Infiltration is widely cited as a control on the presence of clay minerals in granular sediments. Although there seem to have been few studies of modern sedimentary environments where infiltration has been proved, there is a burgeoning soil-science literature that proves that illuviation is accepted as a major control on redistribution of fine materials in a granular soil matrix (Buurman et al., 1998; Skolasinska, 2006). In contrast however, recent work on the Ravenglass estuary in NW England has found no evidence of infiltration of clay minerals into the top 1 m of intertidal sediments (Griffiths et al., 2018b; Wooldridge et al., 2018); this is significant as many studies of chlorite cemented estuarine sandstones assert that infiltration has added chlorite-precursor phases to the sandy sediment. The assumed importance of infiltration for the origin of clay minerals in sandstones may need to be re-examined.

## Depositional and hydrodynamic processes that influence the accumulation of chlorite and its precursors

Chlorite-bearing sandstones occur in all depositional environments (Fig. 10) but chlorite-coated sandstones are most common from estuarine and deltaic environments of deposition but are also reported in turbidites and in fluvial-alluvial sediments (Dowey et al., 2012). A key issue is that the components needed to generate chlorite during burial and diagenesis (the chlorite-precursor minerals) need either to be co-deposited with sand-grade sediment or incorporated after deposition. There have been attempts (Ehrenberg, 1993) to understand chlorite-cemented sandstone by reference to the seminal work on green marine clays in fine-grained sediments (Odin, 1988). However, the relationship between chlorite-bearing marginal marine sandstones and Fe-clay rich marine mudstones, the focus of Odin's work, is not necessarily simple due to the hydrodynamic differences between sand-dominated and mud-dominated sediments.

Hydrodynamic processes lead to the physical separation, or fractionation, of sediment of different grain sizes during transport since clay grade materials are routinely transported in suspension during low to high velocity flow, whereas sand grade materials are typically transported by rolling and saltation at relatively high velocity flow. Deposition processes also tend to lead to the separation of grain sizes since, during waning flow, coarse sediment is deposited first and clay grade material is deposited last under negligible flow velocities. Therefore, consideration is required to account for the presence of clay minerals in sandstones. In theory, sandstones can become chlorite-bearing if: (i) there were chlorite-precursor coats created in situ in the environment of deposition (Wooldridge et al., 2017b), or (ii) there were chlorite-precursor-bearing (allogenic) lithic sand grains (Griffiths et al., 2019c), or (iii) there were chlorite-precursor-bearing autogenic grains, such as Fe-ooids or Fe-clay rich intraclasts (Vanhousten, 1992). Post-depositional processes can re-incorporate fine-grained chlorite-precursor minerals (e.g. berthierine, odinite, phyllite-V, Fe-smectite, Fe-oxyhydroxides), originally deposited as discrete mudstone beds, into sand-dominated sediment due to processes such as (iv) bioturbation (McIlroy et al., 2003; Needham et al., 2004; Needham et al., 2005; Taylor and Goldring, 1993), (v) sediment ingestion and excretion (McIlroy et al., 2003; Needham et al., 2005; Worden et al., 2006b), (vi) soft-sediment deformation due to slumping or dewatering (Porter et al., 2000), or (vii) clay infiltration into sand due to infiltration of suspended clay into vadose zone sand (Matlack et al., 1989).

There are numerous processes that can be invoked to explain how chlorite-precursor minerals are incorporated into sandstones. The likelihood of the various processes, listed above, occurring in the range of clastic environments has here been evaluated and represented in Figure 19. For estuarine and deltaic sediments, it seems likely that all seven processes listed above (i-vii) can occur perhaps helping to explain why chlorite grain coats are most common in estuarine and deltaic sediments.

Detailed studies of the modern Ravenglass estuarine sedimentary environment (Daneshvar and Worden, 2018; Griffiths et al., 2018b; Griffiths et al., 2019b; Griffiths et al., 2019c; Wooldridge et al., 2017a; Wooldridge et al., 2017b; Wooldridge et al., 2018; Wooldridge et al., 2019a; Wooldridge et al., 2019b) have revealed that it is imperative to define specific sub-environments of deposition to fully understand and predict chlorite grain coats in ancient and deeply buried sandstones. A study of bulk iron, the key element required to allow chlorite formation and measured using a portable X-ray fluorescence (pXRF) device under careful laboratory conditions, showed that iron sediment concentration is highly heterogeneous across the estuary with highest concentrations in inner estuary sandflats and mixed sand-mudflats (Fig. 20). Analysis of the distribution of detrital chlorite, the dominant Fe-mineral in Ravenglass, revealed that it is most concentrated relative to other clays in outer and mid estuary sand-rich sediment (Fig. 21A-C) because this clay mineral is predominantly not in clay-grade sediment (Fig 21B) (Griffiths et al., 2019c). The absolute concentration of chlorite in Ravenglass is highest in inner estuary, sand-dominated environments such as sand bars (Fig. 22). A sequence-type approach to describing an estuary infill (Dalrymple et al., 1992), shows that clean barrier and shoreface sands will have poorer reservoir quality than clay-rich (chlorite-rich) inner estuary (sand flat and tidal bar) sands, in rocks buried to > 80 to 100°C, because quartz cementation will run unhindered in the absence of chlorite coats (Fig.22) (Griffiths et al., 2018b). The Ravenglass modern analogue study has also revealed the routine presence of detrital clay coats, including chlorite-bearing coats, especially in inner estuary sediments (Fig. 23) (Wooldridge et al., 2017b; Wooldridge et al., 2019a). The detrital coats studied from Ravenglass provided conclusive proof that authigenic chlorite coats commonly sit on top of detrital clay “root” grain coats (Fig. 6b) in deeply buried sandstones and strongly suggest that authigenic coats may partly be recrystallized detrital clay coats. Studies of modern grain coats has also revealed that biofilms are common in estuarine sandy sediment and that diatoms are commonly associated with these coats (Fig. 18D) (Dowey et al., 2017; Wooldridge et al., 2017a). Grain coats are heterogeneously distributed in Ravenglass estuarine sediment (Fig. 23a) with the greatest concentration occurring in inner estuarine sediment. The grain coat distribution pattern closely matches the distribution of a biomarker for diatoms (chlorophyll-a) implying



that diatom life activities have created biofilms that have subsequently adhered clays and clay minerals to sand grain surfaces (Wooldridge et al., 2017a) (Fig. 23B). Thus proto-chlorite coats are created due to the development of biofilms and the concentration of chlorite in inshore tidal sandy sediments.

There is growing appreciation of the preferential localization of Fe-clays, such as berthierine or other chlorite-precursor phases, in marginal marine sediments (Ketzer et al., 2003; Morad et al., 2010; Saïag et al., 2016; Worden and Morad, 2003) (Fig. 17A). Estuaries and deltas share a lot of common characteristics. Deltas are sites where river water and seawater meet, and where there is net sediment accumulation due to the rate of fluvial sediment supply exceeding the rate of dispersal within the ocean basin (Nichols, 2009). Estuaries are partly enclosed coastal bodies of mixed river water and seawater, typically where rising sea level has flooded river mouths and the lower reaches of river valleys (Dalrymple et al., 1992; Nichols, 2009). It has been reported that the dominant process (tide, wave or river) can have a large impact on the accumulation of the amount and type of clay minerals in marginal marine sediments (Ainsworth et al., 2017; Longhitano et al., 2012). Both estuaries and deltas can be wave-, tide- or fluvial-dominated or have mixed characteristics. Wave-dominated deltas tend to have mouth bars parallel to the shoreline. Wave-dominated estuaries tend to have coastally-attached sand bars that extend across the embayment and partly enclose the central part of the estuary. Tide-dominated deltas tend to have mouth bars roughly perpendicular to the shoreline with the bars extending beyond the coastline either side of the river-inlet point. Tide-dominated estuaries tend to have sand bars, within the embayment, roughly perpendicular to the shoreline facing an open sea-inlet; estuarine sand bars lie behind the coastline either side of the river inlet point. Tide-dominated estuaries typically contain a bayhead delta. Estuarine deposits develop during periods of rising relative sea level where the sediment is confined within palaeo-valleys, where the fluvial-supplied sediment is trapped within increasingly proximal locations, and where there is limited net transport of the primary fluvial sediment into the marine basin. Berthierine and other Fe-chlorite precursor phases are most commonly found within tide-dominated estuarine sandstones (Saïag et al., 2016).

Why should estuaries be a locus of berthierine or Fe-clay occurrence in the sediment record? There are several possible contributing factors: (i) the enclosed estuarine embayment (Fig. 17) may serve to trap the flocculated fluvial Fe-oxides and -hydroxides rather than allow them to be flushed out into the open marine realm (Odin, 1988), (ii) the rising sea level pushes back the site of sand accumulation, including chlorite precursor lithic (allogenic, extrabasinal) grains or even Fe-ooids (autogenic, intrabasinal) grains, and serves to localise these materials, probably at the head of the estuary, (iii) the semi enclosed nature of estuaries will limit the salinity, and thus aqueous sulphate, of the interstitial waters, and thus minimise Fe-sulphide growth at the expense of Fe-clay minerals (Fig. 17D), (iv) rising sea levels may minimise the accumulation of peaty or proto-coal deposits and thus limit the amount of rotted organic matter and the concomitant elevated aqueous bicarbonate and consequently minimise siderite growth at the expense of Fe-clay minerals (Fig. 17C), (v) the rising sea-level, typical during the formation of estuaries may encourage the development of Fe-ooids in ephemeral coastal lagoons that trap flocculated and sand-grade Fe-rich sand grains, these Fe-ooids may then be flushed into the upper reaches and proximal parts of the estuary thus localising autogenic Fe-rich sand-grade materials in these sediment (Fig. 17B).

Note that the Brent Group, deposited as part of a deltaic succession, is highly Fe-rich, with abundant detrital biotite, but seems to contain little or no authigenic chlorite (Giles et al., 1992). The deltaic, Fe-rich Brent group is demonstrably siderite cemented (Ashcroft and Ridgway, 1996) instead of Fe-clay bearing, suggesting that an abundant supply of organic-derived aqueous bicarbonate in the groundwater locked up the abundant iron as siderite rather than leaving it available to Fe-clay minerals (Fig. 17C). Brent deltaic sediments contain abundant plant remains, and thin coals (Nicolas et al., 1997; Ruau et al., 1996), testifying to the lush vegetation on the coastal plain that led to bicarbonate-enriched groundwater

and interstitial waters, and helping to explain why chlorite is absent despite the Fe-enriched primary Brent sediment supply and deltaic environment of deposition.

### **Types of Fe-minerals that survive deposition and early diagenesis and that generate chlorite during mesodiagenesis**

There is a wide range of Fe-minerals that can be incorporated into sediment, at the time of deposition, to create chlorite (Table 4). Numerous depositional and early diagenetic Fe-minerals have been proposed to generate chlorite during subsequent burial and mesodiagenesis (Fig. 24). Detrital clay minerals, especially berthierine (Beaufort et al., 2015; Ehrenberg, 1993) and trioctahedral smectite (Beaufort et al., 2015; Chang et al., 1986) have been proposed as the source of the key ingredients of chlorite. Siderite, a product of early diagenesis, has been proposed to break down during mesodiagenesis, at temperatures > 120°C, to produce chlorite (presumably with extremely high Fe/(Fe+Mg ratios) values) (Curtis et al., 1985). It has also been proposed that ankerite, probably a product of the intermediate stages of diagenesis, can break down to produce Fe-Mg chlorite (Smith and Ehrenberg, 1989). Fe-Mg-rich lithic fragments have been proposed to be a source of authigenic chlorite (Worden et al., 2018c), such lithic fragments must have survived early diagenesis and so probably will include biotite and chlorite, as higher temperature igneous and metamorphic minerals (e.g. hornblende, pyroxene) are less likely to survive transport, deposition and initial burial (eodiagenesis) than lower temperature minerals. Fe-rich heavy minerals, such as ilmenite, garnet or haematite, can be present at the low percentage levels in sands; ilmenite has been suggested as a key source of Fe for chlorite (Gould et al., 2010). However, it has been noted that heavy mineral populations decrease in progressively buried sandstones (Walderhaug and Porten, 2007) so that at least a small proportion of Fe may be supplied by the diagenetic alteration of a range of heavy minerals.

To summarise the main detrital and early diagenetic minerals that have been reported to lead to the growth of authigenic chlorite during mesodiagenesis are berthierine, smectite, siderite, ankerite, detrital chlorite and biotite, ilmenite and other Fe-rich heavy minerals (Fig. 24).

### **Fe-minerals and chlorite during burial (meso-) diagenesis**

#### **Chlorite generating mesogenetic reactions in sandstones**

As mentioned in the discussion of the types of materials that survive deposition and early diagenesis, there are many processes and reactions that have been proposed to generate chlorite (Fig. 24). These processes fall into several groups; broadly isochemical replacement of Fe-clay (berthierine), replacement of smectite by chlorite, replacement of kaolinite by chlorite, and an ill-defined cluster of processes that involve Fe-rich detrital minerals and grains. Figure 24 largely assumes closed system (isochemical) diagenesis; if an external source of Fe (e.g. from neighbouring mudstones) is predicted then this could allow chlorite to replace alumino-silicate clays such as kaolinite or illite or alumina-silicate framework grains such as detrital feldspars. Note that replacement of alumino-silicate clays and feldspars is rarely reported. The lack of reported replacement of alumina-silicate clays and feldspars strongly supports the assumed isochemical nature of chlorite diagenesis as proposed in Figure 24

The berthierine origin of chlorite in sandstones has been proved experimentally by Aagaard et al. (2000); the neoformed chlorite notably had the same chemical composition as the precursor berthierine. It has been proposed that the transformation of berthierine into chlorite occurs at temperatures greater than about 60°C (Aagaard et al., 2000; Ehrenberg, 1993; Jahren and Aagaard, 1989; Worden and Morad, 2003) (Fig. 24).

The replacement of smectite by chlorite involves flux of material, possibly at the pore- or bed-scale; it requires either a source of aluminium, iron and magnesium (Chang et al., 1986) or distinct loss of silica, calcium and magnesium to balance the reaction (Chang et al., 1986; Niu et al., 2000). Chlorite coats in the Gulf Coast Nophlet Formation have been interpreted to result from transformation of detrital Mg-rich smectite in aeolian interdune settings with iron supplied by cannibalization of detrital haematite coats (Ajdukiewicz et al., 2010). The replacement of smectite by chlorite involves dissolution and reprecipitation; it probably occurs at relatively low temperatures (> 60 or 70°C) and involves intermediate, mixed-layer (initially smectite-dominant chlorite-minor and then chlorite-dominant smectite-minor) stages (known as S-C and C-S) as temperature increases to 120 to 130°C (Fig. 24) (Ryan et al., 1998; Worden and Morad, 2003).

The replacement of kaolinite by chlorite has been proposed in numerous studies including: (i) siderite-kaolinite reaction (Curtis et al., 1985), (ii) ankerite-kaolinite reaction (Muffler and White, 1969; Smith and Ehrenberg, 1989), typically at temperatures > 120°C. Presumably the siderite reaction produces chlorite with a higher Fe/(Fe+Mg) value than the ankerite reaction. Others have proposed a reaction between kaolinite and an unspecified source of Fe and Mg (Boles and Franks, 1979); the source of these divalent metals may be lithic rock fragments or grains. In the absence of kaolinite, perhaps after its reaction with K-feldspar (Bjorkum and Gjelsvik, 1988), it has been further suggested that ankerite will react with illite, at temperatures a lot higher than 120°C, producing Fe-Mg chlorite and quartz (Smith and Ehrenberg, 1989).

Fe-Mg-rich lithic grains (Dutton et al., 2018) and detrital chlorite and biotite (Worden et al., 2018c), ilmenite and other heavy minerals (Gould et al., 2010) have all been reported to be responsible for authigenic chlorite although the ilmenite source proposed by Gould et al. (2010) was interpreted to be via early diagenetic berthierine. The reported progressive loss of heavy minerals, many Fe-rich phases such as amphibole, garnet, staurolite and epidote, during progressive diagenesis (Walderhaug and Porten, 2007) may lead to chlorite growth, for example in kaolinite-rich sandstones.

### Role of interbedded, neighbouring lithologies and mass flux into chlorite-bearing sandstones

Is there any role of either mass flux or diffusion from stratigraphically or spatially neighbouring sediments for authigenic chlorite? Based on the isochemical (closed system) argument for oxides of Fe, Al and Si developed earlier (Table 3, Figure 12), it seems highly unlikely that mass flux of dissolved iron can lead to the development of Fe-chlorite. However, magnesium is definitely mobile in the subsurface as demonstrated by the process of dolomitization in carbonates (Jiang et al., 2016; Jiang et al., 2014) and the common growth of late-stage dolomite cements in sandstones (Worden and Burley, 2003). Table 3 demonstrates that > 130,000 pore volumes are needed to convert aluminosilicate clay into Fe-chlorite, whereas only > 652 pore volumes are needed to convert aluminosilicate clay into Mg-chlorite. A study of the composition of different types of chlorite in some Lower Jurassic sandstones revealed two main compositional types of chlorite: one was Mg-rich chlorite in lithic grains, the other was Fe-rich grain-coating and pore-filling chlorite (Worden et al., 2018c). The more Mg-rich type of chlorite was detrital whereas the more Fe-rich types of chlorite was authigenic, grain-coating and pore-filling, suggesting that mass flux of magnesium has not occurred since, if it had, the authigenic chlorite might have been expected to be more Mg-rich than the detrital chlorite. However, analysis of chlorite in Permian aeolian sandstones showed that they showed a distinct compositional (Fe/(Fe+Mg)) difference across the basin; the variation of Mg was ascribed to lateral migration of Mg-rich brines during early stages of burial (Hillier et al., 1996). From this example, it seems to be possible that the Mg-component in other examples of chlorite may be influenced by an influx of externally-derived Mg, analogous to burial diagenetic dolomitization of limestone (Worden et al., 2018a).

Sandstone reservoirs are rarely reported to be sour, i.e. rich in H<sub>2</sub>S (Worden and Smalley, 2001; Worden et al., 2003). High concentrations of H<sub>2</sub>S are typically the result of thermochemical sulphate reduction (Worden and Smalley, 1996; Worden and Smalley, 2001; Worden et al., 1995) but can also result from the normal thermo-catalytic breakdown of either S-bearing kerogen in source rocks or S-bearing organic molecules in oil accumulations (Hunt, 1995). The lack of sour gas accumulations in sandstones is because, unlike many carbonates, sandstones tend to be Fe-bearing and so have the capacity to react with H<sub>2</sub>S. Any Fe-minerals, except Fe-sulphides, can react with H<sub>2</sub>S, so that any pre-existing Fe-bearing chlorite will react with any H<sub>2</sub>S, from whatever source, in a reservoir and lead to the growth of late-stage euhedral pyrite at the expense of chlorite (Worden et al., 2003). Mass influx of sour gas may serve to degrade grain-coating chlorite.

Most reservoirs contain some CO<sub>2</sub>, either dissolved in oil or in the gas phase. CO<sub>2</sub> in sedimentary basins can derive from many sources (Baines and Worden, 2004; Hunt, 1995; Pearce et al., 2004; Wycherley et al., 1999). An influx of CO<sub>2</sub>, especially at a temperature of less than 100 to 120°C (Smith and Ehrenberg, 1989), may have consequences for chlorite since this mineral is preferentially soluble under acidic conditions (Armitage et al., 2013) and the liberated Fe may react with aqueous CO<sub>2</sub> to generate authigenic siderite (Xu et al., 2005). Mass influx of late-stage CO<sub>2</sub>, like H<sub>2</sub>S, may also serve to degrade grain-coating chlorite.

### Compaction of chlorite-cemented sandstones

Compaction represents a family of processes that can be broadly split into mechanical and chemical end-members. Mechanical compaction includes grain rearrangement, grain bending (Lundegard, 1992), ductile grain deformation (Worden et al., 2000), and brittle grain fracturing, e.g. during the generation of deformation bands (Griffiths et al., 2018a). Chemical compaction is the enhanced dissolution of minerals at grain-grain contacts as a function of increasing effective stress, typically during burial (Bjørlykke et al., 1986) but also potentially due to tectonic processes (Worden et al., 2018a). Pressure solution is another term that is often used synonymously with chemical compaction (Houseknecht, 1984). However, there are some who consider that effective stress plays no part in chemical compaction (Bjørkum and Nadeau, 1998) despite the observation that effective stress is required to provide the driving force for diffusion from grain boundaries to unconstrained grain surfaces adjacent to pores (Sheldon et al., 2003). Use of the term chemical compaction is less controversial than the term pressure solution and is useful contrast to the term mechanical compaction. Chemical compaction in sandstones is usually studied in terms of quartz dissolution either at intergranular microstylolites or at macrostylolites.

It was suggested, by Line et al. (2018), that normal mechanical compaction was the main porosity-loss mechanism in chlorite-cemented sandstones from the Barents Sea although no porosity-depth data were presented to help support that assertion. As stated, deeply-buried chlorite-coated sandstones have anomalously high porosity, with examples of porosity of 25% at 3,500 to 5,000 m not uncommon (Bloch et al., 2002) (Fig. 25). Typical compaction curves for sandstones suggest that mechanical compaction, on its own, can reduce porosity to about 25 or 26 % during burial to > 3,000 m, simply by grain rearrangement, etc. (Paxton et al., 2002) (Fig. 25). This suggests that chlorite-coated sandstones follow normal mechanical compaction curves for sandstones. Chlorite coats therefore seem not to inhibit mechanical compaction.

Conversely, deeply-buried sandstones that have continuous chlorite coats tend to be free of micro- or macro-stylolites, and they typically contain much less quartz cement than non-chlorite-coated sandstones that have had a similar effective stress- and temperature history (Peng et al., 2009). It can thus be concluded that chlorite coats with no breaks in coverage, inhibit pressure solution (Fisher et al., 2000). The inhibition of stylolite development may be because any supersaturated dissolved silica has nowhere to precipitate (as quartz cement) so that quartz cannot further dissolve at any quartz-quartz

grain contacts. Another cause could be the result of there being few clean quartz-quartz grain contacts due to pervasive chlorite coats physically separating quartz grains. However, it has been commonly noted, during SEI examination of chlorite-coated sandstones, that chlorite grain coats are usually absent at grain-grain contacts (Fig. 8A) (Billault et al., 2003; Line et al., 2018; Sun et al., 2014). This suggests that authigenic chlorite coats develop, from whatever source, after the initial stages of mechanical compaction and grain rearrangement. Note that the absence of chlorite coats at grain-grain contacts does not suggest that the ingredients required for chlorite growth (oxides of Fe, Al, Si) were externally sourced by mass flux (Table 3). Rather, the absence of chlorite coats at grain-grain contacts might suggest that increasing effective stress on chlorite-precursor minerals, e.g. berthierine, during burial increased the local solubility of the chlorite precursor mineral and allowed pore-scale transport out into lower stress regions (e.g. of grain surfaces adjacent to open pores) and encouraged precipitation of chlorite on free grain surfaces. In addition, the absence of chlorite at quartz-quartz grain contacts suggests that quartz precipitation is the inhibited process, rather than quartz dissolution.

## **Inhibition of quartz cement: is it possible to have too much of a good thing?**

### **Good chlorite: why does chlorite inhibit quartz cement?**

A compilation of 46 published case studies of grain coating chlorite is presented in Table 8. Chlorite, that is good for reservoir quality because it coats sand grains (Table 1) and inhibits quartz cementation in deeply buried sandstones, has been reported from rocks from North Africa, NW Europe, N America, SE Asia, China, Australia and South America. It has also been reported in rocks ranging in age from Devonian through to Miocene. Although this benign clay mineral is not ubiquitous in sandstones, it is sufficiently widespread as to be of sustained interest to those exploring for and developing oil and gas fields in deeper sedimentary basins.

Chlorite can indiscriminately coat all framework grains, including quartz, K-feldspar, plagioclase and Fe-oxides, lithic grains (Figs. 4 to 8). Authigenic chlorite grows as crystals that are perpendicular to grain surfaces typically forming extensive coats, commonly covering all exposed surfaces. Chlorite coats tend to be roughly equal thickness (isopachous, Figs. 4A and 4B, 5, 6B, 7A, 8A). It is possible that supersaturated silica cannot access quartz grain surfaces to grow quartz by normal epitaxial processes (Barclay and Worden, 2000; Worden and Morad, 2000). However, a nano-scale examination of the interface between a quartz grain and chlorite, using TEM, revealed that chlorite crystals are embedded within quartz (Billault et al., 2003). Quartz surfaces at the contact with authigenic chlorite coats are characterised by nm-scale knobs corresponding to very small quartz overgrowths that grew in the interstices between the perpendicular chlorite crystals. Chlorite crystals look as if they are partially inserted *into* the quartz grain because of the development of small authigenic quartz crystals that grew around the base of chlorite crystals. The work by Billault et al. (2003) suggested that quartz cement tried to grow, and had some access to supersaturated silica in the formation water, but was limited by the ability of authigenic quartz crystals to merge and grow out into the open pore. A similar effect was observed in hydrothermal experiments undertaken by Ajdukiewicz and Larese (2012) during which isolated nanoquartz cements begin to nucleate between clay particles at high temperatures; the clay minerals in the coat acted as barriers (discontinuities) which inhibited epitaxial growth of quartz. In conclusion, it is possible that chlorite inhibits quartz cement by wholly isolating quartz grains from silica saturated formation water, but it is also possible that inhibition of outward and lateral quartz growth is equally important.

The crystals in authigenic chlorite coats typically are platy with the dominant chlorite (001) faces perpendicular to the underlying grain; individual chlorite crystals in authigenic coats are usually no more than 10  $\mu\text{m}$  long parallel to the (001) face and clusters of plate-like chlorite crystals occur as apparently

randomly oriented rosettes (Bloch et al., 2002; Hillier et al., 1996; Saïag et al., 2016) (Figs. 7B and 8B). Chlorite coats grow indiscriminately on any mineral substrate at any orientation (Fig. 5) so there can be no epitaxial control on chlorite growth. Chlorite coats appear to be isopachous because the lengths of the platy crystals are roughly equal and never seem to exceed 10  $\mu\text{m}$ . Cho and Fawcett (1986) experimentally reproduced rosettes and surface-coating forms of chlorite that look exactly like those found in sandstones. They showed that there are three phases of chlorite growth (Figs. 26 and 27): (i) three-dimensional nucleation on all surfaces; (ii) two-dimensional nucleation or layer growth mechanism during which the plates grow as very thin sheets to a maximum dimension (Fig. 27); and (iii) spiral growth mechanism during which the plates thicken but did not get any longer or wider (Fig. 27). Experimentally grown chlorite first underwent three-dimensional nucleation at multiple sites indiscriminately on the vessel wall when the system was at the highest state of supersaturation. These multiple nuclei then developed into pore-extending rosette aggregates of extremely thin plates that resulted from subsequent layer growth. In time the experimental chlorite developed into somewhat thicker hexagonal platelets up to 10  $\mu\text{m}$  in diameter, by a (001)-parallel spiral growth mechanism. The experimental chlorite growth sequence was: random three-dimensional nucleation when the system was at the highest state of supersaturation, followed by edge, or two dimensional, growth parallel to the (001) surface growth as saturation decreased, finally followed by surface thickening by spiral growth on the (001) face as a final event. The experimental system reached some sort of equilibrium as there was finite plate thickening. By analogy to the experimental work (Cho and Fawcett, 1986), it seems that authigenic chlorite can easily and indiscriminately nucleate on all available surfaces at the initial stage when the system is most supersaturated with chlorite. This must be followed, as the saturation state falls, by the growth, out into the open pore, of very thin (001) sheets of chlorite that extend to a maximum of 10  $\mu\text{m}$ ; this may be followed a thickening process as a final stage, but the authigenic chlorite crystals do not get any longer or wider (Figs. 26 and 27).

### Is Fe-chlorite better at preserving porosity than Mg-chlorite

The compositional difference between continental (Mg-rich) and estuarine (Fe-rich) chlorite, illustrated in Figure 10, may influence the location of chlorite within the pore network and thus the effect on the diagenetic and petrophysical response of the rock. Fe-dominated, authigenic chlorite seems to occur as highly regular crystals that preferentially coat grains, while Mg-dominated chlorite occurs as less regular (Cornflake-like" crystals), that may partially coat grains, but which also occur as pore-filling clusters (Hillier, 1994; Worden and Morad, 2003). However, according to data compiled by Dowe et al. (2012), there is no simple relationship between the Fe-Mg composition of chlorite and its effect on reservoir quality. Although, it is true that most porosity-preserving chlorite is found in marginal marine (estuarine and deltaic) settings and these environments generally have the most Fe-rich chlorite (Fig. 10A), but this does not prove that Fe-rich chlorite is better at inhibiting quartz cement than Mg-rich chlorite.

### What if there are gaps or breaks in a chlorite coat?

Even a small break or gap in a chlorite coat can allow quartz cement to grow. There are many published examples of quartz cement growing through a gap in the chlorite and spreading over the chlorite coat (Berger et al., 2009; Sun et al., 2014; Worden and Morad, 2003). Algorithms that predict quartz cement growth as a function of thermal history, grain size, and detrital mineralogy and the degrees of grain coat coverage (Walderhaug, 1994a; Walderhaug, 1994b; Walderhaug et al., 2000), reveal the theoretical impact of different degrees of chlorite coat coverage (Fig. 28). Even a 20 % gap in the grain coat cover by chlorite (i.e., 80 % coverage) can lead to a large loss of porosity compared to the 100% coverage case.

## Bad chlorite: what happens if chlorite coats are very thick or there is pore-filling chlorite

Some chlorite coats are vanishingly thin, on the scale of a few micrometres (Chen et al., 2011; Churchill et al., 2017; Skarpeid et al., 2017) and yet manage to inhibit quartz cement growth. Other chlorite coats are relatively thick, on the scale of 10  $\mu\text{m}$ , and these too inhibit quartz cement (Bloch et al., 2002). This suggests that the thickness of the chlorite coat is not especially important for the inhibition of quartz growth.

Bloch et al. (2002) suggested that as little as 1 to 2 volume % clay coat (bulk rock volume) can coat a relatively large surface area of sandstone grains. The most favourable amount of chlorite to preserve porosity was reported to be 4 to 7 volume % for the Berea Sandstone and 5 to 13 volume % for the Tuscaloosa Sandstone (Pittman et al., 1992). Dutton et al. (2018) showed that more than about 8% chlorite led to 75 % grain coat coverage in fluvial and estuarine Tuscaloosa Formation sandstones. The volume of chlorite needed to coat all sand grain surfaces partly depends on the grain size of the sandstone since specific surface area is inversely proportional to grain size in sandstones (Rabbani and Jamshidi, 2014); finer grained sandstones will need a greater volume of chlorite to coat all surfaces since there is a greater surface area. Furthermore, poorly sorted sediment will have a lower primary-depositional porosity and will therefore be more susceptible to pore-filling chlorite.

Some sandstones have very thick authigenic chlorite coats, locally sitting on top of detrital clay coats, that tend to block pore throats (Table 1). This explains the optimum ranges provided by Bloch et al. (2002) and Pittman et al. (1992). If chlorite coats become too thick, or if they develop on top a pre-existing detrital clay coat, they will merge from either side of a pore and block the pore throat. Some chlorite cemented sandstones have so much chlorite that the permeability is in the nano Darcy range making the chlorite-bearing rock a profound barrier (thus working as a baffle or barrier to flow instead of working as a reservoir) to fluid flow instead of allowing the rock to be a good quality reservoir (Armitage et al., 2013; Armitage et al., 2011; Armitage et al., 2010).

The components for pore-filling chlorite might originate as ductile rock fragments (Galloway, 1979; Thomson, 1979), deformed and partly recrystallised Fe-ooids (Bloch et al., 2002) or excess fine-grained sand entrained into the sand due to soft-sediment deformation, bioturbation or even infiltration. Pore-filling chlorite is detrimental to reservoir quality since it serves to occupy pores (reducing porosity, Fig. 25) and blocks pore throats (reducing permeability) (Cao et al., 2018; Ma et al., 2017) (Fig. 1). Measuring the bulk quantity of chlorite in a sandstone, for example using XRD or bulk spectroscopic methods, is not a helpful way to predict reservoir quality since the location of chlorite in the pore network is paramount. Grain-coating chlorite in sandstones buried to depths hotter than about 80 to 100°C will inhibit quartz cement and preserve porosity, pore-filling chlorite will do nothing but damage porosity and permeability at all depth of burial. Point counting, or some sort of automated spatially-resolved SEM-EDS approach, is essential to understand the impact of chlorite on sandstone reservoir quality.

## Ugly chlorite: the effects of grain replacive chlorite

Grain replacive chlorite (Fig. 4) develops when a detrital Fe-Mg-Al-bearing mineral, or rock fragment, undergoes authigenic replacement by chlorite. For this to happen, it is imperative that the pore fluids do not contain excess  $\text{H}_2\text{S}$  as pyrite (Worden et al., 2003) would preferentially develop instead of chlorite. Similarly, the pore fluids must not contain too much  $\text{CO}_2$  as siderite or ferroan dolomite would result instead of chlorite. Rock fragments, and pore-filling mineral assemblages, that contain replacive chlorite and pyrite, or replacive chlorite and Fe-carbonate (or all three) represent a dynamic equilibrium controlled by the evolving pore fluid chemistry. Grain replacive chlorite therefore requires a specific type of provenance and a specific range of pore fluid compositions.

Grain replacive chlorite is incapable of inhibiting quartz cementation and has therefore received relatively little attention. Chlorite-rich rock fragments are at risk of being mechanically weak and undergoing ductile compaction, creating microporous pseudo-matrix and so leading to low permeability sandstones (Worden et al., 2000). Grain-replacive chlorite is also of importance to those undertaking XRD quantification of chlorite in sandstones because it cannot be discriminated from grain-coating chlorite using bulk techniques.

Primary Fe ooids represent concentration of chlorite in sandstones. Although they probably supply much of the Fe-clay to allow chlorite coats to develop during burial and mesodiagenesis, they represent ductile, pore-filling chlorite that will resemble pseudo-matrix at advanced stages of burial. Where present in large quantities, Fe ooids locally do not help reservoir quality in sandstones (Figs. 4 and 5).

## **Effects of chlorite on log responses**

Different petrographic and petrophysical types of chlorite are schematically illustrated in Figure 29, which has been modified from a general diagram about clay minerals in sandstones from Shedid and Saad (2017) and made specifically relevant to chlorite. Each sedimentary/petrographic type of chlorite will have different petrophysical and geomechanical effects on the overall clastic rock. Laminar and structural chlorite are primary depositional features controlled by a combination of hinterland-controlled sediment supply and hydrodynamic conditions during deposition. Dispersed chlorite could be due to either addition of clay minerals soon after deposition (e.g. via infiltration or bioturbation) or be due to diagenetic alteration of pre-existing minerals (Fig. 24). Grain coating chlorite could be either detrital or authigenic (Table 1).

Laminar chlorite will lead to very low vertical permeability values and will lead to clastic rocks susceptible to mechanical compaction. Structural chlorite (i.e. sand grains rich in chlorite such as volcanic rock fragments and Fe-ooids) will result in ductile deformation, loss of porosity and creation of pseudo-matrix during burial and compaction. Dispersed chlorite, i.e. that which fills pore space and occurs as patches, will at best occupy pore space and at worst block pore-throats and so is detrimental to reservoir quality. The only type of chlorite that is good for reservoir quality is grain coating chlorite as it inhibits quartz cement (Table 8, Fig. 29); clean sandstone will be susceptible to quartz cementation and progressive porosity-loss in deeply buried sandstones. The presence of chlorite is of great interest during the wireline and petrophysical investigation and characterisation of sandstones; however, as shown by Figures 4 to 8 and 28, it is not simply the presence of chlorite that is important; to be beneficial to reservoir quality, the right textural type of chlorite needs to be present (and see Tables 1 and 8).

## **Modelled effects of different amounts of chlorite on wireline logs**

Wireline logs represent the most common sources of information about subsurface reservoirs since they are routinely run either during or after drilling whereas core is expensive to collect and is relatively rare (Rider and Kennedy, 2011). Given the importance of grain coating chlorite for reservoir quality in many deeply buried sandstone reservoirs (Table 8), it is therefore imperative to understand the type of wireline responses produced by chlorite-bearing sandstones. A suite of wireline logs from some variably chlorite cemented sandstones from Jurassic sandstones from the North Sea are presented in Figure 30, along with core porosity values for comparison. Chlorite in sandstones has been reported to result in low-resistivity pay, i.e., oil-bearing sandstone that has anomalously low electric resistivity despite the emplacement of non-conductive oil at the expense of conductive formation water (Worthington, 2000).

Some theoretical, end-member core (porosity, permeability, grain density) and log (gamma, sonic, density, neutron, resistivity) characteristics of variably chlorite cemented sandstones compared to



variably quartz cemented quartz arenites and illite-, calcite- and dolomite-cemented sandstones (for comparison) are presented in Table 9. The proportions of different minerals in these simple end-member rock types are defined in the second column of Table 9.

Typical porosity and permeability values for these types of sandstones have been taken from Primmer et al. (1997). Flow Zone Indicator (FZI), listed in Table 9, is a petrophysically-defined measure of the connectedness of pores and has been used to define “reservoir quality facies” (Tiab and Donaldson, 2015). FZI is defined as  $(0.0314 \cdot (k/\phi)^{0.5}) / (\phi / (1 - \phi))$  where  $k$  is horizontal permeability and  $\phi$  is fractional porosity.

Solid (i.e. mineral) grain density values, data that are produced during routine core analysis, have been derived for each sandstone-type based on the stated mineral proportions in column 2 and typical end-member mineral density values reported in Table 10 (Peters, 2012; Rider and Kennedy, 2011; Tiab and Donaldson, 2015; Zinszner and Pellerin, 2007). The bulk density of the sandstones (combined signal from the grains and the pores, RHOB), as derived using wireline logging of boreholes, has been calculated based on the derived solid grain density (Table 10) and the assumed porosity ( $RHOB = \text{grain density} - (\phi * (\text{grain density} - 1))$ ), where 1 represents the density of the drilling fluid in the invaded zone of the borehole and  $\phi$  is the fractional porosity.

Matrix (i.e. mineral) compressional sonic values have been derived for each sandstone-type based on the stated mineral proportions in column 2 and end-member mineral compressional sonic values reported in Table 10. The theoretical wireline-logged compressional sonic values (DTC) of the sandstones has been calculated based on the derived bulk mineral compressional sonic values (Table 10) and the assumed porosity ( $DTC = \text{matrix compressional sonic} - (\phi * (\text{matrix compressional sonic} - 200))$ ), where 200  $\mu\text{s}/\text{ft}$  represents the compressional sonic of the drilling fluid in the invaded zone of the borehole and  $\phi$  is the fractional porosity (Rider and Kennedy, 2011).

Matrix (i.e. mineral) neutron values have been derived for each sandstone-type based on the stated mineral proportions in column 2 and end-member mineral neutron values reported in Table 10. The wireline-logged neutron values (NPHI) of the sandstones has been calculated based on the derived bulk mineral neutron values (Table 10) and the assumed porosity ( $NPHI = \text{matrix neutron} - (\phi * (\text{matrix neutron} - 1))$ ), where 1 represents the neutron response of the drilling fluid in the invaded zone of the borehole and  $\phi$  is the fractional porosity (Rider and Kennedy, 2011).

The theoretical logged deep resistivity (RD) of the various rock types has been derived based on a rearranged Archie equation ( $RD = (a \cdot R_w) / (S_w^n \cdot \phi^m)$ ) (Rider and Kennedy, 2011), using the specific porosity ( $\phi$ ) for each sandstone type, assumed (constant) fluid resistivity ( $R_w$ , here assumed to be 0.02 ohm.m) and water saturations ( $S_w$ , see Table 9), and typical “a”, “m” and “n” Archie constants. In practice, a more sophisticated approach can be adopted to derive water saturation in low resistivity chlorite-bearing sandstones (Tudge et al., 2014).

The theoretical effects of different amounts of chlorite and other diagenetic minerals are listed in Table 9 and are presented in Figure 31.

### Specific effects of different amounts of chlorite on wireline logs

Log and core data from chlorite-coated sandstones from a Jurassic reservoir from the North Sea Basin are shown in Figure 32.

Chlorite is a high-density mineral (Table 10) so that chlorite-enriched sandstones may have a slightly higher bulk density than chlorite-free sandstones (Fig. 32A) since the matrix density will be higher.

However, since as little as 3 or 4 % chlorite can coat all sand grain surfaces (see previous), this may not show up significantly on a suite of log responses. The additional porosity that results from the prevention of quartz cement growth would lead to a low bulk density and this difference may swamp the signal from the additional grain density. Chlorite-coated sandstones will have a low bulk density, but it might not be obvious from this log alone as to the cause of the elevated porosity.

The compressional sonic response of chlorite is not especially well defined but can be assumed, like other clay minerals, to be slightly higher than framework minerals such as quartz (Table 10) (Rider and Kennedy, 2011). Chlorite-cemented sandstones therefore may have a slightly higher sonic response (in terms of  $\mu\text{s}/\text{ft}$ ) than chlorite-free sandstone (Fig. 32B). However, as with the density log, the additional porosity that results from the prevention of quartz cement growth would lead to a high overall sonic response and this difference may swamp the chlorite-specific effect on the sonic log. Chlorite-coated sandstones will have a high sonic response but, as with the density log, it might not be obvious from the sonic log alone what has caused the elevated porosity.

In theory, chlorite has no effect on a gamma ray log since chlorite does not contain any potassium and cannot contain thorium or uranium in its crystal lattice (Table 10). Gamma ray logs are thus not useful for studying chlorite except that they are notable in giving a distinct neutron signal but no gamma signal, unlike illite-dominated clay suites that give both neutron and gamma responses.

Neutron logs respond to the amount of hydrogen in a given volume of sediment (Rider and Kennedy, 2011). Hydrogen is generally present in pore-filling fluids in the invaded, near-wellbore region (i.e., water, oil) and in hydroxyls within clay minerals. Chlorite has a marked neutron response because it contains lot of hydrogen atoms per unit cell (Table 10, Fig. 2). Chlorite contain eight hydrogen atoms for every 20 oxygen atoms whereas illite contains only two hydrogen atoms for every 20 oxygen atoms. While the additional porosity that results from the inhibition of quartz cement will lead to a marked neutron response, having chlorite present will lead to an unusually high neutron response due to the additional hydrogen in the chlorite (Fig. 32C). Rocks with 10's of % of chlorite are quite distinct as they have low gamma but high neutron responses.

Chlorite in oil-bearing sandstones has a distinct character on resistivity logs because it leads to rocks that have unusually high residual (irreducible) water saturation (Fig. 32D) even at the crests of oil fields. This is not the result of the high quantity of hydroxyl molecules in chlorite (Henn et al., 2007). The low resistivity is the result of the microporous nature of grain-coating, and pore-filling, chlorite (Figs. 4-8) that allows water to remain trapped within the clay network, even after oil-filling (Durand et al., 2001; Pratama et al., 2017; Tudge et al., 2014). Chlorite-cemented sandstones routinely have up to 30 to 40 % water saturation ( $S_w$ ) compared to interbedded chlorite-free sandstones that will typically have 5 to 10 % water saturation. The main consequence of this elevated water content is very low resistivity deep within the uninvaded zone of the borehole. Another consequence is a lower volume of recoverable hydrocarbon resource. Chloritic sandstones are known as low resistivity pay.

The bulk density, compressional sonic, neutron and resistivity log data from the variably chlorite-cemented sandstones in Figure 30 have been compared to core analysis porosity in Figure 32, which is analogous to the theoretical data displayed in Figure 31 and Table 9. The sections that contain chlorite are indicated by dashed outlines. It can be seen that chlorite cemented sandstones are especially visible on the resistivity plot, but also on the neutron plot and even the bulk density plot.

### **Overview on log-recognition of chlorite-coated oil-field sandstones**

Based on Table 9 and Figures 31 and 32, low resistivity and relatively high neutron responses characterise chlorite-coated sandstones with inhibited quartz cement growth (and commensurately high porosity for

the depth of burial). Compressional sonic and bulk density logs are not necessarily distinct in sandstones with a few percent chlorite since they have high sonic and low bulk density values that are characteristic of any high porosity sandstone.

## **Synthesis: prediction and modelling of chlorite**

The ability to predict the presence of grain-coating chlorite, and any other reservoir quality-influencing authigenic mineral, would lead to better informed decisions during oil and gas exploration and field appraisal and development. As with many areas of geoscience, there are many variables and assumptions need to be made to facilitate chlorite prediction.

It is first important to understand whether the authigenic mineral growth is the result of the import of materials in an open geochemical system at the bed-scale. If chlorite is the result of open system diagenesis then the net flux of material needs to be understood and modelled. This is no easy matter given the vast lengths of time involved and the complexity of needing to know the mineralogy, water composition and transport properties of all relevant formations within a basin (Brosse et al., 2003; Giles et al., 2000; Sanjuan et al., 2003). There is good evidence that Fe-chlorite at least is probably the result of closed-system diagenesis at the bed scale; the volumes of water that would be needed to import the required amounts of Fe given typical aqueous iron concentrations are improbably huge (Fig. 10, Table 3), the typical growth pattern of chlorite must be the result of the bed-scale water-rock system being massively supersaturated with respect to chlorite due to the presence of unstable Fe-clay minerals or mineralogically unstable lithic fragments containing all the ingredients to create chlorite (Fig. 26). Extreme supersaturation cannot be the result of the geologically slow influx of components; it must be due to the components being present within the system but chlorite being unable to grow due to a large activation barrier inhibiting nucleation (Fig. 26-A2). On this evidence, we can assume that grain-coating chlorite growth probably results from a closed, or isochemical, system at the bed-scale.

Chlorite, being an Fe-rich mineral, requires an Fe-rich sediment supply (Figs. 13, 14, 15). There needs to be an understanding or knowledge of sedimentary provenance and mineralogy to make predictions of chlorite presence in sandstones. Even more important is that any iron, that is required to create chlorite, is not first locked up as either siderite or pyrite at the expense of Fe-clay minerals. Siderite grows in pore waters that are rich in dissolved bicarbonate; elevated bicarbonate is a characteristic of organic-rich sedimentary environments. Pyrite grows in pore waters rich in dissolved reduced sulphur (aqueous sulphide); elevated sulphide is a characteristic of marine pore waters when aqueous sulphate is bacterially reduced to sulphide (Fig. 16). Leaving the deposited iron available to produce chlorite requires specific sedimentary geochemical conditions during and soon after deposition (Fig. 17); an understanding of the environment of deposition of any sediment (Fig. 19), and the geochemical conditions in that sediment is needed to make predictions about the presence of chlorite in sandstones.

Numerous geochemical processes have been cited as leading to the growth of authigenic chlorite, over a range of temperatures (Fig. 24). Fe-ooids (Figs. 5, 6, 7), commonly associated with deltaic and estuarine chlorite-coated sandstones (Fig. 19), originate in transient clay rich deposits in, and around, the final site of sediment deposition. Fe-ooids initially contain low temperature Fe-clay minerals that become metastable as the sediment is buried and heated and so need to transform into chlorite to become more stable. Having Fe-ooids present in a sandstone will greatly encourage the growth of grain coating chlorite as they introduce the correct mineral chemistry in the form of grains, but these grains need to dissolve and recrystallise as chlorite during burial and heating. This process is energetically difficult due to the high activation barrier resulting from the complex crystal structure of chlorite; once the energy barrier has been overcome, spontaneous nucleation occurs on all surfaces, followed by slower growth of small plates, perpendicular to grain surfaces, into the open pore (Fig. 26). The presence of laminae of low

temperature Fe-rich clay within a sandstone could plausibly have the same effect as Fe-ooids (Fig. 29) but these seem to be seldom recorded in sandstones. Being able to predict the presence of Fe-ooids within a sedimentary system would be great step forward in making predictions about chlorite presence within a sandstone. This approach requires a good knowledge of sedimentary sub-environments and how sediment supply has interacted with evolving sea level (Figs. 20, 21, 22, 23).

Volcanic rock fragments are also a way of introducing the appropriate Fe-rich chemistry in an unstable mineral form into sandstones; this has been suggested to be a common source of chlorite in some deeper marine sandstones (Figs. 19, 24) (Anjos et al., 2003; Bonnell et al., 2014; Grigsby, 2001). Prediction of this source of chlorite requires a detailed understanding of sediment provenance and mineral and grain fractionation during transport (Griffiths et al., 2019b). Identical issues for chlorite prediction arise if Fe-rich heavy minerals such as ilmenite (Fig. 24) are considered to be source of the key ingredient in chlorite (Gould et al., 2010).

Detrital clay coats are common in marginal marine sedimentary systems; these introduce clay minerals in otherwise sand-rich systems (Figs. 7, 18). If the detrital clay is Fe-clay-bearing, then this may result of chlorite grain coats. This takes us to the questions of how detrital grain coats develop, overall sediment provenance and how iron is introduced into coarse-grained sediments (Figs. 11, 17, 18, 19). Grain coats in marginal marine sediments have been shown to result from biofilms that derive from the normal life activities of diatoms (Wooldridge et al., 2017a); diatoms are heterogeneously distributed within sediment environments (Figs. 18, 23) so that understanding the exact sub-environment of deposition is important to facilitate prediction of detrital grain coats.

The role of temperature in chlorite growth is subject to some uncertainty (Fig. 24) but, for chlorite to inhibit quartz cement growth, the sandstone must develop authigenic chlorite coats before quartz growth starts (Fig. 28). The important chlorite-producing reactions in sandstones (from berthierine, volcanic rock fragments and Fe-heavy minerals such as ilmenite) all seem to occur at about 60 to 70°C which is well below the commonly accepted threshold of 80°C for quartz cementation (Lander et al., 2008; Walderhaug, 1990; Walderhaug, 1994b; Walderhaug et al., 2000). On this basis, the growth of grain-coating chlorite during burial can be assumed to occur at temperatures lower than quartz cement potentially making redundant the use of thermal modelling for chlorite prediction. If the correct geochemical ingredients are present and in available form in a sandstone and if the rock has had enough thermal stress to grow quartz cement, then it has had enough time to grow chlorite.

Prediction of chlorite based on wireline log analysis, the most common way that sandstones are characterised, requires a careful and subtle examination of the full suite of logs (Figs. 30 to 32). Revealing the presence of chlorite may be undertaken on a log-by-log basis but integrated approaches using modern data analytical tools. This log-based prediction only reveals what is in the formation directly adjacent to the borehole, but it still is likely to be the first step in making field-wide predictions at the discovery scale and during appraisal and field development when more wells are drilled. Assessment of grain coating chlorite from wireline logs, linked to a detailed assessment of specific sedimentary sub-environments of deposition, offers great potential for chlorite prediction at the field scale.

## Conclusions

1. Chlorite is a 14Å aluminosilicate clay mineral that contains abundant Mg and Fe as well as Al and Si. It is compositionally like low temperature 7Å Fe-clay berthierine, but has a more complex crystal structure. Chlorite has a vast range of compositions; mainly variable Fe/(Fe+Mg) values in octahedral sites, Fe+Mg substitutions for Al on octahedral sites and Al-substitutions for Si on the tetrahedral sites.

2. Chlorite can be detrital, originating as single mineral grain, as a component in lithic fragments, as part of fine-grained matrix or as part of a detrital grain coat. Chlorite can be derived from lithic grains such as volcanic rock fragments or Fe-oxides that were created in, or near, the environment of deposition.
3. Chlorite can also be authigenic, occurring as a grain-coating, pore-filling or grain replacing mineral.
4. Only grain-coating chlorite is good for reservoir quality since it stops quartz cement growth on detrital quartz grain surfaces. Chlorite grain coats inhibit the normal porosity-loss process of quartz cementation that occurs at temperatures > 80 to 100°C since the chlorite coat physically isolates the surface of quartz grains from the formation water required to allow quartz to grow.
5. Clay minerals in sandstones, in the form of grain-coating chlorite, can therefore be good for reservoir quality in deeply-buried, higher temperature (> 80 to 100°C) sandstones.
6. Roughly 3 to 10 % grain-coating chlorite is needed to fully coat quartz grains depending on sandstone grain size, sorting, and chlorite coat thickness. Thicker coats are not necessarily better but gaps or breaks in chlorite coats allow quartz to grow, albeit at a slower rate than if no chlorite coats were present.
7. Pore-filling chlorite and chlorite-rich lithic grains reduce porosity and permeability and are bad for reservoir quality. The precise location of chlorite in a pore-network is therefore paramount for its effect on rock properties.
8. Coats of clay on detrital grains form in modern, marginal marine (deltaic-estuarine) sedimentary environments due to biological processes. Remnant detrital grain coats can be observed underlying authigenic chlorite coats deep in sedimentary basins.
9. Chlorite in continental sandstones tends to be Mg-rich, chlorite in marginal marine sandstones is Fe-rich, suggesting different suites of reactions are responsible in sandstones deposited in different sedimentary environments.
10. The local enrichment of iron in estuarine and deltaic sediment compared to open marine sediments may be the result of flocculation of fluvial Fe oxide-humic complexes where rivers meet the sea, or hydrodynamic concentration of Fe-rich sand grains at the heads of estuaries.
11. The process that lead to the concentration of sedimentary iron and the greatest likelihood of grain coats occur preferentially in the marginal marine setting of estuaries and deltas. Thus deeply buried estuarine and deltaic sandstones, deep in sedimentary basins, are more likely to be chlorite coated and have inhibited rates of quartz cementation than sandstones from other depositional environments.
12. The supply of sediment into a sedimentary environment needs to be moderately iron rich to allow authigenic chlorite-precursor minerals to accumulate.
13. Chlorite has many possible origins in sandstones, but the most important ones seem to be: early diagenetic berthierine (Fe-clay), smectite (especially for Mg-rich chlorite), and kaolinite reacting with a source of Fe, for example from Fe-carbonate, Fe-rich lithic grains, and Fe-bearing heavy minerals at elevated temperatures (> 120°C).
14. Fe-chlorite components (Fe, Al, Si) are probably broadly isochemical (closed system) at the bed scale, what was deposited gets transformed into new minerals. This is evidenced by the unreasonably large volumes of water required to import aqueous iron into sandstones and the presence of grain-coating morphology which must be the result of a closed system at extreme degrees of chlorite supersaturation.
15. In contrast, magnesium is part of open systems as proved by large scale dolomitization, so that the magnesium in Mg-rich chlorite may be part of a more open diagenetic system at the bed-scale, i.e. related to large scale water flux.
16. Chlorite tends to develop as authigenic coats, on all sand grains, at about 60 to 90°C and is typically absent from grain-grain contacts suggesting that any detrital grain coats at grain-to-grain contacts were removed by stress-related enhanced dissolution.

17. Wireline logs from sandstones contain distinct signals of the presence of chlorite since this mineral has high neutron, low gamma, high density and high sonic log responses, plus it leads to high residual water saturation and thus results in anomalously low resistivity in oil-filled sandstones that would otherwise have high resistivity.

## Figure captions

Figure 1. Schematic porosity-permeability diagram of samples from the same formation, depth and temperature histories illustrating the effects of different types of chlorite diagenesis: grain-coating chlorite, pore-filling chlorite, lack of chlorite leading to quartz cement.

Figure 2. Crystal structure of chlorite, after McMurchy (1934), and end-member XRD traces for Fe-rich and Mg-rich chlorite, modified from Hillier (2003).

Figure 3. Chemical types of chlorite based on the definition of Hey (1954).

Figure 4. SEM-EDS images of chlorite-coated sandstones. Image from chlorite-rich Lower Jurassic sandstones from the North Sea Basin. (A) Low resolution SEM-EDS image using the colour scheme shown to the right. (B) High resolution enlargement of part of (A). These SEM-EDS images reveal three morphological and compositional types of chlorite: relatively Fe-depleted chlorite that has replaced detrital biotite grain, relatively Fe-enriched chlorite that forms grain coats, and relatively Fe-enriched chlorite that forms irregular pore-filling patches (pseudo-matrix). Chlorite coats both quartz and detrital feldspar grains. The black arrows reveal that the chlorite grain coat lies on a “root” layer of another clay mineral suggesting that the development of the burial diagenetic Fe-rich chlorite coat was facilitated by a non-chlorite grain coat, formed earlier, possibly in the sedimentary depositional environment.

Figure 5. SEM-EDS image of Fe-oid-bearing sandstone from chlorite-rich Jurassic sandstones from the > 4,000m depth TDV ss (> 145°C) in the North Sea Basin, using the colour scheme shown in Figure 5. A largely intact, although deformed, Fe-oid is present in the lower left of the image; the original concentric layers of chlorite (green) and illite (browns and grey) are still visible although now delaminated and with secondary porosity now present in the Fe-oid. The more chaotic remnants of another deformed Fe-oid are present in the middle right of the image with hints of the original chlorite-illite layering visible although the outer margins are hard to differentiate from pore-filling chlorite-dominated clay, that could also be classified as pseudo-matrix. All grain surfaces have a chlorite coat and quartz cement is absent despite the thermal stress that this sample has experienced. A secondary pore after dissolution of a rock fragment is present in the upper left that is only visible due to the preservation of the pre-dissolution chlorite grain coat.

Figure 6. Light optical images of (A) Fe-oid with a quartz core and (B) chlorite-coated sandstone, Lower Jurassic Norwegian North Sea samples from ~4000 m TVD ss. This sample is at about 145°C and would typically be highly cemented with quartz if the chlorite grain coat was absent. Grain-coating chlorite has a green colour and a diffuse outline in light optical images.

Figure 7. BSEM images of chlorite coated sandstone, Lower Jurassic Norwegian North Sea samples from ~4400 m TVD ss. (A) Low resolution image showing Fe-oids, open pores, and minimal quartz cement due to the presence of chlorite grain coats. (B) Higher resolution image of the inner part of detrital chlorite-rich coat with a chaotic structure. There is also a more ordered authigenic coat made of bladed crystals set perpendicular to the host grain and growing out, or on top, of the detrital coat. There is a chlorite silt grain entrained within the detrital chlorite coat suggesting a mechanism for the delivery of chlorite into this sedimentary environment. (C) Enlarged part of the Fe-oid from part A showing the microporous

nature of the Fe-oid, likely due to dissolution of this type of detrital chlorite and probably resulting in the creation of authigenic chlorite coats.

Figure 8. Medium resolution SEI images of chlorite cemented sandstone, Lower Jurassic Norwegian North Sea, samples from ~4000 m TVD ss. (A) The chlorite grain coat is absent from grain-grain contacts suggesting that any detrital clay may have undergone effective stress-induced dissolution and diffusion of the components to low stress regions facing open pores. The chlorite coat is uniformly thin but complete in this sample. (B) Higher resolution image revealing details of the perpendicular chlorite crystals, apparently with random orientation of the C-axes on the grain surface.

Figure 9. Histogram showing the range of Fe/(Fe+Mg) values found in authigenic chlorite in sandstones with the sources of compositional data taken from sources listed in Table 2. Chlorite can have a wide range of Fe/(Fe+Mg) values with modes at Fe<sub>30</sub>Mg<sub>70</sub>, Fe<sub>50</sub>Mg<sub>50</sub>, Fe<sub>65</sub>Mg<sub>35</sub>, and Fe<sub>75</sub>Mg<sub>25</sub>. Chlorite grain coats are not universally enriched in iron.

Figure 10. Variation of chlorite and berthierine composition as a function of environment of deposition of sandstone with compositional data taken from sources listed in Table 2. Same colour scheme as Figure 9. The term n represents the count total for each category, med represents the median value. (A and B) Chlorite is increasingly Fe-enriched going from continental (aeolian, fluvial) through to deltaic and estuarine conditions. Estuarine chlorite has the highest Fe/(Fe+Mg) ratio which is remarkably similar to the berthierine Fe/(Fe+Mg) values. Turbidite sandstones have variably but low Fe/(Fe+Mg) values suggesting that they are not related to estuarine or coastal processes. (C and D) Chlorite and berthierine seem to have highly variable tetrahedral Al concentrations that bear no relationship to environment of deposition (Dowey et al., 2012). (E and F) Chlorite displays decreasing octahedral Al going from continental to shallow marine-estuarine environments of deposition. Berthierine has variable octahedral Al and shows no relationship to estuarine chlorite.

Figure 11. Co-variation of total Si and the Fe/(Fe+Mg) index for chlorite, based on the diagram of Hey (1954), with data taken from sources listed in Table 2. Same colour scheme as Figures 9 and 10. Chlorite and berthierine in sandstones display a wide range of compositions; diabanite, brunsvigite, ripidolite, chamosite and thuringite being common; true clinocllore apparently not present in any sedimentary environment. Estuarine samples having the highest Fe/(Fe+Mg) and relatively high Si concentrations per unit cell. Chlorite is most commonly found in deltaic and estuarine sedimentary environments, suggesting that an elevated supply or availability of Fe is paramount for the growth of this mineral in sandstones.

Figure 12. Compilation of published formation water compositions from UK oil and gas fields (Warren and Smalley, 1994; Worden et al., 2006a). The term n represents the count total for each category, m represents the median value. (A) Magnesium concentrations in mol/L. (B) Iron concentrations in mol/L. (C) Log ratio of magnesium to iron concentrations. Many published reports of formation water do not contain the concentrations of iron and have therefore not been included here. The data have been subdivided into different stratigraphic intervals (Devonian to Eocene) and represented by box and whisker diagrams. There are no available iron concentration data from Upper Triassic, Lower Jurassic and Eocene reservoirs. The number of data points (n) and the median (m) for each category is presented. The magnesium concentrations are always much higher than the iron concentrations. These data have been used in the mass balance calculations used to show how many pore volumes of water would be needed for non-isochemical reaction of aluminosilicate minerals into chlorite (Table 3).

Figure 13. Fe-variation in estuaries as a function of salinity, data from Boyle et al. (1977). Sea water contains approximately 0.0003 µm/L dissolved iron (Liu and Millero, 2002) so that the elevated iron concentrations typical of river waters are not found in the marine setting. The plot shows that the

concentration of aqueous iron diminishes with increasing salinity in estuarine settings (and replicated in deltaic environments). This is caused by destabilisation of the dominant form of dissolved iron (iron-organic complexes) in increasingly saline water; flocculation of iron happens as a consequence. These flocs settle out from suspension during periods of slack water and enter the sediment realm. The significance of this process is that fluvially transported “dissolved” iron gets preferentially trapped in the sediment column within the zone where river water mixes with seawater.

Figure 14. Compositions of possible sand-hinterland rocks (and their metamorphic equivalents). Rock compositional data based on Hill et al. (2000), Parker (1967) and Krauskopf (1979) (Table 5). Basic igneous rocks and their weathered equivalents have the highest Fe concentrations. Andesitic rocks are intermediate between basalt and granite.

Figure 15. Theoretical compositions of sandstones with specific mineralogy including low and high concentration chlorite-bearing sandstones, siderite-bearing sandstones, mixed chlorite and siderite sandstones and biotite-ilmenite-pyrite bearing rocks (Table 6). Compositions are based on end-member mineral compositions, taken from Deer et al. (2013b). Rocks with the best concentration of chlorite for reservoir quality (roughly 5-10%) have relatively limited compositions but note that the effect of carbonate and sulphide are not represented in these diagrams. Chlorite cemented sandstones do not have unique compositions; similar bulk compositions could also result in siderite- or pyrite-bearing sandstones.

Figure 16. Redox and bioturbation in estuarine, deltaic and coastal sediments. (A) Relatively shallow redox boundary (~10 cm) in clean sand (finger for scale). The oxidised sand is pale, the reduced sand, where bacterial sulphate reduction has occurred, is dark due to the growth of Fe-sulphide. Penetrating burrows by *Arenicola marina* (the common lugworm) have brought oxidised waters 30-40 cm into the surface during the lugworm's normal irrigation activities; the result is a re-oxidation of the sulphidic sand, showing that some redox processes are rapid and reversible. (B) Early stage burrowing by a lugworm into mixed sand and clay showing that primary bedding is disturbed (aka bioturbation); cm-scale shown. (C) Late stage bioturbation showing that normal life activities of burrowing animals mixes together hydrodynamically-separated sand and clay-grade materials thus allowing the fine-grained result of Fe-flocculation to be mixed in to clean, previously Fe-mineral-free sand (same scale as B) (McIlroy et al., 2003; Needham et al., 2006; Needham et al., 2004; Needham et al., 2005; Worden et al., 2006b).

Figure 17. Schematic diagrams adapted from the late transgressive stage block diagram of Fe-clay accumulation, modified from Saiag et al. (2016). (A) fluvial, alluvial, sand-bar, tidal flat and marine environments of deposition labelled. Fe-clay can only develop if there is enough iron supplied by the fluvial system (Tables 5 and 6). Flocculation of the dominant organically-complexed form of iron preferentially occurs at the head of the estuary during the initial interactions of low salinity river water with seawater (Fig. 13). Fe-rich allogenic (created in the environment of deposition) sand grains will tend to have higher density than normal quartz- or feldspar-rich sand grains and will be deposited at the head of the estuary rather than being preferentially swept through the system towards the open ocean. Fe-rich clay and any chlorite precursor minerals will tend to be concentrated in the proximal estuarine (bayhead delta) sediments. (B) Fe-ooids are likely to be created in hypersaline, ephemeral lagoons as a result of Fe-rich sediment supply, and algal or bacterial processes, leading to the sequential growth of layers of Fe-oxides or clay minerals around the ooid core. Such conditions will lead to the creation of mechanically-weak autogenic (derived from hinterland) Fe-rich grains (that are ductile during burial but likely to be friable during sediment transport) that can be flushed into the estuary following flooding events. The mechanical weakness of these grains means they are unlikely to be able to withstand prolonged transport and will be deposited in near shore, proximal sand bars. (C) If the coastal plain is especially verdant, then it is likely that there will be elevated bacterial processes leading to elevated aqueous bicarbonate (effectively due to the collection of processes related to rotting and oxidation of organic matter). Elevated bicarbonate will lead to preferential growth of siderite, at the expense of Fe-clay minerals, whereby the flocculated Fe-oxides and hydroxides and Fe-rich lithic grains will react with  $\text{HCO}_3^-$  to create  $\text{FeCO}_3$ . (D) Reduced rates of sediment supply will lead to prolonged interaction of the



sediment with seawater. Sulphate from seawater is converted to aqueous sulphide during the dominant process of bacterial sulphate reduction. The aqueous sulphide will lead to preferential growth of Fe-sulphide minerals whereby the flocculated Fe-oxides and hydroxides and Fe-rich lithic grains will react with sulphide to create FeS at the expense of Fe-clay minerals.

Figure 18. Details of grain coats in modern estuarine sediments of the Ravenglass estuary in NW England (Wooldridge et al., 2017a; Wooldridge et al., 2017b; Wooldridge et al., 2018; Wooldridge et al., 2019a; Wooldridge et al., 2019b). Backscattered electron and environmental scanning electron microscope (SEM) images of clay-coated grains. Arrows indicate clay coatings. Dashed lines (parts C and D) outline the extent of the biofilm coats on the grain surface. (A) Thin section of clay-coated sand grains from an intertidal estuarine setting with abundant grain coat clay, including chlorite, present. (B) SEM image of loose sediment with abundant grain-coating detrital clay. (C) SEM image of loose sediment with the biofilm circled with a white dashed line, with clay and silt being adhered to grains only where the biofilm is present. (D) Environmental SEM image of hydrated sediment. Triangle in top right points to a diatom with excreted extracellular polymeric substance grain attachment outlined. The chaotic detrital clay coats found lying underneath authigenic grain coats in ancient and deeply-buried sandstones (e.g. Fig. 7B) has a precedent routinely found in estuarine sediments (Dowey et al., 2012; Dowey et al., 2017).

Figure 19. Qualitative evaluation of the likelihood of different chlorite-precursor incorporation processes happening in sand deposited in different clastic sedimentary environments. To simplify this diagram, a binary approach was taken although it is acknowledged that there are likely to be probabilities for each scenario that are hitherto ill-defined and thus impossible to quantify.

Figure 20. Depositional environments and distribution of total iron in the sediments of the Ravenglass Estuary, NW England. Bulk sediment chemical analyses were undertaken using portable XRF of dried sediment samples collected from nearly 500 sites across the estuary. Iron is preferentially concentrated in the upper reaches of the estuary confirming that fluvially-transported iron is trapped at the site of mixing between river water and seawater. Key to depositional environments: De1: Gravel bed, De2: Mud flat, De3: Mixed flat, De4: Sand flat, De5: Tidal bar/dunes, De6: Tidal inlet, De7: Backshore, De8: Foreshore, De9: Pro-ebb delta (Daneshvar and Worden, 2018; Griffiths et al., 2019a; Griffiths et al., 2018b; Griffiths et al., 2019c; Wooldridge et al., 2017a; Wooldridge et al., 2017b; Wooldridge et al., 2018; Wooldridge et al., 2019a; Wooldridge et al., 2019b; Worden et al., 2018b; Worden et al., 2018c).

Figure 21. Variation of the relative concentration detrital chlorite in the modern Ravenglass Estuary, NW England (Griffiths et al., 2019a; Griffiths et al., 2018b; Griffiths et al., 2019c). (A) Mapped distribution of >150 data points revealing the heterogenous distribution of chlorite in a modern sedimentary environment. (B) Variation of chlorite concentration as a function of grain size fraction revealing that, in this setting, chlorite is concentrated in the silt and fine sand fractions and is least abundant in the clay fraction. Hydrodynamic processes will thus lead to physical fraction of chlorite partly explaining the heterogenous distribution displayed in Figure 21A. (C) Relative concentration of chlorite (compared to the other clay minerals) as a function of sedimentary environment (De1: Gravel bed, De2: Mud flat, De3: Mixed flat, De4: Sand flat, De5: Tidal bar/dunes, De6: Tidal inlet, De7: Backshore, De8: Foreshore, De9: Pro-ebb delta) showing that chlorite is relatively concentrated in specific sediment sub-environments within the overall estuarine context. This suggests that all studies of chlorite-bearing core from reservoirs needs to have highly detailed interpretation of the specific sub-environment of deposition. It is not sufficient to simply classify a chloritic sandstone as being estuarine; sedimentologists need to define the specific part of the estuarine environment in which a sample was deposited.

Figure 22. Schematic summary of key primary sedimentary and diagenetic characteristics for end-member wave-dominated estuarine depositional environments (facies), as well as predicted reservoir quality for analogous ancient and deeply-buried estuarine sandstones (temperatures exceeding 80–100°C) based on data from the modern analogue for ancient, deeply-buried sandstones from the

Ravenglass Estuary, NW England (Griffiths et al., 2019a; Griffiths et al., 2018b; Griffiths et al., 2019c). The schematic stratigraphic cross-section was modified from Dalrymple et al. (1992). Chlorite is most likely to be present in quantities sufficient to coat grains, but not too much to destroy reservoir quality, within inshore, sandy tidal sub-environments such as tidal bars. In sandstones buried to temperatures > 80 to 100°C, there is a distinct risk of poorer reservoir quality in the cleaner shoreface sandstones, due quartz cementation, whereas the inshore sandstones may experience inhibited quartz cementation due to chlorite grain coats. This assumes that early diagenetic processes have not led to siderite or pyrite growth instead of allowing detrital Fe-minerals to generate authigenic chlorite.

Figure 23. Maps of clay-coated sand grain distribution and biomarker proxy for tidal flat biofilm abundance on sand grains in modern estuarine sediments of the Ravenglass estuary in NW England (Wooldridge et al., 2017a). (A) Clay-coat coverage of sand grains established from quantitative petrography. (B) Chlorophyll-a concentrations where chlorophyll is a biomarker that represents the net concentration of biofilm-creating diatoms in estuarine sedimentary environments. Darker shades in A and B represent greater extent of clay-coat coverage and greater abundance of sediment biofilm (chl-a is chlorophyll-a). Detrital clay coats are the result of biofilms rendering sand grains adhesive, with the biofilms being the result of the normal life activities of diatoms. Here it is not claimed that all detrital clay coats are due to biofilms from diatoms, it is possible that other organisms produce biofilms (McIlroy et al., 2003; Needham et al., 2006; Needham et al., 2004; Needham et al., 2005; Worden et al., 2006b) and that clay minerals adhere to sand grains by other mechanisms but the Ravenglass case study has demonstrated, for the first time, why and where clay coats (including detrital chlorite) are present in surface sediments.

Figure 24. Diagram showing the range of largely isochemical reactions that have been reported as being capable of producing authigenic chlorite in deeply-buried sandstones (>60 or 70°C) (modified from Worden and Morad, 2003). In theory, there are many ways of generating chlorite in sandstones including: siderite-kaolinite reaction (Curtis et al., 1985), ankerite-kaolinite (Muffler and White, 1969; Smith and Ehrenberg, 1989), ankerite-illite reaction (Smith and Ehrenberg, 1989), trioctahedral smectite breakdown reaction (Chang et al., 1986), berthierine reaction (Ehrenberg, 1993; Šegvić et al., 2020 in press), Fe-Mg-rich lithic grains and detrital chlorite and biotite conversion to chlorite (Worden et al., 2018c), ilmenite and other heavy mineral reactions (Gould et al., 2010; Walderhaug and Porten, 2007).

Figure 25. Core analysis porosity versus depth for some variably chlorite-cemented deltaic Jurassic sandstones from the North Sea Basin. A typical combined “compaction plus cementation” porosity-loss curve for North Sea sandstones has been added based on Aase et al. (1996) and Bloch et al. (2002). The modelled compaction-only porosity-loss curve was taken from Ramm et al. (1997). Sandstones with elevated porosity contain grain coating chlorite; sandstones with very low porosity are highly quartz-cemented; sandstones with intermediate porosity values contain pore-filling chlorite and some quartz cement. The high porosity, chlorite-cemented sandstones seem to have undergone normal mechanical compaction processes as they do not exceed porosity values for compacted clean quartz arenites.

Figure 26. Schematic diagram of growth of authigenic grain-coating chlorite in sandstones, based on descriptions of experimental chlorite growth in Cho and Fawcett (1986). Parts A to D represent the four stages of grain-coating chlorite growth. (A1) Chlorite grows indiscriminately on all detrital grain surfaces, irrespective of mineralogy or orientation. (A2) Schematic diagram representing energy of the system versus time involving nucleation and then growth of chlorite with the four stages revealed by letters A to D. Before chlorite growth, the water-rock geochemical system must have been extremely supersaturated with respect to chlorite. This extreme supersaturation may have arisen as a result of the large activation energy of nucleation to overcome and the presence within the sandstone of unstable precursor Fe-rich clays (such as berthierine, in Fe-ooids, or volcanic rock fragment) and the slow rate of crystal growth of complex silicate minerals. (B1) Once supersaturation reaches a critical point, randomly oriented three-dimensional nuclei of chlorite form on all available surfaces and create a vanishingly thin coat of chlorite. (B2) Enlarged area of part of B1 revealing that small but randomly oriented three-dimensional nuclei on

detrital grain surfaces. (C1) As supersaturation decreases following initial chlorite nucleation, very thin chlorite plates extend into the open pore to a maximum length and width of about 10  $\mu\text{m}$ . (C2) Enlarged area of part of C1 revealing that nuclei with their (001) surfaces (c-axes) perpendicular to the grain surface can most easily grow by two-dimensional growth at the edges of (001) sheets. Nuclei with other orientations (e.g., (001) parallel to detrital grain surfaces) will not easily be able to grow because they will impinge on other chlorite crystals. These other oriented chlorite nuclei may remain as very small crystals or they may dissolve and contribute to plates that are growing. (D1) As supersaturation decreases further, the 10  $\mu\text{m}$  wide and 10  $\mu\text{m}$  long plates become thicker but do not grow any further into the pore. (D2) Enlarged area of part of D1 revealing that the perpendicular plates become thicker by a spiral growth mechanism on the (001) surfaces (Fig. 27) but do not grow further out into the open pores.

Figure 27. Schematic illustration of the various stages of chlorite growth based on the deductions of Cho and Fawcett (1986). (A) Nucleation involves the growth of necessarily small by 3-dimensional crystals of chlorite on a sand grain surface. These grow at edges of the (001) plane and extend into the pore. Only crystals which have the (001) plane perpendicular to the grain surface will be able to successfully grow without impinging into other competing chlorite crystals. Initial chlorite crystals only extend 10  $\mu\text{m}$  into the open pore. (B) The next stage of growth, at lower degrees of supersaturation, is by dislocation-controlled spiral growths on the (001) surface. Clockwise accretion of new chlorite layers occurs as the growth spiral builds onto the thin chlorite sheet. The result is a degree of thickening of the initial 2-dimensional 10  $\mu\text{m}$  sheets.

Figure 28. Simple model showing the effect of different degrees of quartz grain coverage by chlorite in an early Jurassic (200 Ma) sandstone. The model is based on quartz kinetic models (Walderhaug, 1994a; Walderhaug et al., 2000), an assumed simple heating history (see inset) with the rock reaching nearly 140°C during continuous and steady heating, for a 300  $\mu\text{m}$  grain size sandstone that is made up of solely of quartz grains. Quartz cement is assumed to start growing at temperatures > 80 to 100°C, after normal compactional processes have reduced porosity to 25%. Porosity-loss from 90 Ma to the present is the result of variable amounts of quartz cementation. Even 20% gaps in the chlorite coat (the 80% case) can reduce porosity from 25% to about 12%; it is likely that this loss of porosity would reduce permeability by several orders of magnitude.

Figure 29. Various petrophysical types of chlorite that can be found in sandstones (Table 1) and how they relate to petrographic characteristics of chlorite distribution and occurrence in sandstones); diagram modified from Shedid and Saad (2017). Parts A, C, E, G and I represent petrographic images that are summarised into a petrophysics summary view of the location of chlorite in the rock in parts B, D, F, H and J.

Figure 30. Representative wireline logs and core analysis data through a variably chlorite-cemented, oil-bearing Jurassic succession from the North Sea Basin; (A) bulk density and neutron, (B) gamma, (C) compressional sonic, (D) deep resistivity, (E) core porosity. The high porosity part of the section, at about 4380 m, is characterised by high neutron, low gamma, low density, high sonic, and low resistivity.

Figure 31. Diagrammatic representation of the modelled (theoretical) wireline log responses of different types of sandstones including: chlorite-bearing sandstones, quartz arenites with variable amounts of quartz cement and illite-kaolinite- and dolomite-cemented quartz arenites (see Table 9); (A) core porosity versus bulk density, (B) core porosity versus compressional sonic, (C) core porosity versus neutron, (D) core porosity versus deep resistivity. Chlorite-cemented sandstones have some well-defined log attributes as well as inhibiting quartz cement and leading to anomalously high porosity deep in sedimentary basins. For a given porosity, chlorite-cemented sandstones tend to have slightly elevated bulk density and compressional sonic responses. Chlorite-cemented sandstones also have rather distinct

neutron responses due to the eight hydroxyls per unit cell of chlorite and the tendency for chlorite grain coats to result in unusually high irreducible water saturations in oil fields (Durand et al., 2001). The high irreducible water saturations found in chlorite cemented sandstones result in them having low resistivity in oil fields as there is more fluid capable of conducting the current from the deep resistivity logging tool (Tudge et al., 2014). Chlorite cemented sandstones with inhibited quartz cement growth (and commensurately high porosity for the depth of burial) are thus primarily characterised by low resistivity and relatively high neutron. For sandstones with a few percent chlorite, compressional sonic and bulk density logs are not necessarily distinct in that they will have high sonic and low bulk density values that are characteristic of any high porosity sandstone.

Figure 32. Representative wireline log and core analysis data, analogous to Figure 30, from the same Jurassic North Sea data as shown in Figure 30 to differentiate the effects of quartz-cemented (chlorite-free) and chlorite-coated sandstones: (A) porosity versus bulk density, (B) porosity versus compressional sonic, (C) porosity versus neutron, (D) porosity versus deep resistivity. The good reservoir quality chlorite-bearing sandstones are indicated by the dashed outline for each of the four logs. The gamma log proved not helpful at discerning the presence of chlorite in sandstones because chlorite contains no common radioactive elements (K, U, Th, Table 10).

Table 1: Definitions of key terms used in this paper to describe chlorite and its genesis. \*: adapted from Dowey et al. (2017). #: adapted from Wooldridge et al. (2019a). § modified from Shedid and Saad (2017).

| Group                         | Term                     | Definition  | Commentary  |
|-------------------------------|--------------------------|---|---|
| Origin of clasts and chlorite | Autogenic grains         | Grains formed in situ, near or within the depositional environment. E.g. Fe-ooids, mudclasts  | Equivalent to intraclasts   |
|                               | Allogenic grains         | Grains formed away from (outside of) the depositional environment, e.g. lithic grains, as well as quartz, micas and feldspar grains, from hinterlands   | Equivalent to "extraclasts"   |
|                               | Detrital chlorite        | Chlorite present in sand or sandstone at the time of deposition: could be chlorite grains, chlorite-bearing lithics, chlorite-bearing matrix or part of a detrital clay coat  | As opposed to authigenic chlorite   |
| Timing and basic definitions  | Eogenetic                | Either: (i) resulting from processes near or at the depositional environment, typically when the sediment is in equilibrium with the atmosphere (redox, pH, saturation state) or (ii) resulting from low temperature (< 60-70°C) and low effective stress.  | Equivalent to early diagenetic  |
|                               | Mesogenetic              | Resulting from conditions during burial to > 60-70°C and increasing effective stress; follows eogenetic conditions  | Equivalent to burial diagenetic   |
|                               | Authigenic               | In situ mineral growth resulting from chemical, physical and biological processes after deposition  | Equivalent to diagenetic mineral  |
|                               | Authigenic chlorite      | In situ chlorite growth resulting from chemical, physical and biological processes after deposition   | As opposed to detrital chlorite   |
|                               | Chloritization           | Generic term for the diagenetic growth of any textural type of chlorite and does not automatically mean the development of chlorite grain-coats in sandstone  | Texturally non-specific term; best <b>not</b> to be used as a synonym for the development of grain-coating chlorite |
| Scale of diagenetic system    | Open system diagenesis   | Diagenesis of a sandstone that is geochemically open to the movement of (specific) components, such as H <sub>2</sub> O, CO <sub>2</sub> , aqueous Na <sup>+</sup> or aqueous HCO <sub>3</sub> <sup>-</sup> , at a defined scale (e.g. at the bed-scale)  | Non-isochemical system  |
|                               | Closed system diagenesis | Diagenesis of a sandstone that is geochemically shut-off to the movement of (specific) components such as SiO <sub>2</sub> , Al <sub>2</sub> O <sub>3</sub> or TiO <sub>2</sub> , at a defined scale (e.g. at the bed-scale)  | Isochemical system  |
| Coat vs rim                   | Grain coat*              | Any coat that either partly or completely covers a sand grain in three dimensions (e.g. like a coat of fur on an animal) found on a sand grain in modern or ancient and deeply buried sandstones. A coat has different mineralogy (and/or no crystallographic orientation relationship) to the host grain | May be partial or total coverage of detrital grains. See grain rim  |
|                               | Grain rim*               | A coat on a sand grain observed in <i>thin section</i> or in a polished block - giving the appearance of a two dimensional texture (e.g. like the rim of a wheel or the rim of a cup)   | See grain coat  |
| Origin of clay coats          | Inherited clay coat*     | A clay mineral-dominated coat that formed in one environment (e.g., fluvial or alluvial) prior to deposition, and was subsequently transported into, and deposited in, another sedimentary environment  | See detrital clay coat  |

|                                |                                      |  |   |
|--------------------------------|--------------------------------------|--|---|
|                                | In-situ clay coat*                   | A clay-dominated coat on a sand grain that formed during, or immediately after, deposition (i.e. while still within the depositional environment). Formed at the very earliest stages of eodiagenesis.   | See detrital clay coat  |
|                                | Detrital clay coat#                  | A clay mineral-dominated coat on a sand grain that formed before, during or immediately after deposition (i.e. while still in the depositional environment) via the physical attachment of clay minerals (includes both inherited and in-situ grain coats) | Appears as discontinuous micron-scale accumulations of clay- to silt-sized material, typically occurring as clumps, tangentially attached coats or strand-like bridges between grains |
|                                | Diagenetic clay coat#                | Clay coat formed following initial deposition, probably limited to late eodiagenesis and mesodiagenesis (typically burial >1000 m and 40-50°C) with an unknown origin  | Generic definition; not split between recrystallized and authigenic clay coats  |
|                                | Diagenetic-recrystallized clay coat# | Depositionally-controlled: recrystallization of the primary attached clay mineral assemblage, emphasizing the importance of clay coats formed in depositional environments   | Appears as tangentially-oriented (parallel to grain surface), densely packed mass of platy-anhedral mineralogically-mixed clay minerals   |
|                                | Diagenetic-authigenic clay coat#     | Provenance-controlled: unstable mineralogy of the sediment assemblage breaks down and provides material required for clay coat creation  | Appears as euhedral, regularly spaced clay crystals, perpendicular (radial) to grains. Often reported to nucleate on underlying detrital clay-coat root-layer                         |
| Petrographic descriptive terms | Isopachous chlorite                  | Petrographic description of chlorite that forms equal thickness layers on detrital grains, typically with crystals that are perpendicular to grain surfaces.   | Description made using light optical, or better still, SEM (SEI or BSEM) microscopy. See also: grain-coating chlorite   |
|                                | Grain-coating chlorite               | Petrographic description of a thin layer, or coat, of chlorite on grain surfaces, that may be isopachous   | As above. Description focused on the solid portion of the rock  |
|                                | Pore-lining chlorite                 | Petrographic description of chlorite that forms a layer, or liner, between detrital, and earlier diagenetic, grains and minerals and the open pore   | Description focused on pores, probably used during SEI imaging of broken rock chips   |
|                                | Pore-throating blocking chlorite     | Petrographic description of chlorite cement that preferentially blocks, or closes, pore throats. Chlorite typically extends from opposite grain surfaces and meets at the narrowest point, i.e. the pore throat  | Description focused on pores, probably used during SEI imaging of broken rock chips   |
|                                | Pore filling chlorite                | Petrographic description of chlorite that fills pores, as opposed to coats grains. Emphasis is filling intergranular spaces as well as pore throats  | Can have many possible origins: grain-replacive chlorite, deformed Fe-oids, detrital matrix   |
|                                | Grain replacive chlorite             | Petrographic description of chlorite that has grown within a mineral, or a lithic grain, and that replaces depositional minerals, e.g. biotite replaced by chlorite. Chlorite effectively fills intragranular pores  | As above. See also structural chlorite  |
|                                | Pseudo-matrix                        | Petrographic description of chlorite in pores between grains that originated as weak chloritic grains, that have been deformed (squeezed) between more competent grains.   | As above. See also dispersed chlorite. As opposed to primary matrix (present at the time of deposition)   |
| Petrophysical terms            | Clean sandstone§                     | Sandstone with negligible detrital (or authigenic) clay (< 1 % clay minerals)  | Petrographic-petrophysical description, strongly affecting wireline-log responses   |
|                                | Laminar chlorite§                    | Petrophysical definition of primary bedded layers of mudstone dominated by chlorite  | As above  |

|                        |  |   |
|------------------------|--|---|
| Structural chlorite§   | Petrophysical definition of primary or secondary lithic grains dominated by chlorite (see grain-replacive chlorite and chlorite pseudo-matrix) | As above. See also grain-replacive chlorite |
| Dispersed chlorite§    | Petrophysical definition of patches of authigenic chlorite sitting in primary pores  | As above. See also pseudo-matrix            |
| Grain-coating chlorite | Petrophysical definition of isopachous layers of primary or authigenic chlorite sitting on all or most detrital grain surfaces                 | As above. See also isopachous chlorite      |

Table 2 Sources of chlorite (and berthierine) compositional data (GoM; Gulf of Mexico)

| Mineral name          | Country   | Basin name                  | Ref                              |
|-----------------------|-----------|-----------------------------|----------------------------------|
| Chlorite              | Brazil    | Santos                      | Anjos et al. (2003)              |
| Chlorite              | Pakistan  | Indus                       | Berger et al. (2009)             |
| Chlorite              | USA       | GoM-Wilcox Fm               | Boles and Franks (1979)          |
| Chlorite              | USA       | GoM-Tuscaloosa Fm           | Bourdelle et al. (2013)          |
| Chlorite              | UK        | N Sea                       | Curtis et al. (1985)             |
| Chlorite              | USA       | GOM-Woodbine and -Vicksburg | Genuise (1991)                   |
| Chlorite              | USA       | GoM-Vicksburg Fm            | Grigsby (2001)                   |
| Chlorite              | Germany   | N German                    | Hillier et al. (1996)            |
| Berthierine/chlorite  | Norway    | Haltenbanken                | Hillier and Velde (1992)         |
| Berthierine           | Canada    | W Canada                    | Hornibrook and Longstaffe (1996) |
| Chlorite              | India     | Surat                       | Huggett et al. (2015)            |
| Chlorite              | UK        | N Sea                       | Humphreys et al. (1989)          |
| Chlorite              | Indonesia | N Sumatra                   | Humphreys et al. (1994)          |
| Chlorite              | Norway    | N Sea                       | Jahren and Aagaard (1989)        |
| Serpentinite/chlorite | USA       | GoM-Tuscaloosa Fm           | Ryan and Reynolds (1996)         |
| Chlorite              | USA       | GoM-Tuscaloosa Fm           | Whittle (1986)                   |



Table 3 Mass balance calculation of the relative number of pore volumes of formation water needed to non-isochemically convert various detrital or early diagenetic Al-bearing minerals such as kaolinite, muscovite or K-feldspar into Fe-chlorite or Mg-chlorite. kaolinite =  $\text{Al}_2\text{Si}_2\text{O}_5(\text{OH})_4$ , chlorite =  $(\text{M}2+)_5\text{Al}_2\text{Si}_3\text{O}_{10}(\text{OH})_8$ , muscovite =  $\text{KAl}_3\text{Si}_3\text{O}_{10}(\text{OH})_2$ , K-feldspar =  $\text{KAlSi}_3\text{O}_8$ . The initial rock is assumed to contain mineral proportions of 4 % each of kaolinite and muscovite, 8% K-feldspar and 84% quartz. The initial rock is also assumed to contain 20% porosity at the time of chlorite growth.

| % of solid reactant % (in 20% porosity sandstone) | Reactant mol/m <sup>3</sup> | Reaction  | % of solid product | Moles of Fe <sup>2+</sup> needed/m <sup>3</sup> | Pore volumes of water needed to supply Fe <sup>2+</sup> at 0.000077 mol/L, for 20% sandstone | Moles of Mg <sup>2+</sup> needed/m <sup>3</sup> | Pore volumes of water needed to supply Mg <sup>2+</sup> at 0.01544 mol/L, for 20% sandstone |
|---|-----------------------------|---|--------------------|---|--|---|---|
| 4% kaolinite                                      | 402.9                       | $1\text{kaol}+5\text{Fe}^{2+}+1\text{qtz}+7\text{H}_2\text{O} = 1\text{FeChl} + 10\text{H}^+$                 | 9.2% Fe-chlorite   | 2014.5  | 130812   | -   | -   |
| 4% kaolinite                                      | 402.9                       | $1\text{kaol}+5\text{Mg}^{2+}+1\text{qtz}+7\text{H}_2\text{O} = 1\text{MgChl} + 10\text{H}^+$                 | 8.4% Mg-chlorite   | -   | -  | 2014.5  | 652   |
| 4% muscovite                                      | 282.3                       | $2\text{musc}+15\text{Fe}^{2+}+3\text{qtz}+24\text{H}_2\text{O} = 3\text{FeChl} + 28\text{H}^+ + 2\text{K}^+$ | 9.7% Fe-chlorite   | 2117.25   | 137484   | -   | -   |
| 4% muscovite                                      | 282.3                       | $2\text{musc}+15\text{Mg}^{2+}+3\text{qtz}+24\text{H}_2\text{O} = 3\text{MgChl} + 28\text{H}^+ + 2\text{K}^+$ | 8.4% Mg-chlorite   | -   | -  | 2117.25   | 686   |
| 8% K-feldspar                                     | 581.8                       | $2\text{Ksp}+5\text{Fe}^{2+}+\text{H}_2\text{O} = 1\text{FeChl} + 3\text{qtz} + 8\text{H}^+ + 2\text{K}^+$    | 6.6% Fe-chlorite   | 1454.5  | 94448  | -   | -   |
| 8% K-feldspar                                     | 581.8                       | $2\text{Ksp}+5\text{Mg}^{2+}+\text{H}_2\text{O} = 1\text{MgChl} + 3\text{qtz} + 8\text{H}^+ + 2\text{K}^+$    | 6.1% Mg-chlorite   | -   | -  | 1454.5  | 471   |

Table 4: Common sedimentary iron mineral names and compositions. Fe<sup>II</sup> represents divalent (ferrous) iron. Fe<sup>III</sup> represents trivalent (ferric) iron.

| Mineral name     | Alternative name | Approximate formula  |
|------------------|------------------|--|
| Limonite         |                  | Fe <sup>III</sup> (OH) <sub>3</sub> or Fe <sub>2</sub> O <sub>3</sub> ·nH <sub>2</sub> O   |
| Goethite         |                  | Fe <sup>III</sup> OOH  |
| Haematite        |                  | Fe <sub>2</sub> O <sub>3</sub> (Fe <sup>II</sup> Fe <sup>III</sup> O <sub>3</sub> )  |
| Greigite         |                  | Fe <sub>3</sub> S <sub>4</sub> (Fe <sup>II</sup> Fe <sup>III</sup> <sub>2</sub> S <sub>4</sub> )   |
| Magnetite        | Ferrite          | Fe <sub>3</sub> O <sub>4</sub> (Fe <sup>II</sup> Fe <sup>III</sup> <sub>2</sub> O <sub>4</sub> )   |
| Fe-smectite      | Nontronite       | Na <sub>0.3</sub> Fe <sup>III</sup> <sub>2</sub> (SiAl) <sub>4</sub> O <sub>10</sub> (OH) <sub>2</sub> · n(H <sub>2</sub> O)   |
| Glauconite       |                  | (KNa)(Fe <sup>III</sup> AlMg) <sub>2</sub> (SiAl) <sub>4</sub> O <sub>10</sub> (OH) <sub>2</sub>   |
| Odinite          | Phyllite-V       | (Fe <sup>II</sup> <sub>0.6</sub> Mg <sub>1.4</sub> Fe <sup>III</sup> <sub>1.4</sub> Al <sub>1.0</sub> )(Si <sub>3.6</sub> Al <sub>0.4</sub> )O <sub>10</sub> (OH) <sub>8</sub>                         |
| Berthierine      | 7Å chamosite     | (Fe <sup>II</sup> <sub>2.1</sub> Mg <sub>0.9</sub> Fe <sup>III</sup> <sub>0.5</sub> Al <sub>1.5</sub> )(Si <sub>3.5</sub> Al <sub>0.5</sub> )O <sub>10</sub> (OH) <sub>8</sub> · 0.8(H <sub>2</sub> O) |
| Daphnite         | Chamosite        | (Fe <sup>II</sup> <sub>5</sub> Al <sub>1</sub> )(Si <sub>3</sub> Al <sub>1</sub> )O <sub>10</sub> (OH) <sub>8</sub>  |
| Fe-rich chlorite |                  | (Fe <sup>II</sup> <sub>4</sub> Mg <sub>1</sub> Al <sub>1</sub> )(Si <sub>3</sub> Al <sub>1</sub> )O <sub>10</sub> (OH) <sub>8</sub>  |
| Fe-Mg chlorite   |                  | (Fe <sup>II</sup> <sub>2.5</sub> Mg <sub>2.5</sub> Al <sub>1</sub> )(Si <sub>3</sub> Al <sub>1</sub> )O <sub>10</sub> (OH) <sub>8</sub>  |
| Mg-rich chlorite |                  | (Fe <sup>II</sup> <sub>1</sub> Mg <sub>4</sub> Al)(Si <sub>3</sub> Al <sub>1</sub> )O <sub>10</sub> (OH) <sub>8</sub>  |
| Clinochlore      |                  | (Mg <sub>5</sub> Al)(Si <sub>3</sub> Al <sub>1</sub> )O <sub>10</sub> (OH) <sub>8</sub>  |
| Biotite          |                  | K(Fe <sup>II</sup> Mg <sub>1</sub> ) <sub>3</sub> Al <sub>1</sub> Si <sub>3</sub> O <sub>10</sub> (OH) <sub>2</sub>  |
| Siderite         |                  | Fe <sup>II</sup> CO <sub>3</sub>   |
| Pyrrhotite       |                  | Fe <sup>II</sup> S   |
| Pyrite           |                  | Fe <sup>II</sup> S <sub>2</sub>  |
| Garnet           | Almandine        | Fe <sup>II</sup> <sub>3</sub> Al <sub>2</sub> Si <sub>3</sub> O <sub>12</sub>  |
| Ilmenite         |                  | Fe <sup>II</sup> TiO <sub>3</sub>  |

Table 5: Summary of rock types in hinterlands to sedimentary basins. Note that metamorphic equivalents of these rocks will have similar compositions assuming broadly isochemical metamorphism.

| Hinterland rock type | Oxide %<br>Source of data | SiO <sub>2</sub> | Al <sub>2</sub> O <sub>3</sub> | FeO        | MgO        | CaO        | Na <sub>2</sub> O | K <sub>2</sub> O | TiO <sub>2</sub> |
|----------------------|---------------------------|------------------|--------------------------------|------------|------------|------------|-------------------|------------------|------------------|
| Sandstone avg Fe     | Liverpool                 | 83.1             | 6.6                            | 2.4        | 1.3        | 2.6        | 1.4               | 1.7              | 0.3              |
| Sandstone low Fe     |                           | 94.8             | 4.0                            | 0.9        | 0.5        | 0.2        | 1.2               | 1.0              | 0.1              |
| Sandstone hi Fe      |                           | 56.2             | 13.0                           | 9.6        | 3.3        | 1.3        | 1.5               | 3.0              | 0.7              |
| Sandstone            | Parker (1967)             | 78.7             | 4.7                            | 1.3        | 1.2        | 5.5        | 0.4               | 1.3              | 0.3              |
| Shale                |                           | 50.9             | 19.7                           | 4.3        | 2.2        | 3.5        | 0.8               | 2.7              | 0.8              |
| Limestone            |                           | 5.1              | 0.8                            | 0.5        | 7.8        | 42.3       | 0.1               | 0.3              | 0.2              |
| Shale                | Krauskopf (1979)          | 50.9             | 17.4                           | 6.0        | 2.3        | 3.5        | 1.2               | 3.0              | 0.8              |
| Acid felsic          |                           | 69.1             | 14.5                           | 3.5        | 0.7        | 2.2        | 3.8               | 3.9              | 0.4              |
| Basic mafic          |                           | 49.2             | 15.9                           | 11.1       | 6.6        | 10.1       | 2.6               | 1.0              | 1.5              |
| Basalt               | Hill et al. (2000)        | 43.94            | 15.15                          | 13.61      | 6.94       | 9.32       | 2.24              | 0.2              | 1.87             |
| Lithomarge           |                           | 37.33            | 27.86                          | 18.03      | 2.32       | 1.8        | 0.37              | 0.11             | 2.64             |
| Laterite             |                           | 21.54            | 33.78                          | 25.03      | 0.37       | 0.45       | 0.15              | 0.04             | 3.99             |
| Iron crust           |                           | 12.72            | 17.51                          | 47.51      | 0.4        | 0.59       | 0.07              | 0.04             | 9.99             |
|                      | element ratio             | Fe/(Fe+Al)       | Fe/(Fe+Mg)                     | Fe/(Fe+Si) | Mg/(Mg+Al) | Al/(Al+Si) | Fe/(Fe+Mg+Al)     | Mg/(Fe+Mg+Al)    | Al/(Fe+Mg+Al)    |
| Sandstone avg Fe     | Liverpool                 | 0.189            | 0.679                          | 0.021      | 0.099      | 0.085      | 0.173             | 0.082            | 0.745            |
| Sandstone low Fe     |                           | 0.134            | 0.691                          | 0.008      | 0.065      | 0.047      | 0.126             | 0.056            | 0.818            |
| Sandstone hi Fe      |                           | 0.343            | 0.791                          | 0.125      | 0.122      | 0.215      | 0.315             | 0.083            | 0.602            |
| Sandstone            | Parker (1967)             | 0.159            | 0.583                          | 0.013      | 0.119      | 0.066      | 0.143             | 0.102            | 0.755            |
| Shale                |                           | 0.133            | 0.713                          | 0.066      | 0.058      | 0.314      | 0.127             | 0.051            | 0.822            |
| Limestone            |                           | 0.304            | 0.075                          | 0.074      | 0.844      | 0.154      | 0.064             | 0.790            | 0.146            |
| Shale                | Krauskopf (1979)          | 0.198            | 0.594                          | 0.090      | 0.145      | 0.287      | 0.174             | 0.119            | 0.706            |
| Acid felsic          |                           | 0.145            | 0.723                          | 0.040      | 0.061      | 0.199      | 0.137             | 0.053            | 0.810            |
| Basic mafic          |                           | 0.331            | 0.483                          | 0.158      | 0.346      | 0.275      | 0.244             | 0.261            | 0.494            |
| Basalt               | Hill et al. (2000)        | 0.389            | 0.486                          | 0.206      | 0.403      | 0.289      | 0.276             | 0.292            | 0.432            |
| Lithomarge           |                           | 0.315            | 0.789                          | 0.288      | 0.109      | 0.468      | 0.290             | 0.078            | 0.632            |
| Laterite             |                           | 0.345            | 0.970                          | 0.493      | 0.016      | 0.649      | 0.341             | 0.010            | 0.649            |
| Iron crust           |                           | 0.658            | 0.983                          | 0.758      | 0.033      | 0.619      | 0.651             | 0.011            | 0.338            |

Table 6: Examples of the compositions of different types of sandstones. Mineral proportions are indicated in the left-hand column. q: quartz, Ks: K-feldspar, FMc: mixed Fe-, Mg-chlorite, pg: albite, s: siderite, m: impure muscovite, b: impure biotite, pyr: pyrite, ilm: ilmenite, ill: illite, ka: kaolinite, d: ferroan dolomite, c: calcite (the compositions of these minerals is defined in Table 7)

| Sandstone composition   oxide % | SiO <sub>2</sub> | Al <sub>2</sub> O <sub>3</sub> | FeO         | MgO         | CaO         | Na <sub>2</sub> O | K <sub>2</sub> O | TiO <sub>2</sub> |
|---------------------------------|------------------|--------------------------------|-------------|-------------|-------------|-------------------|------------------|------------------|
| 90q 5Ks 5FMc                    | 94.5             | 1.6                            | 2.0         | 0.4         | 0.0         | 0.0               | 1.0              | 0.0              |
| 80q 5Ks 15FMc                   | 87.2             | 3.2                            | 6.0         | 1.1         | 0.0         | 0.0               | 1.0              | 0.0              |
| 85q 5Ks 5pg 5FMc                | 92.9             | 2.6                            | 2.0         | 0.4         | 0.0         | 0.6               | 1.0              | 0.0              |
| 60q 20Ks 15pg 5FMc              | 84.2             | 7.2                            | 2.0         | 0.4         | 0.0         | 1.8               | 4.0              | 0.0              |
| 60q 15Ks 15pg 10FMc             | 82.4             | 7.1                            | 4.0         | 0.7         | 0.0         | 1.8               | 3.0              | 0.0              |
| 75q 5Ks 5pg 15FMc               | 85.6             | 4.1                            | 6.0         | 1.1         | 0.0         | 0.6               | 1.0              | 0.0              |
| 90q 5Ks 5s                      | 93.1             | 0.9                            | 3.0         | 0.0         | 0.1         | 0.0               | 1.0              | 0.0              |
| 80q 5Ks 15s                     | 83.1             | 0.9                            | 8.9         | 0.1         | 0.2         | 0.0               | 1.0              | 0.0              |
| 85q 5Ks 5pg 5s                  | 91.6             | 1.9                            | 3.0         | 0.0         | 0.1         | 0.6               | 1.0              | 0.0              |
| 75q 5Ks 5pg 15s                 | 81.6             | 1.9                            | 8.9         | 0.1         | 0.2         | 0.6               | 1.0              | 0.0              |
| 80q 5Ks 5m 5b 3py 2ilm          | 87.4             | 2.5                            | 4.3         | 0.4         | 0.0         | 0.0               | 2.3              | 1.2              |
| 75q 5Ks 5pg 5m 5b 3py 2ilm      | 85.8             | 3.5                            | 4.3         | 0.4         | 0.0         | 0.6               | 2.3              | 1.2              |
| 75q 5Ks 5pg 3m 2b 5FMc 5s       | 85.1             | 3.5                            | 5.7         | 0.6         | 0.1         | 0.6               | 1.6              | 0.1              |
| 75q 5Ks 5pg 3m 5FMc 5S 2s       | 84.3             | 3.4                            | 6.4         | 0.4         | 0.1         | 0.6               | 1.4              | 0.0              |
| 80q 10ill 10ka                  | 89.8             | 7.2                            | 0.2         | 0.1         | 0.0         | 0.0               | 1.0              | 0.0              |
| 80q 10ill 10d                   | 85.1             | 3.2                            | 1.2         | 1.5         | 2.9         | 0.0               | 1.0              | 0.0              |
| 80q 10ill 10c                   | 85.1             | 3.2                            | 0.3         | 0.1         | 5.4         | 0.0               | 1.0              | 0.0              |
| Sandstone composition           | Fe/ (Fe+Al)      | Fe/ (Fe+Mg)                    | Fe/ (Fe+Si) | Mg/ (Mg+Al) | Al/ (Al+Si) | Fe/ (Fe+Mg+ Al)   | Mg/ (Fe+Mg+ Al)  | Al/ (Fe+Mg+ Al)  |
| 90q 5Ks 5FMc                    | 0.463            | 0.873                          | 0.017       | 0.111       | 0.020       | 0.434             | 0.063            | 0.503            |
| 80q 5Ks 15FMc                   | 0.574            | 0.873                          | 0.054       | 0.164       | 0.041       | 0.530             | 0.077            | 0.393            |
| 85q 5Ks 5pg 5FMc                | 0.352            | 0.873                          | 0.018       | 0.073       | 0.032       | 0.334             | 0.049            | 0.617            |
| 60q 20Ks 15pg 5FMc              | 0.164            | 0.873                          | 0.019       | 0.028       | 0.092       | 0.160             | 0.023            | 0.816            |
| 60q 15Ks 15pg 10FMc             | 0.286            | 0.873                          | 0.039       | 0.055       | 0.092       | 0.274             | 0.040            | 0.686            |
| 75q 5Ks 5pg 15FMc               | 0.507            | 0.873                          | 0.055       | 0.130       | 0.054       | 0.473             | 0.069            | 0.459            |
| 90q 5Ks 5s                      | 0.704            | 0.989                          | 0.026       | 0.027       | 0.011       | 0.698             | 0.008            | 0.294            |
| 80q 5Ks 15s                     | 0.877            | 0.989                          | 0.082       | 0.076       | 0.012       | 0.868             | 0.010            | 0.122            |
| 85q 5Ks 5pg 5s                  | 0.532            | 0.989                          | 0.026       | 0.013       | 0.023       | 0.529             | 0.006            | 0.465            |
| 75q 5Ks 5pg 15s                 | 0.773            | 0.989                          | 0.084       | 0.038       | 0.026       | 0.766             | 0.009            | 0.225            |
| 80q 5Ks 5m 5b 3py 2ilm          | 0.544            | 0.934                          | 0.039       | 0.078       | 0.033       | 0.524             | 0.037            | 0.439            |
| 75q 5Ks 5pg 5m 5b 3py 2ilm      | 0.463            | 0.934                          | 0.040       | 0.057       | 0.046       | 0.449             | 0.032            | 0.520            |
| 75q 5Ks 5pg 3m 2b 5FMc 5s       | 0.531            | 0.927                          | 0.053       | 0.082       | 0.047       | 0.510             | 0.040            | 0.450            |
| 75q 5Ks 5pg 3m 5FMc 5S 2s       | 0.570            | 0.952                          | 0.059       | 0.063       | 0.046       | 0.553             | 0.028            | 0.418            |
| 80q 10ill10ka                   | 0.018            | 0.000                          | 0.002       | 0.004       | 0.086       | 0.018             | 0.004            | 0.979            |
| 80q 10ill 10d                   | 0.211            | 0.511                          | 0.012       | 0.204       | 0.043       | 0.176             | 0.168            | 0.656            |
| 80q 10ill 10c                   | 0.067            | 0.000                          | 0.003       | 0.015       | 0.043       | 0.066             | 0.014            | 0.920            |

Table 7: Exact mineral compositions used to construct the compositions of end-member sandstone types represented in Table 6.

| Mineral                | Formula   |
|------------------------|---|
| Quartz                 | $\text{SiO}_2$  |
| K-feldspar             | $\text{KAlSi}_3\text{O}_8$  |
| Albite                 | $\text{NaAlSi}_3\text{O}_8$   |
| Kaolin                 | $\text{Al}_2\text{Si}_2\text{O}_5(\text{OH})_4$   |
| Muscovite-impure       | $\text{K}_{0.95}\text{Na}_{0.04}\text{Al}_{2.2}\text{Ti}_{0.05}\text{Si}_{3.3}\text{O}_{10}(\text{OH})_2$   |
| Biotite-impure         | $\text{K}_{0.89}\text{Na}_{0.06}\text{Al}_{0.55}\text{Ti}_{0.14}\text{Si}_{2.77}\text{O}_{10}(\text{OH})_2$ |
| Illite                 | $\text{K}_{0.65}\text{Al}_{2.65}\text{Si}_{3.35}\text{O}_{10}(\text{OH})_2$                                 |
| Fe-Mg chlorite         | $\text{Fe}_{2.5}\text{Mg}_{2.5}\text{Al}_2\text{Si}_3\text{O}_{10}(\text{OH})_8$                            |
| Ilmenite               | $\text{FeTiO}_3$  |
| Calcite                | $\text{Ca}_{0.97}\text{Mg}_{0.01}\text{Fe}_{0.02}(\text{CO}_3)_2$   |
| Fe-dolomite (ankerite) | $\text{Ca}_{1.0}\text{Mg}_{0.7}\text{Fe}_{0.3}(\text{CO}_3)_2$  |
| Siderite               | $\text{Fe}_{0.95}\text{Ca}_{0.03}\text{Mg}_{0.02}\text{CO}_3$   |
| Pyrite                 | $\text{FeS}_2$  |

Table 8: Collated examples of sandstones that contain chlorite grain coats.

| Formation                              | Age                      | Basin                | Country        | Authors   |
|--|--------------------------|----------------------|----------------|---|
| -                                      | Lower Devonian           | Ahnet-Timimoun Basin | Algeria        | Hirst et al. (2001)   |
| -                                      | Lower Carboniferous      | Timimoun Basin       | Algeria        | Armitage et al. (2010), Tudge et al. (2014)   |
| Upper Cape Hay Formation               | Permian                  | Bonaparte Basin      | Australia      | Saiag et al. (2016)   |
| Itajai-Acu Formation                   | Upper Cretaceous         | Santos Basin         | Brazil         | Anjos et al. (2003), Bahlis and De Ros (2013)   |
| Missisauga Formation                   | Lower Cretaceous         | Scotian Basin        | Canada         | Gould et al. (2010), Pe-Piper and Weir-Murphy (2008)  |
| Clearwater Formation                   | Lower Cretaceous         | Western Canada Basin | Canada         | Hornibrook and Longstaffe (1996)  |
| Shiqianfeng Formation                  | Upper Permian            | Bohai Bay Basin      | China          | Ma et al. (2017)  |
| T <sub>3</sub> x or Xujiache Formation | Upper Triassic           | Sichuan Basin        | China          | Cao et al. (2018), Peng et al. (2009), Sun et al. (2014), Yu et al. (2016)  |
| Yanchang Formation                     | Upper Triassic           | Ordos Basin          | China          | Fan et al. (2017), Xiang et al. (2016), Zhu et al. (2017),  |
| Lista Formation, Heimdal Member        | Palaeocene               | Danish Basin         | Denmark        | Mu et al. (2015)  |
| Rotliegend Formation                   | Lower Permian            | North German Basin   | Germany        | Hillier et al. (1996)   |
| Mahim Formation                        | Miocene                  | Mumbai Basin         | India          | Huggett et al. (2015)   |
| Keutapang Formation                    | Middle and Upper Miocene | North Sumatra Basin  | Indonesia      | Humphreys et al. (1994)   |
| Tilje, Tofte and Garn Formations       | Lower to Middle Jurassic | Haltenbanken         | Norway         | Aagaard et al. (2000), Ehrenberg (1993), Ehrenberg et al. (1998), Hillier and Velde (1992), Jahren et al. (1998), Martinius et al. (2001) |
| Cook Formation                         | Lower Jurassic           | North Sea            | Norway         | Churchill et al. (2017), Skarpeid et al. (2017)   |
| Kobbe and Snadd Formations             | Middle to Late Triassic  | Barents Sea Basin    | Norway         | Line et al. (2018)  |
| Goru Formation                         | Cretaceous               | Indus Basin          | Pakistan       | Berger et al. (2009)  |
| Jauf Formation                         | Devonian                 | Arabian Basin        | Saudi Arabia   | Al-Ramadan et al. (2004), Saner et al. (2006)   |
| Skaggerak Formation                    | Upper Triassic           | Central Graben       | UK and Denmark | Stricker and Jones (2018), Weibel (1999)  |
| Spiro Member, Savanna Formation        | Upper Carboniferous      | Arkoma Basin         | USA            | Pittman and Lumsden (1968), Spotl et al. (1994)   |
| Sundance Formation                     | Upper Jurassic           | Bighorn Basin        | USA            | Ryan and Hillier (2002)   |
| Vicksburg Formation                    | Oligocene                | Gulf of Mexico Basin | USA            | Grigsby and Langford (1996), Grigsby (2001)   |
| Norphlet Formation                     | Upper Jurassic           | Gulf of Mexico Basin | USA            | Ajdukiewicz et al. (2010), Dixon et al. (1989)  |
| Tuscaloosa Formation                   | Late Cretaceous          | Gulf of Mexico Basin | USA            | Dutton et al. (2018), Ryan and Reynolds (1996), Ryan and Reynolds (1997), Thomson (1979), Thomson (1982)                                  |

---

Table 9 Theoretical core (porosity, permeability, grain density) and log (gamma, sonic, density, neutron, resistivity) characteristics of variably chlorite cemented sandstones compared to variably quartz cemented quartz arenites and illite-, calcite- and dolomite-cemented sandstones (Fig. 30). The proportions of different minerals in these simple end-member rock types are defined in the second column. Porosity and permeability values for these types of sandstones have been taken from Primmer et al. (1997) and Cade et al. (1994). Flow Zone Indicator is a petrophysically-defined measure of the connectedness of pores and has been used to define reservoir quality facies (Tiab and Donaldson, 2015) and was determined using  $(0.0314 \cdot (k/\phi)^{0.5}) / (\phi / (1-\phi))$ , where k is horizontal permeability and  $\phi$  is fractional porosity. The density and sonic responses of the various sandstones are the result of inverting the equations normally used to derive porosity from logs (Zinszner and Pellerin, 2007) and sandstone-specific solid grain density and solid grain sonic values (for the differing mineralogies) calculated using mineral end-member values listed in Table 10. Gamma and neutron responses for each rock type have been derived using the same approach. The deep resistivity characteristic of each sandstone type was derived by inverting the Archie equation and using the stated porosity, a constant formation water resistivity and typical Archie constants (Rider and Kennedy, 2011).

(see next page)

| Sandstone type                         | Sandstone mineralogy  | Porosity ( $\emptyset$ , fraction) | Horizontal permeability (kh, mD) | Flow Zone Indicator (FZI, m <sup>3</sup> ) see table caption | Dean & Stark water saturation (Sw, fraction) | Solid grain density (g/cm <sup>3</sup> ) | Log-response bulk density (RHOB, g/cm <sup>3</sup> ) | Log-response gamma ray API | Derived matrix sonic value ( $\mu$ s/ft) | Log-response compressional sonic (DTC, $\mu$ s/ft) | Log-response shear sonic (DTC, $\mu$ s/ft) | Derived matrix neutron value (NPHI) | Log-response compensated neutron hydrogmn index (NPHI, fraction) | Log-response deep resistivity (RD, ohm.m) |
|--|---|------------------------------------|----------------------------------|--|--|--|--|----------------------------|--|--|--|-------------------------------------|--|---|
| Shallow clean sandstone                | Quartz arenite  | 0.30                               | 3000                             | 7.33   | 0.05   | 2.660                                    | 2.16   | 20                         | 55.0                                     | 99   | 165  | -0.020                              | 0.29   | 66.0                                      |
| V thin chlorite-coated sandstone       | Quartz arenite with 3% chlorite (coat) by volume                | 0.22                               | 1500                             | 9.19   | 0.25   | 2.670                                    | 2.30   | 20                         | 55.8                                     | 87   | 146  | -0.004                              | 0.22   | 5.4                                       |
| Chlorite-coated sandstone              | Quartz arenite with 5% chlorite (coat) by volume                | 0.20                               | 1000                             | 8.88   | 0.4  | 2.677                                    | 2.34   | 20                         | 56.3                                     | 85   | 143  | 0.007                               | 0.21   | 2.5                                       |
| Excess-chlorite-coated sandstone       | Quartz arenite with 15% chlorite (coat and pore-fill) by volume | 0.16                               | 25                               | 2.06   | 0.6  | 2.711                                    | 2.44   | 20                         | 58.8                                     | 81   | 135  | 0.061                               | 0.21   | 1.8                                       |
| Pore-filling chlorite sandstone        | Quartz arenite with 25% chlorite (pore-fill) by volume          | 0.12                               | 1                                | 0.66   | 0.7  | 2.745                                    | 2.54   | 20                         | 61.3                                     | 78   | 126  | 0.115                               | 0.22   | 2.3                                       |
| Excess pore-filling chlorite sandstone | Quartz arenite with 40% chlorite (pore-fill) by volume          | 0.08                               | 0.1                              | 0.40   | 0.8  | 2.796                                    | 2.65   | 20                         | 65.0                                     | 76   | 117  | 0.196                               | 0.26   | 4.0                                       |
| 5%-qtz cemented sandstone              | Quartz arenite with 5% quartz cement                            | 0.25                               | 1000                             | 5.96   | 0.1  | 2.660                                    | 2.25   | 20                         | 55.0                                     | 91   | 151  | -0.020                              | 0.24   | 32.0                                      |
| 15%-qtz cemented sandstone             | Quartz arenite with 15% quartz cement                           | 0.15                               | 100                              | 4.59   | 0.2  | 2.660                                    | 2.41   | 20                         | 55.0                                     | 77   | 124  | -0.020                              | 0.13   | 22.2                                      |
| 25%-qtz cemented sandstone             | Quartz arenite with 25% quartz cement                           | 0.05                               | 1                                | 2.67   | 0.7  | 2.660                                    | 2.58   | 20                         | 55.0                                     | 62   | 97   | -0.020                              | 0.03   | 16.3                                      |
| Illite-clay rich sandstone             | Quartz arenite with 20% illite                                  | 0.12                               | 0.05                             | 0.15   | 0.95   | 2.690                                    | 2.49   | 56                         | 60.0                                     | 77   | 128  | -0.001                              | 0.12   | 1.5                                       |
| Calcite-cemented sandstone             | Quartz arenite with 40% calcite                                 | 0.05                               | 0.0001                           | 0.03   | 1  | 2.688                                    | 2.60   | 20                         | 52.6                                     | 60   | 94   | -0.012                              | 0.04   | 6.5                                       |
| Dolomite-cemented sandstone            | Quartz arenite with 25% dolomite                                | 0.10                               | 0.5                              | 0.63   | 0.95   | 2.695                                    | 2.53   | 20                         | 52.5                                     | 67   | 107  | -0.015                              | 0.09   | 1.8                                       |



Table 10. Mineral end-member wireline log responses used to derive the sandstones gamma, bulk density, sonic, and neutron responses in Table 9 and Figure 30 (Peters, 2012; Rider and Kennedy, 2011; Tiab and Donaldson, 2015; Zinszner and Pellerin, 2007).

| Mineral  | Mineral density (g/cm <sup>3</sup> ) | Mineral gamma (API) | Mineral compressional sonic (μs/ft) | Mineral neutron response (NPHI units) |
|----------|--------------------------------------|---------------------|-------------------------------------|---------------------------------------|
| Quartz   | 2.66                                 | 20                  | 55                                  | -0.02                                 |
| Chlorite | 3.00                                 | 20                  | 80                                  | 0.52                                  |
| Illite   | 2.81                                 | 150                 | 80                                  | 0.30                                  |
| Calcite  | 2.73                                 | 20                  | 49                                  | 0.00                                  |
| Dolomite | 2.80                                 | 20                  | 45                                  | 0.01                                  |

## References

- Aagaard, P., Jahren, J.S., Harstad, A.O., Nilsen, O. and Ramm, M., 2000. Formation of grain-coating chlorite in sandstones. Laboratory synthesized vs. natural occurrences. *Clay Minerals*, 35(1): 261-269.
- Aase, N.E., Bjørkum, P.A. and Nadeau, P.H., 1996. The effect of grain-coating microquartz on preservation of reservoir porosity. *American Association of Petroleum Geologists Bulletin*, 80(10): 1654-1673.
- Ainsworth, R.B., Vakarelov, B.K., MacEachern, J.A., Rarity, F., Lane, T.I. and Nanson, R.A., 2017. Anatomy of a shoreline regression: Implications for the high-resolution stratigraphic architecture of deltas. *Journal of Sedimentary Research*, 87(5): 425-459.
- Ajdukiewicz, J.M. and Larese, R.E., 2012. How clay grain coats inhibit quartz cement and preserve porosity in deeply buried sandstones: Observations and experiments. *American Association of Petroleum Geologists Bulletin*, 96(11): 2091-2119.
- Ajdukiewicz, J.M., Nicholson, P.H. and Esch, W.L., 2010. Prediction of deep reservoir quality using early diagenetic process models in the Jurassic Norphlet Formation, Gulf of Mexico. *American Association of Petroleum Geologists Bulletin*, 94(8): 1189-1227.
- Al-Ramadan, K.A., Hussain, M., Imam, B. and Saner, S., 2004. Lithologic characteristics and diagenesis of the Devonian Jauf sandstone at Ghawar Field, eastern Saudi Arabia. *Marine and Petroleum Geology*, 21(10): 1221-1234.
- Andresen, B., Throndsen, T., Barth, T. and Bolstad, J., 1994. Thermal generation of carbon dioxide and organic acids from different source rocks. *Organic Geochemistry*, 21(12): 1229-1242.
- Anjos, S.M.C., De Ros, L.F. and Silva, C.M.A., 2003. Chlorite authigenesis and porosity preservation in the Upper Cretaceous marine sediments of the Santos Basin, offshore eastern Brazil. In: R.H. Worden and S. Morad (Editors), *Clay cements in sandstones*, Special Publication of the International Association of Sedimentologists. Blackwells, Oxford, pp. 291-316.
- Armitage, P.J., Faulkner, D.R. and Worden, R.H., 2013. Caprock corrosion. *Nature Geoscience*, 6(2): 79-80.
- Armitage, P.J., Faulkner, D.R., Worden, R.H., Aplin, A.C., Butcher, A.R. and Iliffe, J., 2011. Experimental measurement of, and controls on, permeability and permeability anisotropy of caprocks from the CO<sub>2</sub> storage project at the Krechba Field, Algeria. *Journal of Geophysical Research-Solid Earth*, 116, Article number B12208.
- Armitage, P.J., Worden, R.H., Faulkner, D.R., Aplin, A.C., Butcher, A.R. and Iliffe, J., 2010. Diagenetic and sedimentary controls on porosity in Lower Carboniferous fine-grained lithologies, Krechba field, Algeria: A petrological study of a caprock to a carbon capture site. *Marine and Petroleum Geology*, 27(7): 1395-1410.
- Ashcroft, W.A. and Ridgway, M.S., 1996. Early discordant diagenesis in the Brent Group, Murchison Field, UK North Sea, detected in high values of seismic-derived acoustic impedance. *Petroleum Geoscience*, 2(1): 75-81.

- Bahlis, A.B. and De Ros, L.F., 2013. Origin and impact of authigenic chlorite in the Upper Cretaceous sandstone reservoirs of the Santos Basin, eastern Brazil. *Petroleum Geoscience*, 19(2): 185-199.
- Baines, S.J. and Worden, R.H., 2004. The long term fate of CO<sub>2</sub> in the subsurface: natural analogues for CO<sub>2</sub> storage. In: S.J. Baines and R.H. Worden (Editors), *Geological Storage of Carbon Dioxide*. Special Publication. The Geological Society, London, pp. 59-85.
- Barclay, S.A. and Worden, R.H., 2000. Geochemical modelling of diagenetic reactions in a sub-arkosic sandstone. *Clay Minerals*, 35(1): 57-67.
- Barrie, G.M., Worden, R.H., Barrie, C.D. and Boyce, A.J., 2015. Extensive evaporation in a modern temperate estuary: Stable isotopic and compositional evidence. *Limnology and Oceanography*, 60(4): 1241-1250.
- Barth, T. and Riis, M., 1992. Interactions between organic-acid anions in formation waters and reservoir mineral phases. *Organic Geochemistry*, 19(4-6): 455-482.
- Beard, D.C. and Weyl, P.K., 1973. Influence of texture on porosity and permeability of unconsolidated sand. *American Association of Petroleum Geologists Bulletin*, 57: 349-369.
- Beaufort, D., Rigault, C., Billon, S., Billault, V., Inoue, A., Inoue, S. and Patrier, P., 2015. Chlorite and chloritization processes through mixed-layer mineral series in low temperature geological systems a - review. *Clay Minerals*, 50(4): 497-523.
- Benbaccar, M., Fritz, B., Sommer, F., Bazin, B. and Brosse, E., 1995. Geochemical modelling of mineral diagenesis in the Brent sandstone reservoirs, Alwyn South and Alwyn North areas, East Shetland Basin, North Sea. *Water-Rock Interaction*, 437-440 pp.
- Berger, A., Gier, S. and Krois, P., 2009. Porosity-preserving chlorite cements in shallow-marine volcanoclastic sandstones: Evidence from Cretaceous sandstones of the Sawan gas field, Pakistan. *American Association of Petroleum Geologists Bulletin*, 93: 595-615.
- Berner, E.K. and Berner, R.A., 2012. *Global environment: water, air and geochemical cycles*. Second edition. Princeton University Press, Princeton, 444 pp.
- Berner, R.A., 1980. *Early diagenesis, a theoretical approach*. Princeton University Press, Princeton.
- Billault, V., Beaufort, D., Baronnet, A. and Lacharpagne, J.C., 2003. A nanopetrographic and textural study of grain-coating chlorites in sandstone reservoirs. *Clay Minerals*, 38(3): 315-328.
- Bjorkum, P.A. and Gjelsvik, N., 1988. An isochemical model for formation of authigenic kaolinite, k-feldspar and illite in sediments. *Journal of Sedimentary Petrology*, 58(3): 506-511.
- Bjørkum, P.A. and Nadeau, P.H., 1998. Temperature controlled porosity/permeability reduction, fluid migration, and petroleum exploration in sedimentary basins. *Australian Petroleum Production and Exploration Association Journal*, 38: 453-464.
- Bjørlykke, K., Aagaard, P., Dypvik, H., Hastings, D.S. and Harper, A.S., 1986. Diagenesis and reservoir properties of Jurassic sandstones from the Haltenbanken area, offshore mid Norway. *Habitat of hydrocarbons on the Norwegian continental shelf*. Proc. conference, Stavanger, 1985: 275-286.

- Bjørlykke, K. and Egeberg, P.K., 1993. Quartz cementation in sedimentary basins. *American Association of Petroleum Geologists Bulletin*, 77(9): 1538-1548.
- Bloch, S., Lander, R.H. and Bonnell, L., 2002. Anomalously high porosity and permeability in deeply buried sandstone reservoirs: Origin and predictability. *American Association of Petroleum Geologists Bulletin*, 86(2): 301-328.
- Boles, J.R. and Franks, S.G., 1979. Clay diagenesis in Wilcox Sandstones of southwest Texas - implications of smectite diagenesis on sandstone cementation. *Journal of Sedimentary Petrology*, 49(1): 55-70.
- Bonnell, L.M., Lander, R.H. and Larese, R.E., 2014. Prediction of the formation of grain coating chlorite by the in situ alteration of volcanic rock fragments (abs), *Reservoir Quality of Clastic and Carbonate Rocks: Analysis, Modelling and Prediction*. Geological Society, London, pp. 112-113.
- Bourdelle, F., Parra, T., Chopin, C. and Beyssac, O., 2013. A new chlorite geothermometer for diagenetic to low-grade metamorphic conditions. *Contributions to Mineralogy and Petrology*, 165(4): 723-735.
- Boyle, E.A., Edmond, J.M. and Sholkovitz, E.R., 1977. Mechanism of iron removal in estuaries. *Geochimica et Cosmochimica Acta*, 41(9): 1313-1324.
- Brosse, E., Margueron, T., Cassou, C., Sanjuan, A., Canham, A., Girard, J.-P., Lacharpagne, J.-C. and Sommer, F., 2003. The formation and stability of kaolinite in Brent sandstone reservoirs: a modelling approach. In: R.H. Worden and S. Morad (Editors), *Clay Mineral Cements in Sandstones*. Special Publication of the International Association of Sedimentologists. Blackwells, Oxford, pp. 383-410.
- Bryant, S., Cade, C. and Mellor, D., 1993. Permeability prediction from geologic models. *American Association of Petroleum Geologists Bulletin*, 77(8): 1338-1350.
- Burley, S.D., 1993. Models of burial diagenesis for deep exploration plays in Jurassic fault traps of the Central and Northern North Sea. In: J.R. Parker (Editor), *Petroleum geology of northwest Europe: proceedings of the 4th conference*. Geological Society, London, pp. 1353-1375.
- Burton, J.H., Krinsley, D.H. and Pye, K., 1987. Authigenesis of kaolinite and chlorite in Texas Gulf-Coast sediments. *Clays and Clay Minerals*, 35(4): 291-296.
- Buurman, P., Jongmans, A.G. and PiPujol, M.D., 1998. Clay illuviation and mechanical clay infiltration - Is there a difference? *Quaternary International*, 51-2: 66-69.
- Cade, C.A., Evans, I.J. and Bryant, S.L., 1994. Analysis of permeability controls - a new approach. *Clay Minerals*, 29(4): 491-501.
- Cao, Z., Liu, G.D., Meng, W., Wang, P. and Yang, C.Y., 2018. Origin of different chlorite occurrences and their effects on tight clastic reservoir porosity. *Journal of Petroleum Science and Engineering*, 160: 384-392.
- Cazier, E.C., Hayward, A.B., Espinoza, G., Velandia, J., Mugniot, J.-F. and Leel, J., W. G. , 1995. Petroleum geology of Cusiana field, Llanos basin foothills, Colombia. *American Association of Petroleum Geologists Bulletin*, 79: 1444-1463.

- Cecil, C.B. and Heald, M.T., 1971. Experimental investigation of effects of grain coatings on quartz growth. *Journal of Sedimentary Petrology*, 41(2): 582-&.
- Chamley, H., 1989. *Clay Sedimentology*. Springer-Verlag.
- Chan, M.A., Parry, W.T. and Bowman, J.R., 2000. Diagenetic hematite and manganese oxides and fault-related fluid flow in Jurassic sandstones, southeastern Utah. *Aapg Bulletin-American Association of Petroleum Geologists*, 84(9): 1281-1310.
- Chang, H.K., Mackenzie, F.T. and Schoonmaker, J., 1986. Comparisons between the diagenesis of dioctahedral and trioctahedral smectite, Brazilian offshore basins. *Clays and Clay Minerals*, 34: 407-423.
- Chen, G.J., Du, G.C., Zhang, G.C., Wang, Q., Lv, C.F. and Chen, J., 2011. Chlorite cement and its effect on the reservoir quality of sandstones from the Panyu low-uplift, Pearl River Mouth Basin. *Petroleum Science*, 8(2): 143-150.
- Cho, M.S. and Fawcett, J.J., 1986. Morphologies and growth mechanisms of synthetic mg-chlorite and cordierite. *American Mineralogist*, 71(1-2): 78-84.
- Churchill, J.M., Poole, M.T., Skarpeid, S.S. and Wakefield, M.I., 2017. Stratigraphic architecture of the Knarr Field, Norwegian North Sea: sedimentology and biostratigraphy of an evolving tide- to wave-dominated shoreline system. In: G.J. Hampson, A.D. Reynolds, B. Kostic and M.R. Wells (Editors), *Sedimentology of Paralic Reservoirs: Recent Advances*. Geological Society Special Publication, pp. 35-58.
- Consonni, A., Frixia, A. and Maragliulo, C., 2018. Hydrothermal dolomitization: simulation by reaction transport modelling. In: P.J. Armitage, A. Butcher, J. Churchill, A. Csoma, C. Hollis, R.H. Lander, J. Omma and R.H. Worden (Editors), *Reservoir Quality of Clastic and Carbonate Rocks: Analysis, Modelling and Prediction*. Special Publication. Geological Society, London, pp. 235-244.
- Curtis, C.D., Hughes, C.R., Whiteman, J.A. and Whittle, C.K., 1985. Compositional variation within some sedimentary chlorites and some comments on their origin. *Mineralogical Magazine*, 49(352): 375-386.
- Curtis, C.D., Ireland, B.J., Whiteman, J.A., Mulvaney, R. and Whittle, C.K., 1984. Authigenic chlorites - problems with chemical analysis and structural formula calculation. *Clay Minerals*, 19(3): 471-481.
- Dalrymple, R.W., Zaitlin, B.A. and Boyd, R., 1992. Estuarine facies models - conceptual models and stratigraphic implications. *Journal of Sedimentary Petrology*, 62(6): 1130-1146.
- Daneshvar, E., 2011. *Role of provenance on clay minerals and their distribution in modern estuaries*, University of Liverpool, 236 pp.
- Daneshvar, E. and Worden, R.H., 2018. Feldspar alteration and Fe minerals: origin, distribution and implications for sandstone reservoir quality in estuarine sediments. In: P.J. Armitage, A.R. Butcher, J.M. Churchill, A.E. Csoma, C. Hollis, R.H. Lander, J.E. Omma and R.H. Worden (Editors), *Reservoir Quality of Clastic and Carbonate Rocks: Analysis, Modelling and Prediction*. Geological Society Special Publication, pp. 123-139.

- De Ros, L.F. and Scherer, C.M.S., 2012. Stratigraphic controls on the distribution of diagenetic processes, quality and heterogeneity of fluvial-aeolian reservoirs from the Reconcavo Basin, Brazil. In: S. Morad, J.M. Ketzer and L.F. DeRos (Editors), *Linking Diagenesis to Sequence Stratigraphy*. Special Publications of the International Association of Sedimentologists. Wiley-Blackwell, Malden, pp. 105-132.
- Decaritat, P., Hutcheon, I. and Walshe, J.L., 1993. Chlorite geothermometry - a review. *Clays and Clay Minerals*, 41(2): 219-239.
- Deer, W.A., Howie, R.A. and Zussman, J., 2013a. Chlorite Group: Clinocllore  $(\text{Mg})_{10}\text{Al}_2[\text{Al}_2\text{Si}_6\text{O}_{20}](\text{OH})_{16}$  - Chamosite  $(\text{Fe}^{2+})_{10}\text{Al}_2[\text{Al}_2\text{Si}_6\text{O}_{20}](\text{OH})_{16}$ . In: W.A. Deer, R.A. Howie and J. Zussman (Editors), *An Introduction to the Rock-Forming Minerals*, Mineralogical Society of Great Britain and Ireland.
- Deer, W.A., Howie, R.A. and Zussman, J., 2013b. *An introduction to the rock-forming minerals*, 3rd edition. The Mineralogical Society, London, 498 pp.
- Dixon, S.A., Summers, D.M. and Surdam, R.C., 1989. Diagenesis and preservation of porosity in Norphlet Formation (Upper Jurassic), Southern Alabama. *American Association of Petroleum Geologists Bulletin*, 73(6): 707-728.
- Dowey, P.J., Hodgson, D.M. and Worden, R.H., 2012. Pre-requisites, processes, and prediction of chlorite grain coatings in petroleum reservoirs: A review of subsurface examples. *Marine and Petroleum Geology*, 32(1): 63-75.
- Dowey, P.J., Worden, R.H., Utley, J. and Hodgson, D.M., 2017. Sedimentary controls on modern sand grain coat formation. *Sedimentary Geology*, 353: 46-63.
- Durand, C., Brosse, E. and Cerepi, A., 2001. Effect of pore-lining chlorite on petrophysical properties of low-resistivity sandstone reservoirs. *SPE Reservoir Evaluation & Engineering*, 4(3): 231-239.
- Durand, C., Rebours, B., Rosenberg, E. and Brosse, E., 2003. Pore lining chlorites in hydrocarbon reservoirs: structure and composition related to their origin. 2001 - a Clay Odyssey, 261-268 pp.
- Dutton, S.P., Hutton, M.E., Ambrose, W.A., Childers, A.T. and Loucks, R.G., 2018. Preservation of reservoir quality by chlorite coats in deep Tuscaloosa sandstones, Centrl Louisiana, USA. . *Gulf Coast Association of Geological Societies*, 7: 46-58.
- Eckert, J.M. and Sholkovitz, E.R., 1976. Flocculation of iron, aluminium and humates from river water by electrolytes. *Geochimica et Cosmochimica Acta*, 40(7): 847-848.
- Ehrenberg, S.N., 1993. Preservation of anomalously high-porosity in deeply buried sandstones by grain coating chlorite - examples from the Norwegian continental shelf. *American Association of Petroleum Geologists Bulletin*, 77(7): 1260-1286.
- Ehrenberg, S.N., Dalland, A., Nadeau, P.H., Mearns, E.W. and Amundsen, H.E.F., 1998. Origin of chlorite enrichment and neodymium isotopic anomalies in Haltenbanken sandstones. *Marine and Petroleum Geology*, 15(5): 403-425.

- Fan, A.P., Yang, R.C., Li, J.B., Zhao, Z.J. and Van Loon, A.J., 2017. Siliceous Cementation of Chlorite-Coated Grains in the Permian Sandstone Gas Reservoirs, Ordos Basin. *Acta Geologica Sinica-English Edition*, 91(3): 1147-1148.
- Fisher, Q.J., Knipe, R. and Worden, R.H., 2000. Microstructures of deformed and non-deformed sandstones from the North Sea: implications for the origins of quartz cements in sandstones. In: R.H. Worden and S. Morad (Editors), *Quartz cementation in sandstones*, Special Publication of the International Association of Sedimentologists. Blackwells, Oxford, pp. 129-146.
- Flemal, R.C., 1969. Iron-bearing heavy minerals in Sespe Formation (California). *Journal of Sedimentary Petrology*, 39(4): 1616-&.
- French, M.W. and Worden, R.H., 2013. Orientation of microcrystalline quartz in the Fontainebleau Formation, Paris Basin and why it preserves porosity. *Sedimentary Geology*, 284: 149-158.
- French, M.W., Worden, R.H., Mariani, E., Larese, R.E., Mueller, R.R. and Kliewer, C.E., 2012. Microcrystalline quartz generation and the preservation of porosity in sandstones: evidence from the Upper Cretaceous of the Sub-Hercynian Basin, Germany. *Journal of Sedimentary Research*, 82(5-6): 422-434.
- Fritz, S.J. and Toth, T.A., 1997. An Fe-berthierine from a Cretaceous laterite .2. Estimation of Eh, pH and pCO<sub>2</sub> conditions of formation. *Clays and Clay Minerals*, 45(4): 580-586.
- Galloway, W.E., 1979. Diagenetic control of reservoir quality in arc-derived sandstones: Implications for petroleum exploration. In: P.A. Scholle and P.R. Schluger (Editors), *Aspects of diagenesis*, SEPM Special Publication. Society and Economic Palaeontologists and Mineralogists, Tulsa, pp. 251-262.
- Genuise, J.J., 1991. Petrography and geochemistry of authigenic chlorite from Cretaceous and Oligocene sandstones of the Texas/Louisiana Gulf Coast, The University of Texas at Austin, 188 pp.
- Gier, S., Worden, R.H. and Krois, P., 2018. Comparing clay mineral diagenesis in interbedded sandstones and mudstones, Vienna Basin, Austria. In: P.J. Armitage, A. Butcher, J. Churchill, A. Csoma, C. Hollis, R.H. Lander, J. Omma and R.H. Worden (Editors), *Reservoir Quality of Clastic and Carbonate Rocks: Analysis, Modelling and Prediction*. Special Publication. Geological Society, London, pp. 389-404.
- Giles, M.R., Indrelid, S.L., Beynon, G.V. and Amthor, J., 2000. The origin of large-scale quartz cementation: evidence from large data sets and coupled heat-fluid mass transport modelling. In: R.H. Worden and S. Morad (Editors), *Quartz cement in sandstones*, Special Publication of the International Association of Sedimentologists. Blackwells, Oxford, pp. 21-38.
- Giles, M.R., Stevenson, S., Martin, S.V., Cannon, S.J.C., Hamilton, P.J., Marshall, J.D. and Samways, G.M., 1992. The reservoir properties and diagenesis of the Brent Group: a regional perspective. In: A.C. Morton, R.S. Haszeldine, M.R. Giles and S. Brown (Editors), *Geology of the Brent Group*. Special Publication. Geological Society Special Publications. Geological Society, London, pp. 289-327.

- Gingele, F.X., De Deckker, P. and Hillenbrand, C.-D., 2001. Clay mineral distribution in surface sediments between Indonesia and NW Australia—source and transport by ocean currents. *Marine Geology*, 179(3): 135-146.
- Golab, A., Arena, A., Barranco, I., Salazar-Tio, R., Hamilton, J., Idowu, N., Rajan, P., Sommanal, S., Young, B., Carnerup, A., Schembre-McCabe, J.M. and Boyle, K., 2015. Mineralogical and petrophysical characterisation of a fine-grained sandstone with significant clay coating using 3d micro-ct and sem imaging from a 5 mm plug, AAPG/SEG International Conference & Exhibition, Search and Discovery Article #41756 (2015). AAPG, Melbourne, Australia.
- Gould, K., Pe-Piper, G. and Piper, D.J.W., 2010. Relationship of diagenetic chlorite rims to depositional facies in Lower Cretaceous reservoir sandstones of the Scotian Basin. *Sedimentology*, 57(2): 587-610.
- Griffiths, J., Faulkner, D.R., Edwards, A.P. and Worden, R.H., 2018a. Deformation band development as a function of intrinsic host-rock properties in Triassic Sherwood Sandstone. In: P.J. Armitage, A. Butcher, J. Churchill, A. Csoma, C. Hollis, R.H. Lander, J. Omma and R.H. Worden (Editors), *Reservoir Quality of Clastic and Carbonate Rocks: Analysis, Modelling and Prediction*. Special Publication. Geological Society, London, pp. 161-176.
- Griffiths, J., Worden, R.H., Wooldridge, L.J., Utley, J.E. and Duller, R.A., 2019a. Compositional variation in modern estuarine sands: predicting major controls on sandstone reservoir quality. *AAPG Bulletin*, 103(4): 797-833.
- Griffiths, J., Worden, R.H., Wooldridge, L.J., Utley, J.E.P. and Duller, R.A., 2018b. Detrital clay coats, clay minerals, and pyrite: a modern shallow-core analogue for ancient and deeply buried estuarine sandstones. *Journal of Sedimentary Research*, 88(10): 1205-1237.
- Griffiths, J., Worden, R.H., Wooldridge, L.J., Utley, J.E.P. and Duller, R.A., 2019b. Compositional variation in modern estuarine sands: Predicting major controls on sandstone reservoir quality. *American Association of Petroleum Geologists Bulletin*, 103(4): 797-833.
- Griffiths, J., Worden, R.H., Wooldridge, L.J., Utley, J.E.P., Duller, R.A. and Edge, R.L., 2019c. Estuarine clay mineral distribution: Modern analogue for ancient sandstone reservoir quality prediction. *Sedimentology*, 66(6): 2011-2047.
- Grigsby, J.D., 2001. Origin and growth mechanism of authigenic chlorite in sandstones of the lower Vicksburg Formation, South Texas. *Journal of Sedimentary Research*, 71(1): 27-36.
- Grigsby, J.D. and Langford, R.P., 1996. Effects of diagenesis on enhanced-resolution bulk density logs in Tertiary Gulf Coast sandstones: An example from the lower Vicksburg Formation, McAllen Ranch field, south Texas. *American Association of Petroleum Geologists Bulletin*, 80(11): 1801-1819.
- Hanor, J.S. and McIntosh, J.C., 2007. Diverse origins and timing of formation of basinal brines in the Gulf of Mexico sedimentary basin. *Geofluids*, 7(2): 227-237.
- Harrison, W.J. and Thyne, G.D., 1992. Predictions of diagenetic reactions in the presence of organic acids. *Geochimica et Cosmochimica Acta*, 56(2): 565-586.
- Hartmann, J., West, A.J., Renforth, P., Kohler, P., De La Rocha, C.L., Wolf-Gladrow, D.A., Durr, H.H. and Scheffran, J., 2013. Enhanced chemical weathering as a geoengineering strategy to



- reduce atmospheric carbon dioxide, supply nutrients, and mitigate ocean acidification. *Reviews of Geophysics*, 51(2): 113-149.
- Heald, M.T. and Anderegg, R.C., 1960. Differential cementation in the Tuscarora sandstones. *Journal of Sedimentary Petrology*, 30: 568-577.
- Heald, M.T. and Larese, R.E., 1974. Influence of coatings on quartz cementation. *Journal of Sedimentary Petrology*, 44(4): 1269-1274.
- Henn, F., Durand, C., Cerepi, A., Brosse, E. and Giuntini, J.C., 2007. DC conductivity, cationic exchange capacity, and specific surface area related to chemical composition of pore lining chlorites. *Journal of Colloid and Interface Science*, 311(2): 571-578.
- Herringshaw, L.G. and McIlroy, D., 2013. Bioinfiltration irrigation-driven transport of clay particles through bioturbated sediments. *Journal of Sedimentary Research*, 83(5-6): 443-450.
- Hey, M.H., 1954. A new review of the chlorites. *Mineralogical Magazine and Journal of the Mineralogical Society*, 30(224): 277-292.
- Hill, I.G., Worden, R.H. and Meighan, I.G., 2000. Geochemical evolution of a palaeolaterite: the Interbasaltic Formation, Northern Ireland. *Chemical Geology*, 166(1-2): 65-84.
- Hillier, S., 1994. Pore-lining chlorite in siliciclastic reservoir sandstones - electron microprobe, SEM and XRD data, implications for their origin. *Clay Minerals*, 29(4): 665-679.
- Hillier, S., 2003. Quantitative analysis of clay and other minerals in sandstones by X-ray powder diffraction (XRPD). In: R.H. Worden and S. Morad (Editors), *Clay mineral cements in sandstones*, Special Publication of the International Association of Sedimentologists. Blackwells, Oxford, pp. 213-252.
- Hillier, S., Fallick, A.E. and Matter, A., 1996. Origin of pore-lining chlorite in the aeolian Rotliegend of northern Germany. *Clay Minerals*, 31(2): 153-171.
- Hillier, S. and Velde, B., 1992. Chlorite interstratified with a 7-A mineral - and example from offshore Norway and possible implications for the interpretation of diagenetic chlorites. *Clay Minerals*, 27(4): 475-486.
- Hirst, J.P.P., Davis, N., Palmer, A.F., Achache, D. and Riddiford, F.A., 2001. The 'tight gas' challenge: appraisal results from the Devonian of Algeria. *Petroleum Geoscience*, 7(1): 13-21.
- Hornibrook, E.R.C. and Longstaffe, F.J., 1996. Berthierine from the Lower Cretaceous Clearwater Formation, Alberta, Canada. *Clays and Clay Minerals*, 44(1): 1-21.
- Houseknecht, D.W., 1984. Influence of grain-size and temperature on intergranular pressure solution, quartz cementation and porosity in quartzose sandstones. *Journal of Sedimentary Petrology*, 54(2): 348-361.
- Huggett, J.M., Burley, S.D., Longstaffe, F.J., Saha, S. and Oates, M.J., 2015. The nature and origin of authigenic chlorite and related cements in Oligo-Miocene reservoir sandstones, Tapti gas fields, Surat Depression, offshore Western India. *Journal of Petroleum Geology*, 38(4): 383-409.

- Humphreys, B., Kemp, S.J., Lott, G.K., Bermanto, Dharmayanti, D.A. and Samsori, I., 1994. Origin of grain-coating chlorite by smectite transformation - an example from Miocene sandstones, North Sumatra Back-Arc Basin, Indonesia. *Clay Minerals*, 29(4): 681-692.
- Humphreys, B., Smith, S.A. and Strong, G.E., 1989. Authigenic chlorite in Late Triassic sandstones from the Central Graben, North-Sea. *Clay Minerals*, 24(2): 427-444.
- Hunt, J.M., 1995. *Petroleum geochemistry and geology*. W. H. Freeman and Company, New York.
- Jahren, J., Olsen, E. and Bjørlykke, K., 1998. Chlorite coatings in deeply buried sandstones - Examples from the Norwegian continental shelf. *Water-Rock Interaction*, 321-324 pp.
- Jahren, J.S. and Aagaard, P., 1989. Compositional variations in diagenetic chlorites and illites, and relationships with formation water chemistry. *Clay Minerals*, 24: 209-213.
- Jiang, L., Cai, C.F., Worden, R.H., Crowley, S.F., Jia, L.Q., Zhang, K. and Duncan, I.J., 2016. Multiphase dolomitization of deeply buried Cambrian petroleum reservoirs, Tarim Basin, north-west China. *Sedimentology*, 63(7): 2130-2157.
- Jiang, L., Worden, R.H., Cai, C.F., Li, K.K., Xiang, L., Cai, L.L. and He, X.Y., 2014. Dolomitization of gas reservoirs: the Upper Permian Changxing and Lower Triassic Feixianguan Formations, northeast Sichuan Basin, China. *Journal of Sedimentary Research*, 84(10): 792-815.
- Jones, S., 2017. Goo, glue, and grain binding: Importance of biofilms for diagenesis in sandstones. *Geology*, 45(10): 959-960.
- Ketzer, J.M., Holz, M., Morad, S. and Al-Aasm, I.S., 2003. Sequence stratigraphic distribution of diagenetic alterations in coal-bearing, paralic sandstones: evidence from the Rio Bonito Formation (early Permian), southern Brazil. *Sedimentology*, 50(5): 855-877.
- King, H.M., 2019. Chlorite, On line encyclopedia at: <https://geology.com/minerals/chlorite.shtml>.
- Konhauser, K.O. and Urrutia, M.M., 1999. Bacterial clay authigenesis: a common biogeochemical process. *Chemical Geology*, 161(4): 399-413.
- Krauskopf, K.B., 1979. *Introduction to geochemistry*. McGraw-Hill, Tokyo.
- Lander, R.H., Larese, R.E. and Bonnell, L.M., 2008. Toward more accurate quartz cement models: The importance of euhedral versus noneuhedral growth rates. *American Association of Petroleum Geologists Bulletin*, 92(11): 1537-1563.
- Lander, R.H. and Walderhaug, O., 1999. Predicting porosity through simulating sandstone compaction and quartz cementation. *American Association of Petroleum Geologists Bulletin*, 83(3): 433-449.
- Line, L.H., Jahren, J. and Hellevang, H., 2018. Mechanical compaction in chlorite-coated sandstone reservoirs - Examples from Middle - Late Triassic channels in the southwestern Barents Sea. *Marine and Petroleum Geology*, 96: 348-370.
- Liu, X.W. and Millero, F.J., 2002. The solubility of iron in seawater. *Marine Chemistry*, 77(1): 43-54.
- Longhitano, S.G., Mellere, D., Steel, R.J. and Ainsworth, R.B., 2012. Tidal depositional systems in the rock record: A review and new insights. *Sedimentary Geology*, 279: 2-22.

- Lundegard, P.D., 1992. Sandstone porosity loss - a big picture view of the importance of compaction. *Journal of Sedimentary Petrology*, 62(2): 250-260.
- Ma, P.J., Lin, C.Y., Zhang, S.Q., Dong, C.M. and Xu, Y.F., 2017. Formation of chlorite rims and the impact of pore-lining chlorite on reservoir quality: a case study from Shiqianfeng sandstones in upper Permian of Dongpu Depression, Bohai Bay Basin, eastern China. *Australian Journal of Earth Sciences*, 64(6): 825-839.
- Macaulay, C.I., Fallick, A.E., Haszeldine, R.S. and McAulay, G.E., 2000. Oil migration makes the difference: regional distribution of carbonate cement delta C-13 in northern North Sea Tertiary sandstones. *Clay Minerals*, 35(1): 69-76.
- Marchand, A.M.E., Haszeldine, R.S., Macaulay, C.I., Swennen, R. and Fallick, A.E., 2000. Quartz cementation inhibited by crestal oil charge: Miller deep water sandstone, UK North Sea. *Clay Minerals*, 35(1): 201-210.
- Markussen, O., Dypvik, H., Hammer, E., Long, H.L. and Hammer, O., 2019. 3D characterization of porosity and authigenic cementation in Triassic conglomerates/arenites in the Edvard Grieg field using 3D micro-CT imaging. *Marine and Petroleum Geology*, 99: 265-281.
- Martinius, A.W., Kaas, I., Naess, A., Helgesen, G. and Kjaerefjord, J.M., 2001. Sedimentology of the heterolithic and tide-dominated Tilje Formation. In: O.J. Martinsen and T. Dreyer (Editors), *Proceedings of the Norwegian Petroleum Society Conference volume 10: Sedimentary Environments Offshore Norway — Palaeozoic to Recent*. Norwegian Petroleum Society, Oslo, pp. 103-144.
- Matlack, K.S., Houseknecht, D.W. and Applin, K.R., 1989. Emplacement of clay into sand by infiltration. *Journal of Sedimentary Petrology*, 59(1): 77-87.
- McIlroy, D., Worden, R.H. and Needham, S.J., 2003. Faeces, clay minerals and reservoir potential. *Journal of the Geological Society*, 160: 489-493.
- McKinley, J.M., Worden, R.H. and Ruffell, A.H., 2003. Smectite in sandstones: A review of the controls on occurrence and behaviour during diagenesis. In: R.H. Worden and S. Morad (Editors), *Clay mineral cements in sandstones*, Special Publication of the International Association of Sedimentologists. Blackwells, Oxford, pp. 109-128.
- McMurchy, R.C., 1934. The crystal structure of the chlorite minerals. *Zeitschrift Fur Kristallographie*, 88(5/6): 420-432.
- Meunier, A., 2005. *Clays*. Springer-Verlag, Berlin.
- Moore, D.M. and Reynolds Jr., R.C., 1997. *X-ray diffraction and the identification and analysis of clay minerals*. Oxford University Press, Oxford, 378 pp.
- Morad, S., Al-Ramadan, K., Ketzer, J.M. and De Ros, L.F., 2010. The impact of diagenesis on the heterogeneity of sandstone reservoirs: A review of the role of depositional facies and sequence stratigraphy. *American Association of Petroleum Geologists Bulletin*, 94(8): 1267-1309.
- Morad, S. and Aldahan, A.A., 1986. Diagenetic alteration of detrital biotite in proterozoic sedimentary-rocks from Sweden. *Sedimentary Geology*, 47(1-2): 95-107.

- Moraes, M.A.S. and De Ros, L.F., 1990. Infiltrated clays in fluvial Jurassic sandstones of Recôncavo Basin, northeastern Brazil. *Journal of Sedimentary Petrology*, 60: 809-819.
- Moraes, M.A.S. and De Ros, L.F., 1992. Depositional, infiltrated and authigenic clays in fluvial sandstones of the Jurassic Sergie Formation, Reconcavo Basin, northeastern Brazil, In: Origin, diagenesis and petrophysics of clay minerals in sandstones (eds. Houseknecht, D.W. and Pittman, E.D.) SEPM Special Publication, pp. 197-208.
- Morton, A.C. and Hallsworth, C.R., 1999. Processes controlling the composition of heavy mineral assemblages in sandstones. *Sedimentary Geology*, 124(1-4): 3-29.
- Mu, N.N., Schulz, H.M., Fu, Y.J., Schovsbo, N.H., Wirth, R., Rhede, D. and van Berk, W., 2015. Berthierine formation in reservoir rocks from the Siri oilfield (Danish North Sea) as result of fluid-rock interactions: Part I. Characterization. *Marine and Petroleum Geology*, 65: 302-316.
- Muffler, L.J.P. and White, D.E., 1969. Active metamorphism of Upper Cenozoic sediments in the salton Sea geothermal field and the Salton Trough, Southeastern California. *Geological Society of America Bulletin*, 94: 161-180.
- Mullis, A.M. and Haszeldine, R.S., 1995. Numerical modeling of diagenetic quartz hydrogeology at a graben edge - Brent oil fields, North Sea. *Journal of Petroleum Geology*, 18(4): 421-438.
- Munawar, M.J., Lin, C.Y., Cnudde, V., Bultreys, Y., Dong, C., Zhang, X., De Boever, W., Zahid, M.A. and Wu, Y., 2018. Petrographic characterization to build an accurate rock model using micro-CT: Case study on low-permeable to tight turbidite sandstone from Eocene Shahejie Formation. *Micron*, 109: 22-33.
- Needham, S.J., Worden, R.H. and Cuadros, J., 2006. Sediment ingestion by worms and the production of bio-clays: a study of macrobiologically enhanced weathering and early diagenetic processes. *Sedimentology*, 53(3): 567-579.
- Needham, S.J., Worden, R.H. and McIlroy, D., 2004. Animal-sediment interactions: the effect of ingestion and excretion by worms on mineralogy. *Biogeosciences*, 1(2): 113-121.
- Needham, S.J., Worden, R.H. and McIlroy, D., 2005. Experimental production of clay rims by macrobiotic sediment ingestion and excretion processes. *Journal of Sedimentary Research*, 75(6): 1028-1037.
- Nichols, G., 2009. *Sedimentology and stratigraphy*. Wiley-Blackwell.
- Nicolas, G., Pradier, B. and Vannier-Petit, F., 1997. Reconstruction of depositional environments of delta plain organic sediments. Application to the sedimentology of the Brent Group (North Sea). *Bulletin Des Centres De Recherches Exploration-Production Elf Aquitaine*, 21(1): 249-264.
- Niu, B., Yoshimura, T. and Hirai, A., 2000. Smectite diagenesis in neogene marine sandstone and mudstone of the Niigata basin, Japan. *Clays and Clay Minerals*, 48(1): 26-42.
- Odin, G.S. (Editor), 1988. *Green Marine Clays*. Elsevier, Amsterdam.
- Odin, G.S., 1990. Clay mineral formation at the continent-ocean boundary - the verdine facies. *Clay Minerals*, 25(4): 477-483.

- Osborne, M.J. and Swarbrick, R.E., 1999. Diagenesis in North Sea HPHT elastic reservoirs - consequences for porosity and overpressure prediction. *Marine and Petroleum Geology*, 16(4): 337-353.
- Parker, R.L., 1967. Chapter D. Composition of the Earth's crust, USGS, Washington.
- Parry, W.T., Chan, M.A. and Beitler, B., 2004. Chemical bleaching indicates episodes of fluid flow in deformation bands in sandstone. *American Association of Petroleum Geologists Bulletin*, 88(2): 175-191.
- Paxton, S.T., Szabo, J.O., Ajdukiewicz, J.M. and Klimentidis, R.E., 2002. Construction of an intergranular volume compaction curve for evaluating and predicting compaction and porosity loss in rigid-grain sandstone reservoirs. *American Association of Petroleum Geologists Bulletin*, 86(12): 2047-2067.
- Pe-Piper, G. and Weir-Murphy, S., 2008. Early diagenesis of inner-shelf phosphorite and iron-silicate minerals, Lower Cretaceous of the Orpheus graben, southeastern Canada: Implications for the origin of chlorite rims. *American Association of Petroleum Geologists Bulletin*, 92(9): 1153-1168.
- Pearce, J., Czernichowski-Lauriol, I., Lombardi, S., Brune, S., Nador, A., Baker, J., Pauwels, H., Hatziannis, G., Beaubien, S. and Faber, E., 2004. A review of natural CO<sub>2</sub> accumulations in Europe as analogues for geological sequestration. In: S.J. Baines and R.H. Worden (Editors), *Geological storage of carbon dioxide*. Special Publication. Geological Society, London, pp. 29-41.
- Peng, J., Liu, J.K., Wang, Y. and Liu, J.F., 2009. Origin and controlling factors of chlorite coatings-an example from the reservoir of T(3)x Group of the Baojie area, Sichuan Basin, China. *Petroleum Science*, 6(4): 376-382.
- Peters, E.J., 2012. *Advanced petrophysics: geology, porosity, absolute permeability, heterogeneity and geostatistics*, 1. Live Oak Book Company, Austin, 229 pp.
- Pittman, E.D., 1992. Relationship of porosity and permeability to various parameters derived from mercury injection-capillary pressure curves for sandstone. *American Association of Petroleum Geologists Bulletin*, 76(2): 191-198.
- Pittman, E.D., Larese, R.E. and Heald, M.T., 1992. Clay coats: occurrence and relevance to preservation of porosity in sandstones. In: *Origin, diagenesis and petrophysics of clay minerals in sandstones* (eds. Houseknecht, D.W. and Pittman, E.D.) SEPM Special Publication, 47: 241-255.
- Pittman, E.D. and Lumsden, D.N., 1968. Relationship between chlorite coatings on quartz grains and porosity, Spiro Sand, Oklahoma. *Journal of Sedimentary Research*, 38(2): 668-670.
- Porter, J.R., Knipe, R.J., Fisher, Q.J., Farmer, A.B., Allin, N.S., Jones, L.S., Palfrey, A.J., Garrett, S.W. and Lewis, G., 2000. Deformation processes in the Britannia Field, UKCS. *Petroleum Geoscience*, 6(3): 241-254.
- Poteet, J.E., Goldstein, R.H. and Franseen, E.K., 2018. Diagenetic controls on location of reservoir spots relative to paleotopographic and structural highs. In: P.J. Armitage, A. Butcher, J. Churchill, A. Csoma, C. Hollis, R.H. Lander, J. Omma and R.H. Worden (Editors), *Reservoir*

Quality of Clastic and Carbonate Rocks: Analysis, Modelling and Prediction. Special Publication. Geological Society, London, pp. 177-215.

- Pratama, E., Ismail, M.S. and Ridha, S., 2017. An integrated workflow to characterize and evaluate low resistivity pay and its phenomenon in a sandstone reservoir. *Journal of Geophysics and Engineering*, 14(3): 513-519.
- Primmer, T.J., Cade, C.A., Evans, J., Gluyas, J., Hopkins, M.S., Oxtoby, N., Smalley, P.C., Warren, E.A. and Worden, R.H., 1997. Global patterns in sandstone diagenesis: their application to reservoir quality prediction for petroleum exploration In: J.A. Kupecz, J. Gluyas and S. Bloch (Editors), *Reservoir quality prediction in sandstones and carbonates*. AAPG Memoir. American Association of Petroleum Geologists, Tulsa, pp. 61-78.
- Pryor, W.A., 1975. Biogenic sedimentation and alteration of argillaceous sediments in shallow marine environments. *Geological Society of America Bulletin*, 86: 1244-1254.
- Quirein, J.A., Gardner, J.S. and Watson, J.T., 1982. Combined Natural Gamma Ray Spectral/Litho-Density Measurements Applied to Complex Lithologies, SPE Annual Technical Conference and Exhibition. Society of Petroleum Engineers, New Orleans, Louisiana, pp. 14.
- Rabbani, A. and Jamshidi, S., 2014. Specific surface and porosity relationship for sandstones for prediction of permeability. *International Journal of Rock Mechanics and Mining Sciences*, 71: 25-32.
- Ramm, M., Forsberg, A.W. and Jahren, J., 1997. Porosity-depth trends in deeply buried Upper Jurassic Reservoirs in the Norwegian Central Graben: an example of porosity preservation beneath the normal economic basement by grain coating microquartz. In: *Reservoir quality prediction in sandstones and carbonates* (eds. Kupecz, J.A., Gluyas, J. and Bloch, S.) AAPG Memoir, 69: 177-200.
- Rateev, M.A., Sadchikova, T.A. and Shabrova, V.P., 2008. Clay minerals in recent sediments of the World Ocean and their relation to types of lithogenesis. *Lithology and Mineral Resources*, 43(2): 125-135.
- Rider, M. and Kennedy, M.J., 2011. *The geological interpretation of well logs*. Rider-French Consulting, Cambridge.
- Ruau, O., Pradier, B., Landais, P. and Gardette, J.L., 1996. Influence of the conditions of deposition on the chemistry and the reflectance variations of the Brent coals. *Organic Geochemistry*, 25(5-7): 325-339.
- Ryan, P.C., Conrad, M.E., Brown, K., Chamberlain, C.P. and Reynolds, R.C., 1998. Oxygen isotope compositions of mixed-layer serpentine-chlorite and illite-smectite in the Tuscaloosa Formation (US Gulf Coast): Implications for pore fluids and mineralogic reactions. *Clays and Clay Minerals*, 46(4): 357-368.
- Ryan, P.C. and Hillier, S., 2002. Berthierine/chamosite, corrensite, and discrete chlorite from evolved verdine and evaporite-associated facies in the Jurassic Sundance Formation, Wyoming. *American Mineralogist*, 87(11-12): 1607-1615.
- Ryan, P.C. and Reynolds, R.C., 1996. The origin and diagenesis of grain-coating serpentine-chlorite in Tuscaloosa Formation sandstone, US Gulf Coast. *American Mineralogist*, 81(1-2): 213-225.

- Ryan, P.C. and Reynolds, R.C., 1997. The chemical composition of serpentine/chlorite in the tuscaloosa formation, United States Gulf Coast: EDX vs. XRD determinations, implications for mineralogic reactions and the origin of anatase. *Clays and Clay Minerals*, 45(3): 339-352.
- Saiag, J., Brigaud, B., Portier, E., Desaubliaux, G., Bucherie, A., Miska, S. and Pagel, M., 2016. Sedimentological control on the diagenesis and reservoir quality of tidal sandstones of the Upper Cape Hay Formation (Permian, Bonaparte Basin, Australia). *Marine and Petroleum Geology*, 77: 597-624.
- Saner, S., Hassan, H.M., Al-Ramadan, K.A. and Abdulghani, W.M., 2006. Mineralogical, pore and petrophysical characteristics of the Devonian Jauf sandstone reservoir, Hawiyah field, Eastern Saudi Arabia. *Journal of Petroleum Geology*, 29(3): 257-272.
- Sanjuan, B., Girard, J.P., Lanini, S., Bourguignon, A. and Brosse, E., 2003. Geochemical modelling of diagenetic illite and quartz cement formation in Brent sandstone reservoirs: example of the Hild Field, Norwegian North Sea. In: R.H. Worden and S. Morad (Editors), *Clay Mineral Cements in Sandstones*. Special Publication of the International Association of Sedimentologists. Blackwells, Oxford, pp. 425-452.
- Šegvić, B., Zanoni, G. and Moscariello, A., 2020 in press. On the origins of eogenetic chlorite in verdine facies sedimentary rocks from the Gabon Basin in West Africa. *Marine and Petroleum Geology*.
- Shedid, S.A. and Saad, M.A., 2017. Comparison and sensitivity analysis of water saturation models in shaly sandstone reservoirs using well logging data. *Journal of Petroleum Science and Engineering*, 156: 536-545.
- Sheldon, H.A., Wheeler, J., Worden, R.H. and Cheadle, M.J., 2003. An analysis of the roles of stress, temperature, and pH in chemical compaction of sandstones. *Journal of Sedimentary Research*, 73(1): 64-71.
- Sholkovitz, E.R., 1976. Flocculation of dissolved organic and inorganic matter during mixing of river water and seawater. *Geochimica et Cosmochimica Acta*, 40(7): 831-845.
- Sholkovitz, E.R., 1978. The flocculation of dissolved Fe, Mn, Al, Cu, Ni, Co and Cd during estuarine mixing. *Earth and Planetary Science Letters*, 41: 77-86.
- Sholkovitz, E.R., Boyle, E.A. and Price, N.B., 1978. Removal of dissolved humic acids and iron during estuarine mixing. *Earth and Planetary Science Letters*, 40(1): 130-136.
- Skarpeid, S.S., Churchill, J.M., Hilton, J.P.J., Izatt, C.N. and Poole, M.T., 2017. The Knarr Field: a new development at the northern edge of the North Sea, Geological Society, London, *Petroleum Geology Conference series*. Geological Society of London, pp. PGC8. 23.
- Skolasinska, K., 2006. Clogging microstructures in the vadose zone—laboratory and field studies. *Hydrogeology Journal*, 14: 1005-1017.
- Smith, J.T. and Ehrenberg, S.N., 1989. Correlation of carbon dioxide abundance with temperature in clastic hydrocarbon reservoirs - relationship to inorganic chemical equilibrium. *Marine and Petroleum Geology*, 6(2): 129-135.

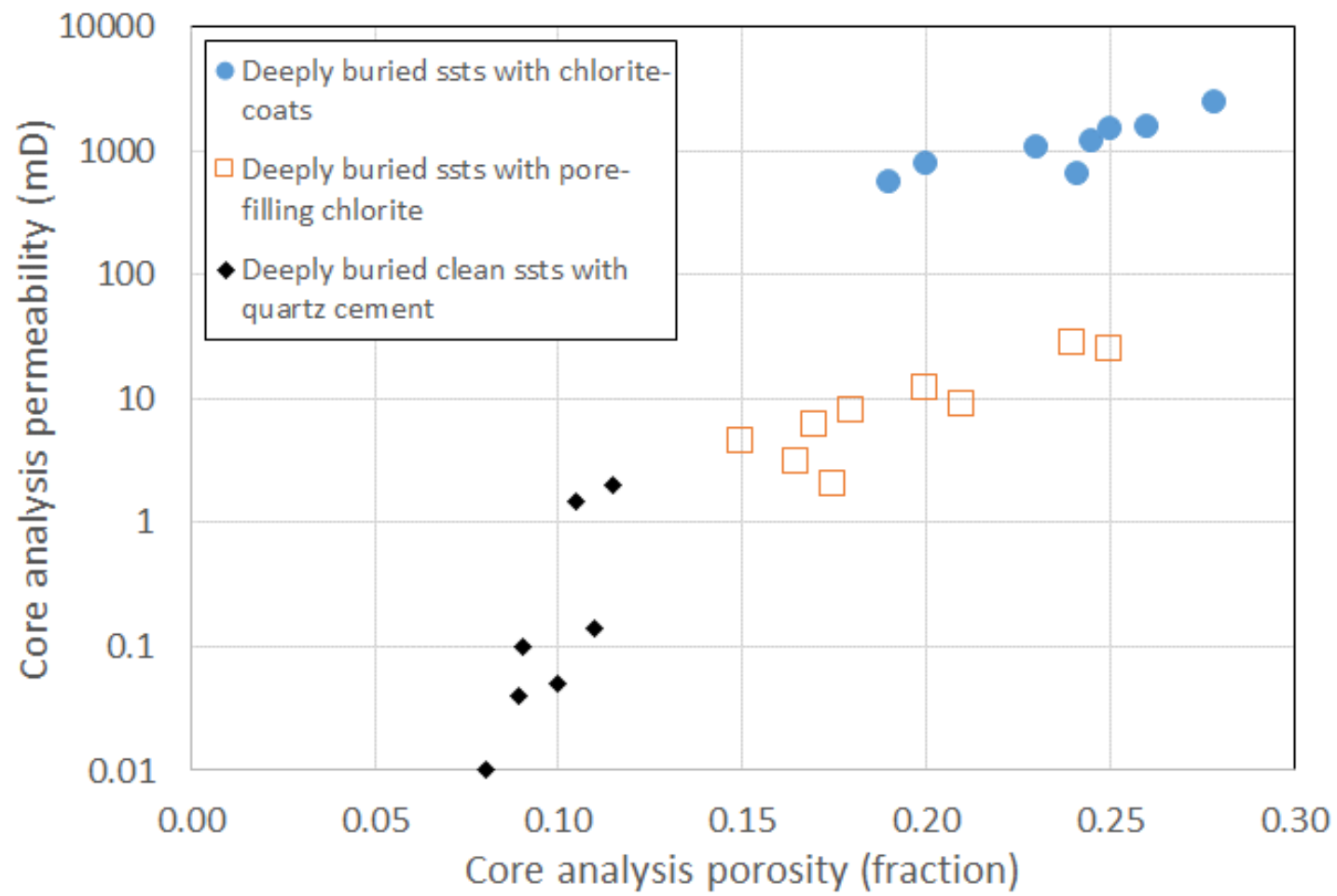
- Spotl, C., Houseknecht, D.W. and Longstaffe, F.J., 1994. Authigenic chlorite in sandstones as indicators of high temperature diagenesis, Arkoma Foreland Basin, USA. *Journal of Sedimentary Research Section a-Sedimentary Petrology and Processes*, 64(3): 553-566.
- Stricker, S. and Jones, S.J., 2018. Enhanced porosity preservation by pore fluid overpressure and chlorite grain coatings in the Triassic Skagerrak, Central Graben, North Sea, UK. In: P.J. Armitage, A.R. Butcher, J.M. Churchill, A.E. Csoma, C. Hollis, R.H. Lander, J.E. Omma and R.H. Worden (Editors), *Reservoir Quality of Clastic and Carbonate Rocks: Analysis, Modelling and Prediction*. Geological Society Special Publication, pp. 321-341.
- Stricker, S., Jones, S.J. and Grant, N.T., 2016. Importance of vertical effective stress for reservoir quality in the Skagerrak Formation, Central Graben, North Sea. *Marine and Petroleum Geology*, 78: 895-909.
- Sun, Z.X., Sun, Z.L., Yao, J., Wu, M.L., Liu, J.R., Dou, Z.Y. and Pei, C.R., 2014. Porosity preservation due to authigenic chlorite coatings in deeply buried Triassic Xujiache Sandstones, Sichuan Basin, Western China. *Journal of Petroleum Geology*, 37(3): 251-267.
- Taylor, A.M. and Goldring, R., 1993. Description and analysis of bioturbation and ichnofabrics. *Journal of the Geological Society*, 150: 141-148.
- Taylor, K.G., Simo, J.A., Yocum, D. and Leckie, D.A., 2002. Stratigraphic significance of ooidal ironstones from the Cretaceous Western Interior Seaway: The Peace River Formation, Alberta, Canada, and the Castlegate Sandstone, Utah, USA. *Journal of Sedimentary Research*, 72(2): 316-327.
- Thomson, A., 1979. Preservation of porosity in the deep Woodbine/Tuscaloosa trend, Louisiana. *Transactions of the Gulf Coast Association of Geological Societies*, 29: 396-403.
- Thomson, A., 1982. Preservation of porosity in the deep Woodbine Tuscaloosa Trend, Louisiana. *Journal of Petroleum Technology*, 34(5): 1156-1162.
- Tiab, D. and Donaldson, E.C., 2015. *Petrophysics*, 4th edition. Elsevier, Amsterdam, 894 pp.
- Toth, T.A. and Fritz, S.J., 1997. An Fe-berthierine from a Cretaceous laterite .1. Characterization. *Clays and Clay Minerals*, 45(4): 564-579.
- Tudge, J., Lovell, M., Davies, S. and Millar, M., 2014. A novel integrated approach to estimating hydrocarbon saturation in the presence of pore-lining chlorites. *Petroleum Geoscience*, 20(2): 201-209.
- Vanhouten, F.B., 1992. Review of Cenozoic ooidal ironstones. *Sedimentary Geology*, 78(1-2): 101-110.
- Velde, B., 1985. *Clay minerals*. Elsevier, Amsterdam.
- Walderhaug, O., 1990. A fluid inclusion study of quartz cemented sandstones from offshore mid-Norway - possible evidence for continued quartz cementation during oil emplacement. *Journal of Sedimentary Petrology*, 60(2): 203-210.
- Walderhaug, O., 1994a. Precipitation rates for quartz cement in sandstones determined by fluid inclusion microthermometry and temperature history modelling. *Journal of Sedimentary Research Section a-Sedimentary Petrology and Processes*, 64(2): 324-333.



- Walderhaug, O., 1994b. Temperatures of quartz cementation in Jurassic sandstones from the Norwegian continental shelf - evidence from fluid inclusions. *Journal of Sedimentary Research Section a-Sedimentary Petrology and Processes*, 64(2): 311-323.
- Walderhaug, O., Lander, R.H., Bjørkum, P.A., Oelkers, E.H., Bjørlykke, K. and Nadeau, P.H., 2000. Modelling quartz cementation and porosity in reservoir sandstones: examples from the Norwegian continental shelf. In: R.H. Worden and S. Morad (Editors), *Quartz cementation in sandstones*, Special Publication of the International Association of Sedimentologists. Blackwells, Oxford, pp. 39-50.
- Walderhaug, O. and Porten, K.W., 2007. Stability of detrital heavy minerals on the norwegian continental shelf as a function of depth and temperature. *Journal of Sedimentary Research*, 77(11-12): 992-1002.
- Warren, E.A. and Pulham, A.J., 2001. Anomalous porosity and permeability preservation in deeply buried tertiary and mesozoic sandstones in the Cusiana Field, Llanos foothills, Colombia. *Journal of Sedimentary Research*, 71(1): 2-14.
- Warren, E.A. and Smalley, P.C., 1994. North Sea formation water atlas. *Geological Society of London Memoir*, 15: 208.
- Weibel, R., 1999. Effects of burial on the clay assemblages in the Triassic Skagerrak Formation, Denmark. *Clay Minerals*, 34(4): 619-635.
- Wentworth, C.K., 1922. A scale of grade class terms for clastic sediments. *Journal of Geology*, 30: 377-392.
- Whittle, C.K., 1986. Comparison of sedimentary chlorite compositions by X-ray-diffraction and analytical TEM. *Clay Minerals*, 21(5): 937-947.
- Wooldridge, L.J., Worden, R.H., Griffiths, J., Thompson, A. and Chung, P., 2017a. Biofilm origin of clay-coated sand grains. *Geology*, 45(10): 875-878.
- Wooldridge, L.J., Worden, R.H., Griffiths, J. and Utley, J.E.P., 2017b. Clay-coated sand grains in petroleum reservoirs: Understanding their distribution via a modern analogue. *Journal of Sedimentary Research*, 87(4): 338-352.
- Wooldridge, L.J., Worden, R.H., Griffiths, J. and Utley, J.E.P., 2018. The origin of clay-coated sand grains and sediment heterogeneity in tidal flats. *Sedimentary Geology*, 373: 191-209.
- Wooldridge, L.J., Worden, R.H., Griffiths, J. and Utley, J.E.P., 2019a. Clay coat diversity in marginal marine sediments. *Sedimentology*, 66: 1118-1138.
- Wooldridge, L.J., Worden, R.H., Griffiths, J. and Utley, J.E.P., 2019b. How to quantify clay-coat grain coverage in modern and ancient sediments. *Journal of Sedimentary Research*, 89: 135-146.
- Worden, R.H., 2018. Halogen elements in sedimentary systems and their evolution during diagenesis. In: D. Harlov, E. and L. Aranovich (Editors), *Role of Halogens in Terrestrial and Extraterrestrial Processes: Surface Crust and Mantle*. Springer, Berlin, pp. 185-260.
- Worden, R.H., Armitage, P.J., Butcher, A., Churchill, J., Csoma, A., Hollis, C., Lander, R.H. and Omma, J., 2018a. Petroleum reservoir quality prediction: overview and contrasting approaches from sandstone and carbonate communities. In: P.J. Armitage, A. Butcher, J. Churchill, A. Csoma,

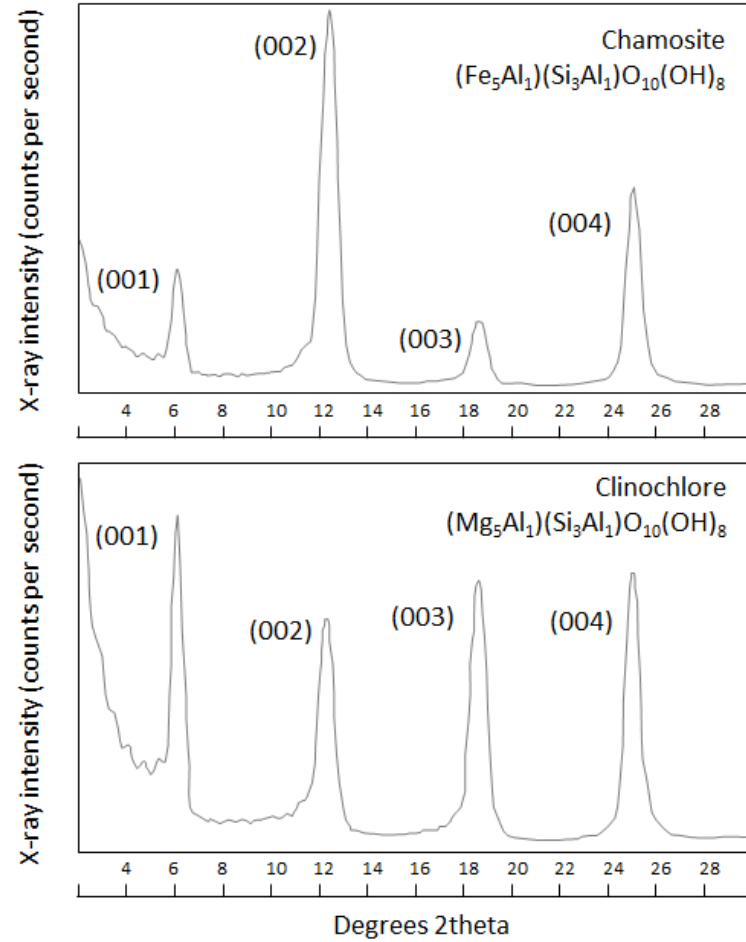
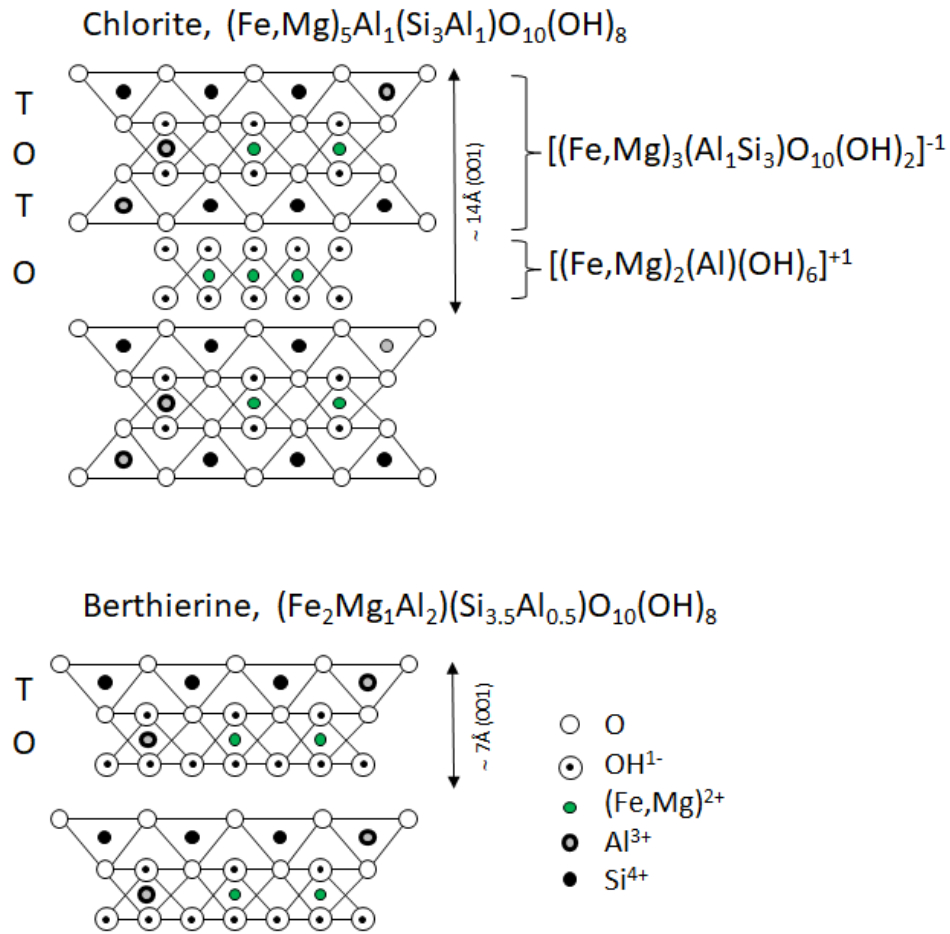
- C. Hollis, R.H. Lander, J. Omma and R.H. Worden (Editors), Reservoir Quality of Clastic and Carbonate Rocks: Analysis, Modelling and Prediction. Special Publication. Geological Society, London, pp. 1-31.
- Worden, R.H., Bukar, M. and Shell, P., 2018b. The effect of oil emplacement on quartz cementation in a deeply buried sandstone reservoir. *American Association of Petroleum Geologists Bulletin*, 102: 49-75.
- Worden, R.H. and Burley, S.D., 2003. Sandstone diagenesis: the evolution from sand to stone. In: S.D. Burley and R.H. Worden (Editors), *Sandstone diagenesis, recent and ancient*. International Association of Sedimentologists Reprint Series, pp. 3-44.
- Worden, R.H., French, M.W. and Mariani, E., 2012. Amorphous silica nanofilms result in growth of misoriented microcrystalline quartz cement maintaining porosity in deeply buried sandstones. *Geology*, 40(2): 179-182.
- Worden, R.H. and Heasley, E.C., 2000. Effects of petroleum emplacement on cementation in carbonate reservoirs. *Bulletin De La Societe Geologique De France*, 171(6): 607-620.
- Worden, R.H., Manning, D.A.C. and Bottrell, S.H., 2006a. Multiple generations of high salinity formation water in the Triassic Sherwood Sandstone: Wytch Farm oilfield, onshore UK. *Applied Geochemistry*, 21(3): 455-475.
- Worden, R.H., Mayall, M. and Evans, I.J., 2000. The effect of ductile-lithic sand grains and quartz cement on porosity and permeability in Oligocene and lower Miocene clastics, South China Sea: Prediction of reservoir quality. *American Association of Petroleum Geologists Bulletin*, 84(3): 345-359.
- Worden, R.H. and Morad, S., 2000. Quartz cementation in sandstones: a review of the key controversies In: R.H. Worden (Editor), *Quartz cementation in sandstones*. Special Publication of the International Association of Sedimentologists. Blackwells, Oxford, pp. 1-20.
- Worden, R.H. and Morad, S., 2003. Clay minerals in sandstones: controls on formation, distribution and evolution. In: R.H. Worden and S. Morad (Editors), *Clay mineral cements in sandstones*. Special Publication of the International Association of Sedimentologists. Blackwells, Oxford, pp. 3-41.
- Worden, R.H., Needham, S.J. and Cuadros, J., 2006b. The worm gut; a natural clay mineral factory and a possible cause of diagenetic grain coats in sandstones. *Journal of Geochemical Exploration*, 89(1-3): 428-431.
- Worden, R.H., Oxtoby, N.H. and Smalley, P.C., 1998. Can oil emplacement prevent quartz cementation in sandstones? *Petroleum Geoscience*, 4(2): 129-137.
- Worden, R.H. and Smalley, P.C., 1996. H<sub>2</sub>S-producing reactions in deep carbonate gas reservoirs: Khuff Formation, Abu Dhabi. *Chemical Geology*, 133(1-4): 157-171.
- Worden, R.H. and Smalley, P.C., 2001. H<sub>2</sub>S in North Sea oil fields: importance of thermochemical sulphate reduction in clastic reservoirs. In: R. Cidu (Editor), *Water-Rock Interaction 2001*. Balkema, Lisse, pp. 659-662.

- Worden, R.H., Smalley, P.C. and Barclay, S.A., 2003. H<sub>2</sub>S and diagenetic pyrite in North Sea sandstones: due to TSR or organic sulphur compound cracking? *Journal of Geochemical Exploration*, 78-9: 487-491.
- Worden, R.H., Smalley, P.C. and Oxtoby, N.H., 1995. Gas souring by thermochemical sulfate reduction at 140 degrees C. *American Association of Petroleum Geologists Bulletin*, 79(6): 854-863.
- Worden, R.H., Utley, J.E.P., Butcher, A.R., Griffiths, J., Wooldridge, L.J. and Lawan, A.Y., 2018c. Improved imaging and analysis of chlorite in reservoirs and modern day analogues: new insights for reservoir quality and provenance. In: P.J. Dowey, M.J. Osborne and H. Volk (Editors), *Application of Analytical Techniques to Petroleum Systems*. Special Publication. Geological Society, London.
- Worthington, P.F., 2000. Recognition and evaluation of low-resistivity pay. *Petroleum Geoscience*, 6(1): 77-92.
- Wycherley, H., Fleet, A. and Shaw, H., 1999. Some observations on the origins of large volumes of carbon dioxide accumulations in sedimentary basins. *Marine and Petroleum Geology*, 16(6): 489-494.
- Xiang, F., Wang, Y.W., Feng, Q., Zhang, D.Y. and Zhao, J.X., 2016. Further research on chlorite rims in sandstones: evidence from the Triassic Yanchang Formation in the Ordos basin, China. *Arabian Journal of Geosciences*, 9(7).
- Xu, T.F., Apps, J.A. and Pruess, K., 2005. Mineral sequestration of carbon dioxide in a sandstone-shale system. *Chemical Geology*, 217(3-4): 295-318.
- Yardley, B.W.D., 1989. *An Introduction to Metamorphic Petrology*. Longman, Harlow.
- Yezerki, D.J. and Shumaker, N., 2017. Improving prediction of porosity preservation in thermally-stressed deep marine sandstones: A synthesis of grain-coating chlorite observations, AAPG 2017 Annual Convention and Exhibition, Search and Discovery Article #51465 (2018). AAPG, Houston, Texas.
- Yu, Y., Lin, L.B. and Gao, J., 2016. Formation mechanisms and sequence response of authigenic grain-coating chlorite: evidence from the Upper Triassic Xujiahe Formation in the southern Sichuan Basin, China. *Petroleum Science*, 13(4): 657-668.
- Zhu, S.F., Wang, X.X., Qin, Y., Jia, Y., Zhu, X.M., Zhang, J.T. and Hu, Y.Q., 2017. Occurrence and origin of pore-lining chlorite and its effectiveness on preserving porosity in sandstone of the middle Yanchang Formation in the southwest Ordos Basin. *Applied Clay Science*, 148: 25-38.
- Zinsner, B. and Pellerin, F.-M., 2007. *A geoscientists guide to petrophysics*. IFP Publications, Paris, 384 pp.



**Figure 1**

**Figure 2**



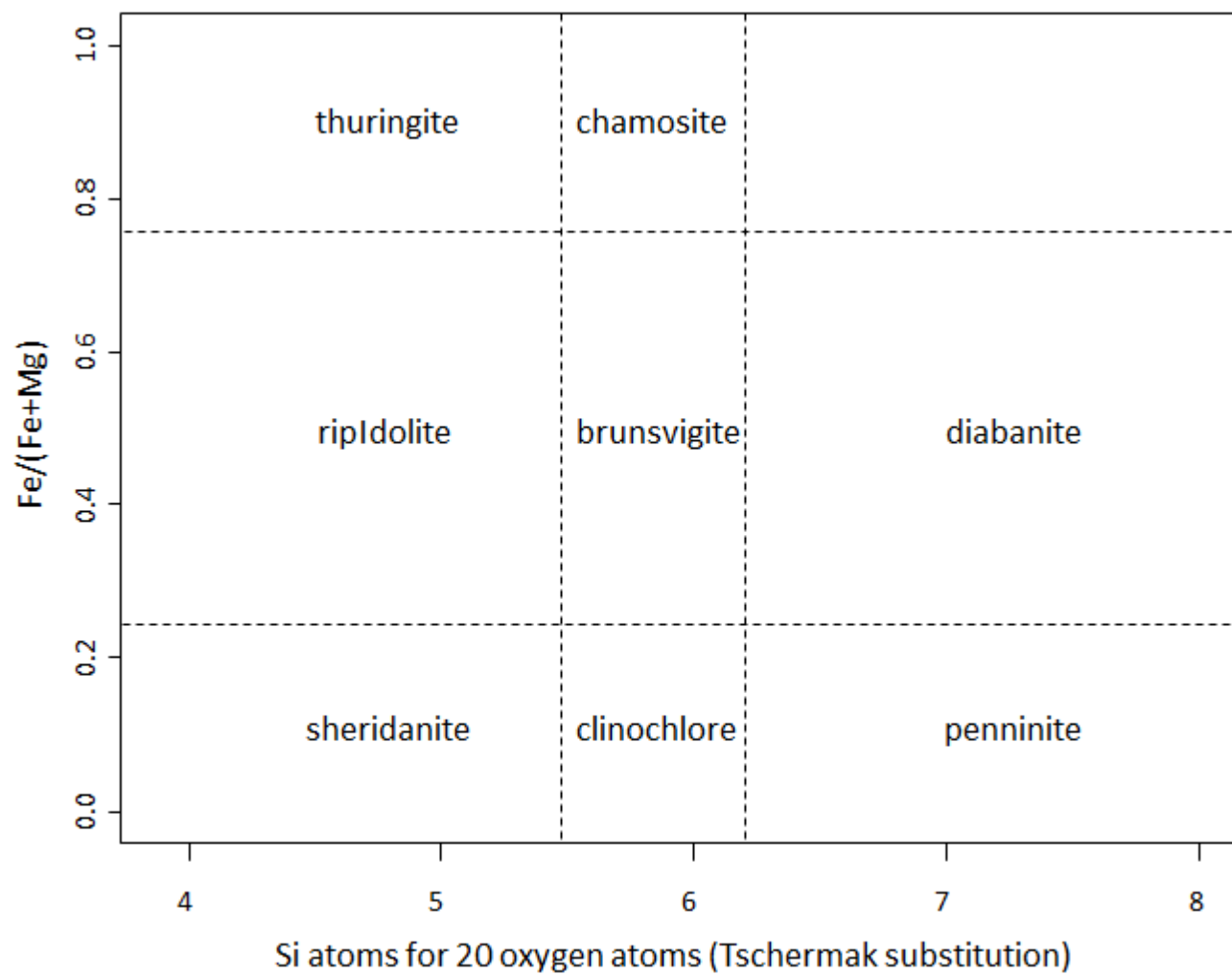


**Figure 3**

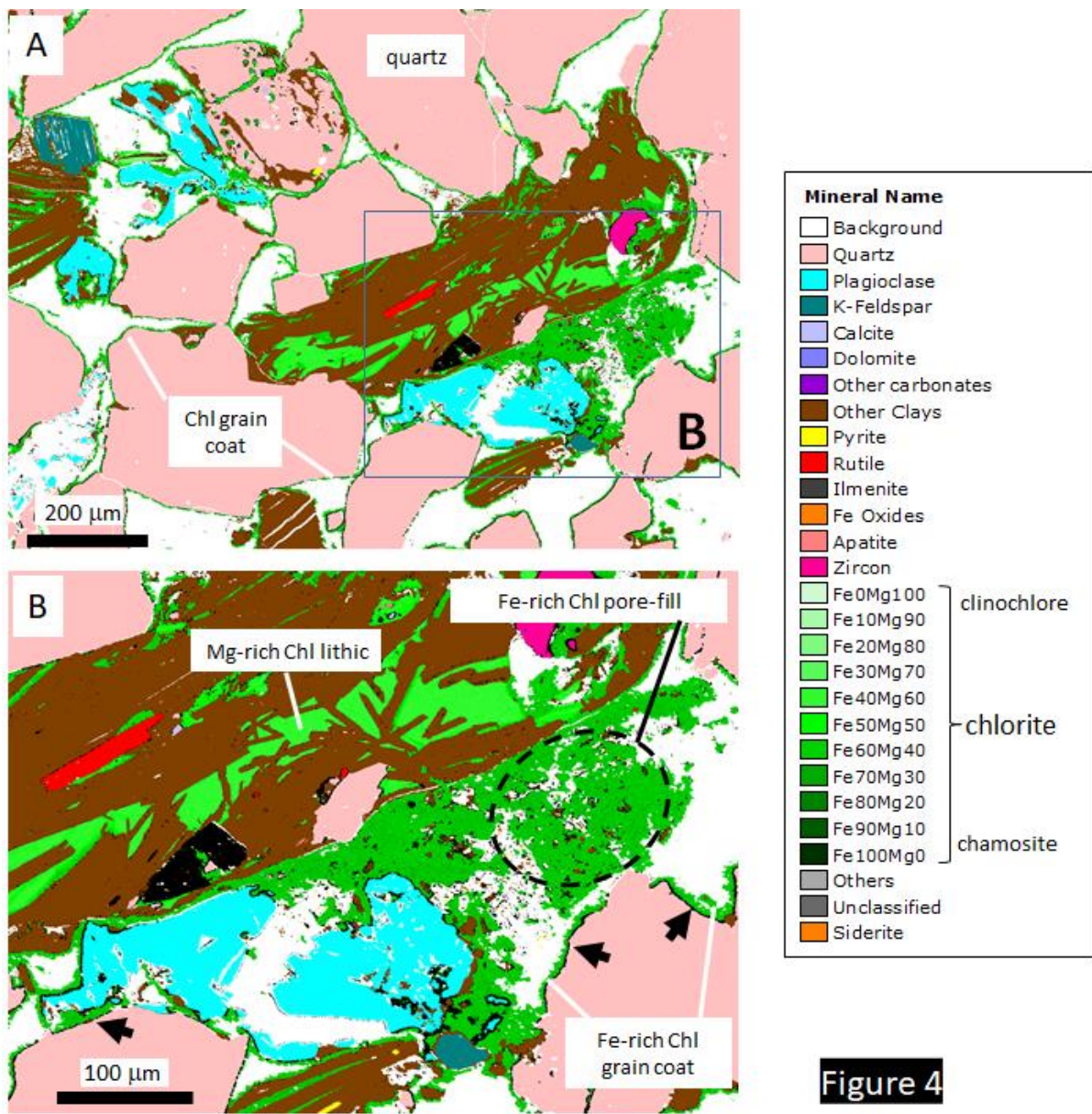


**Figure 4**

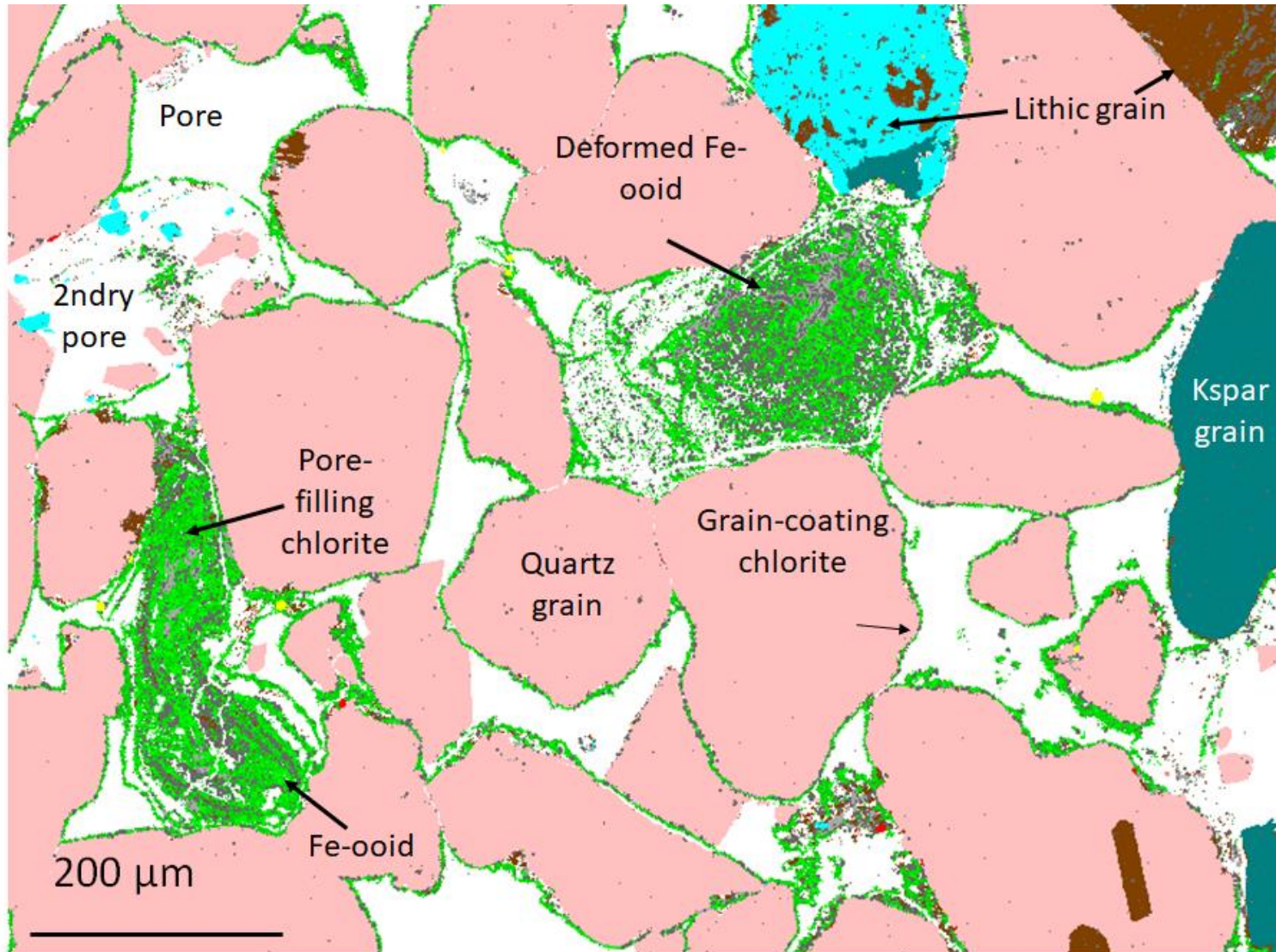


Figure 5



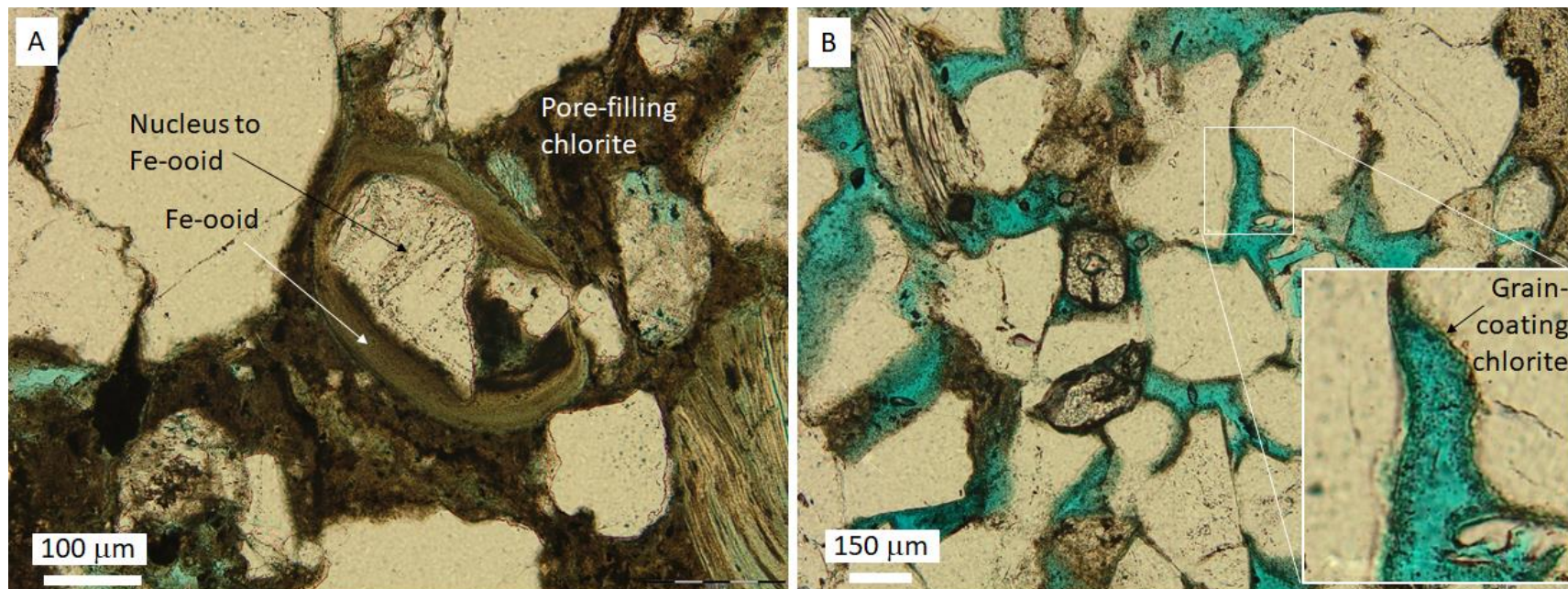
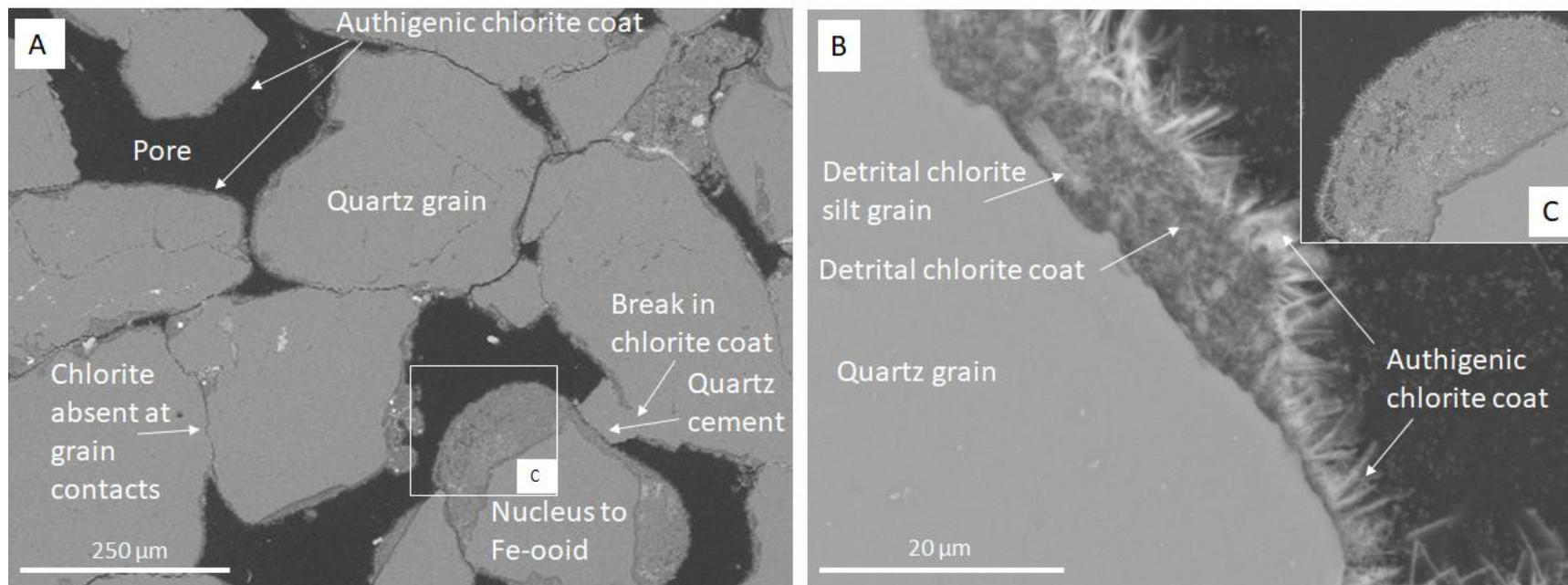
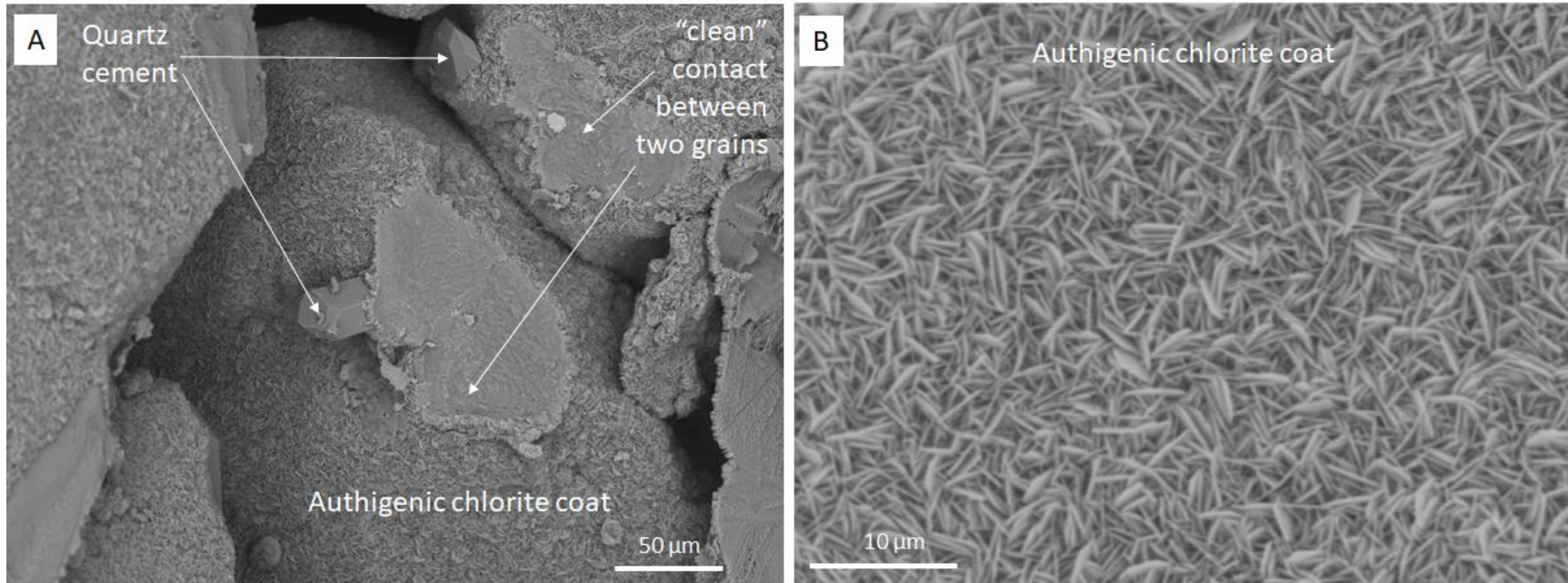


Figure 6



**Figure 7**



**Figure 8**

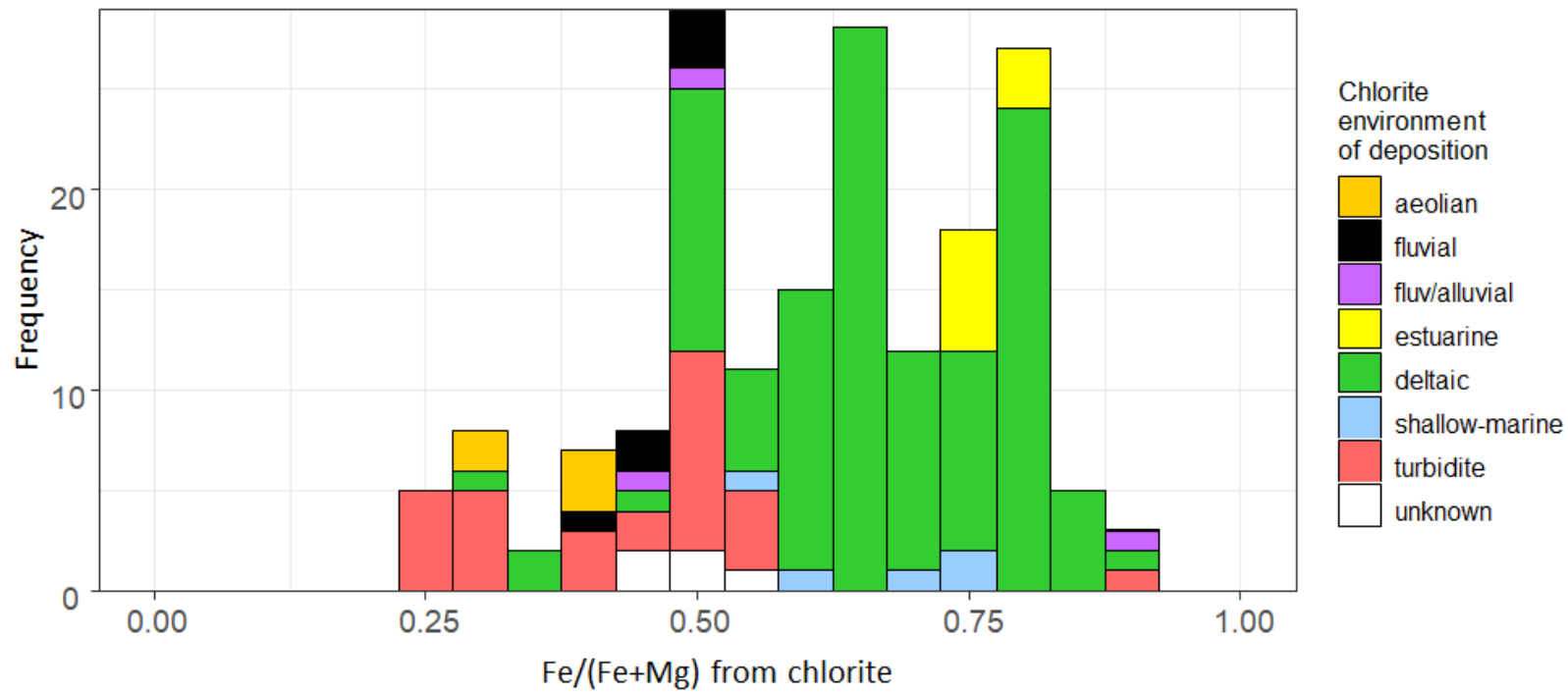


Figure 9

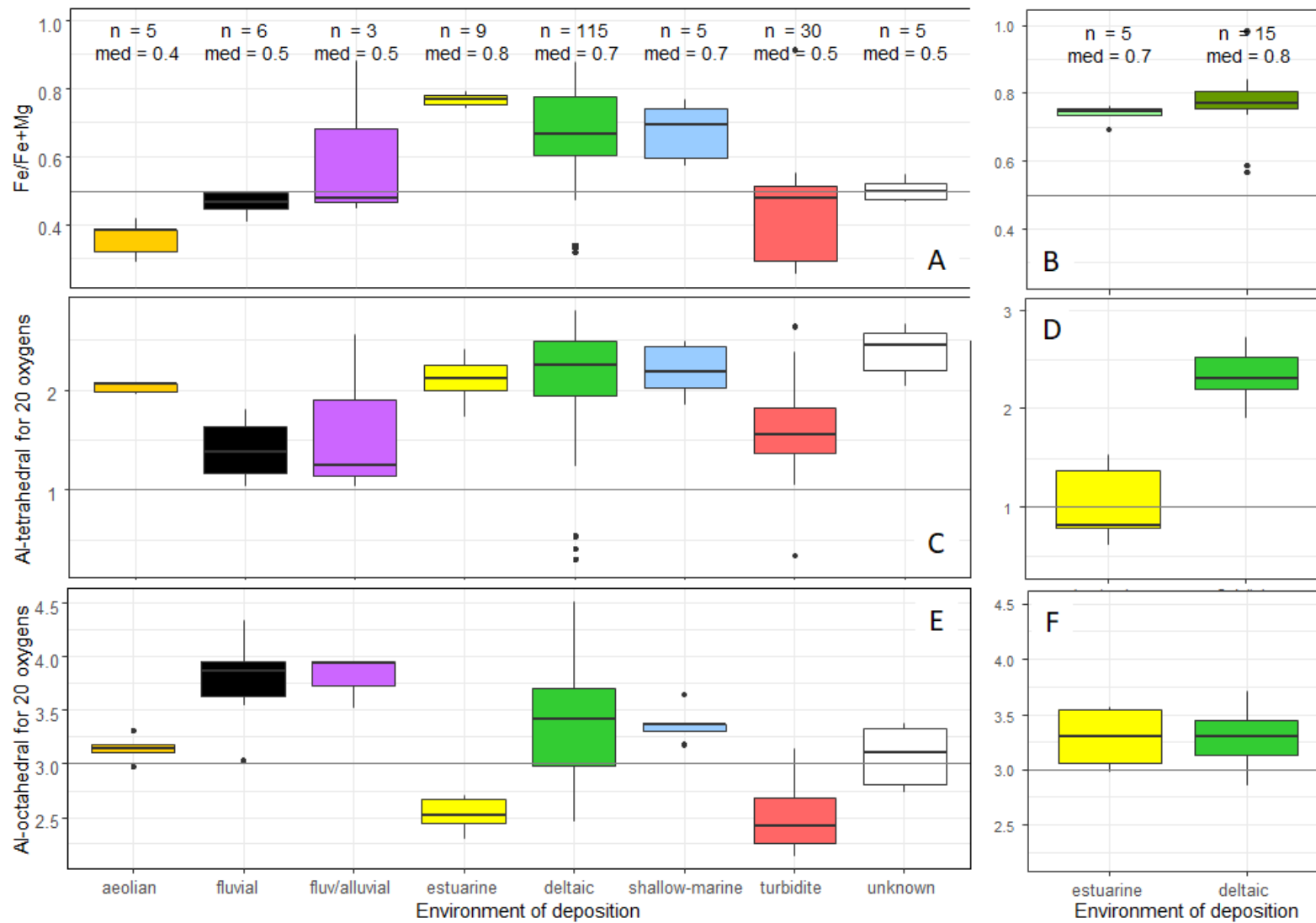
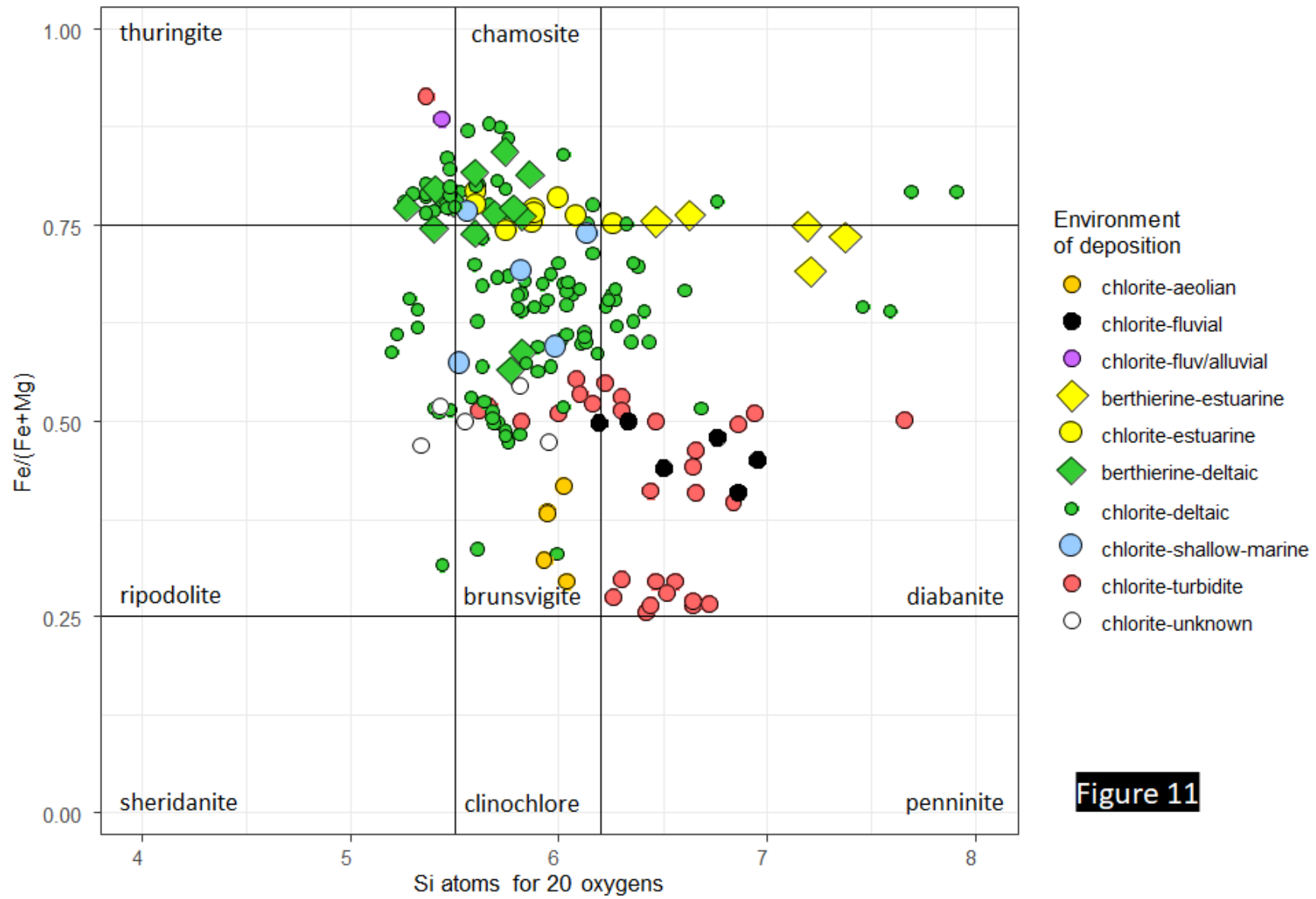
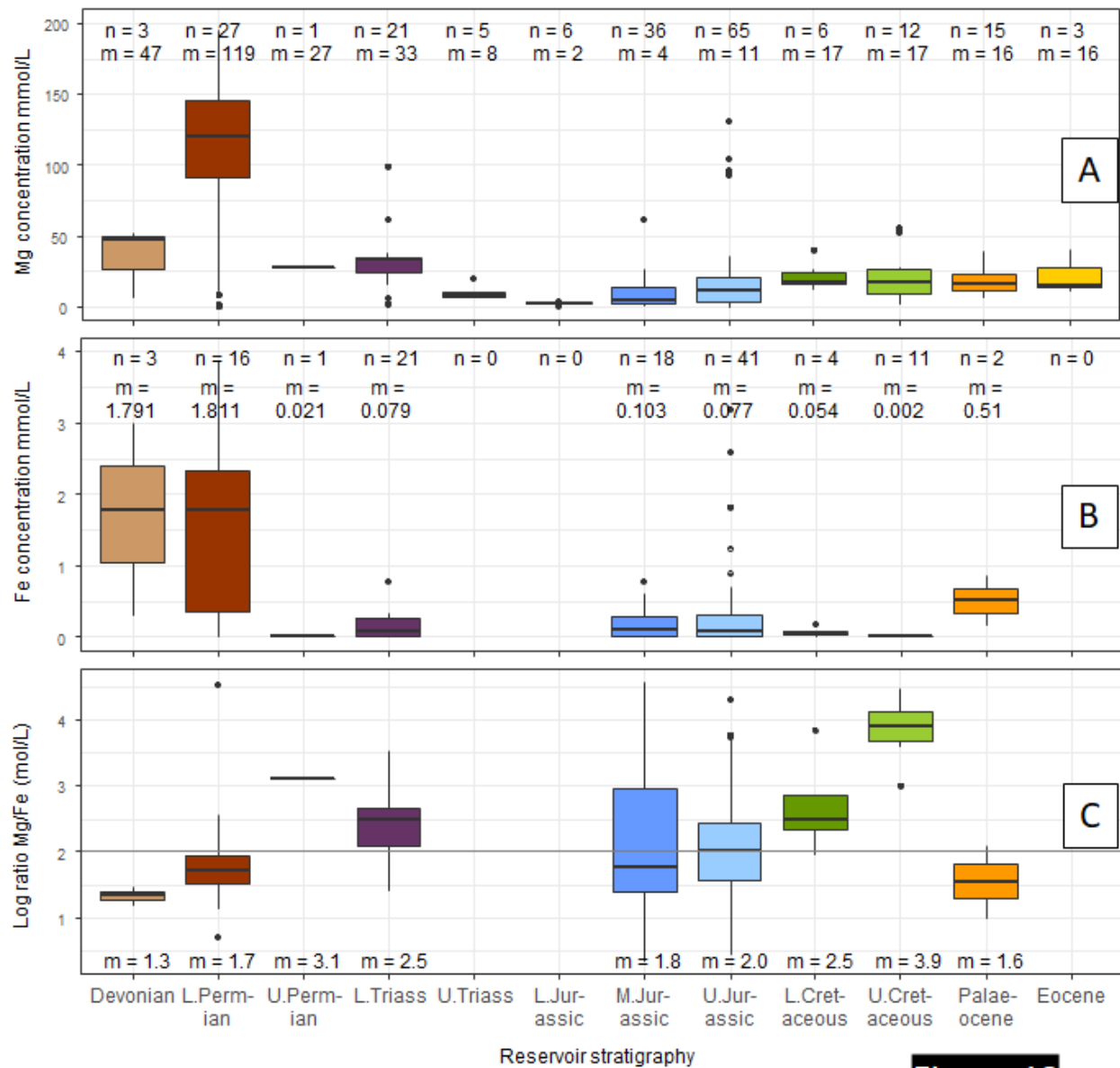


Figure 10





**Figure 11**



**Figure 12**



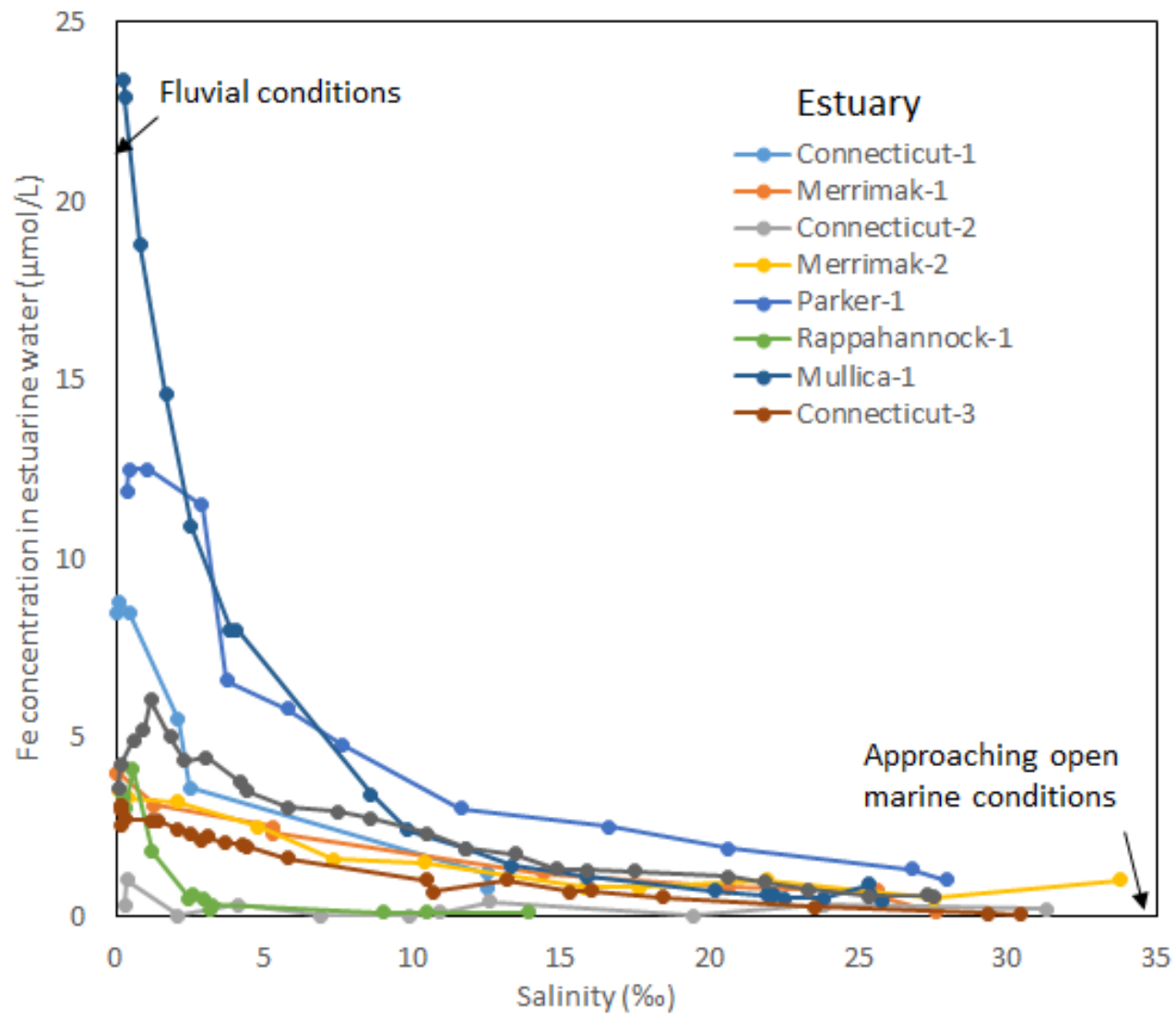


**Figure 13**

Figure 14

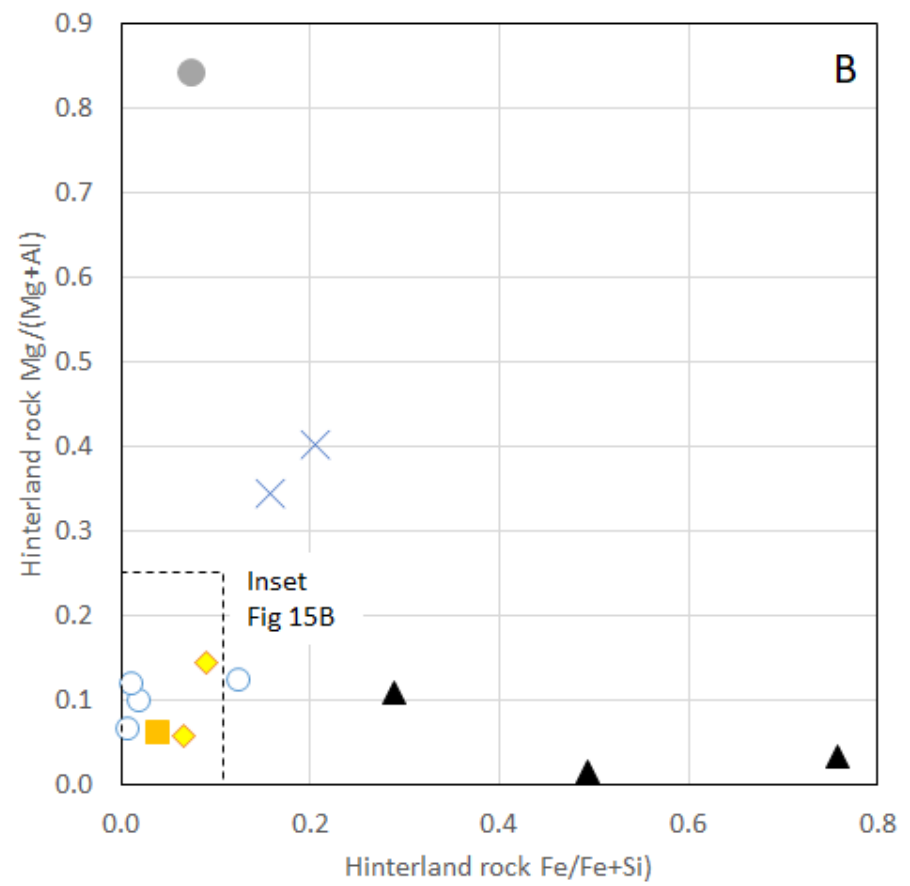
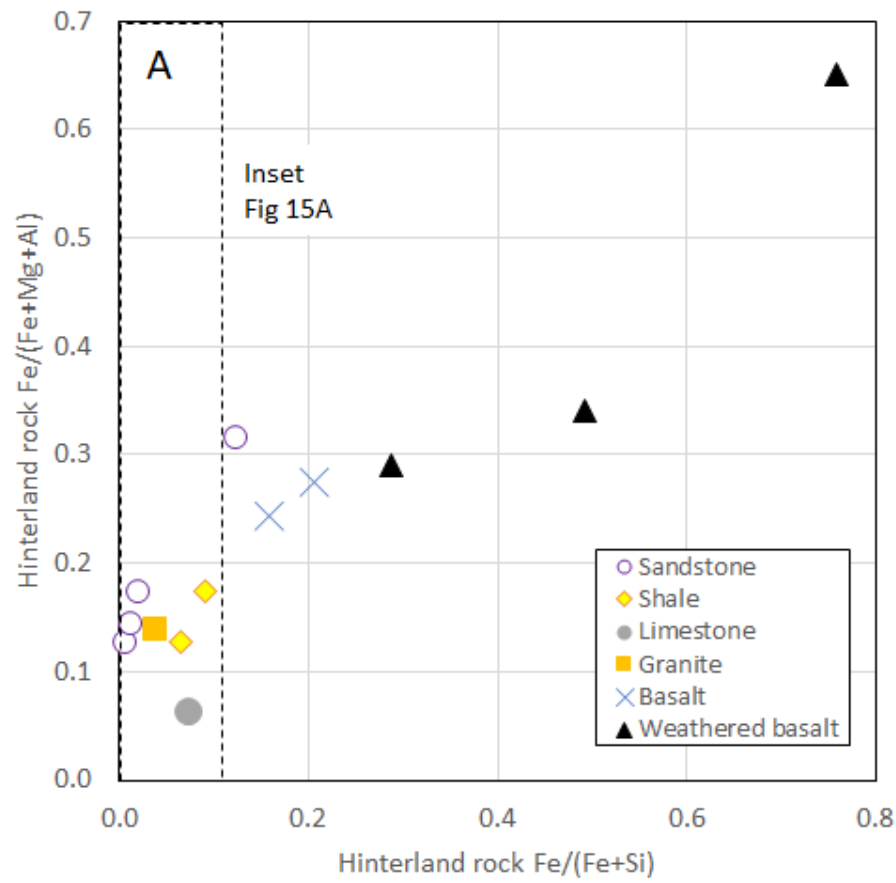


**Figure 15**

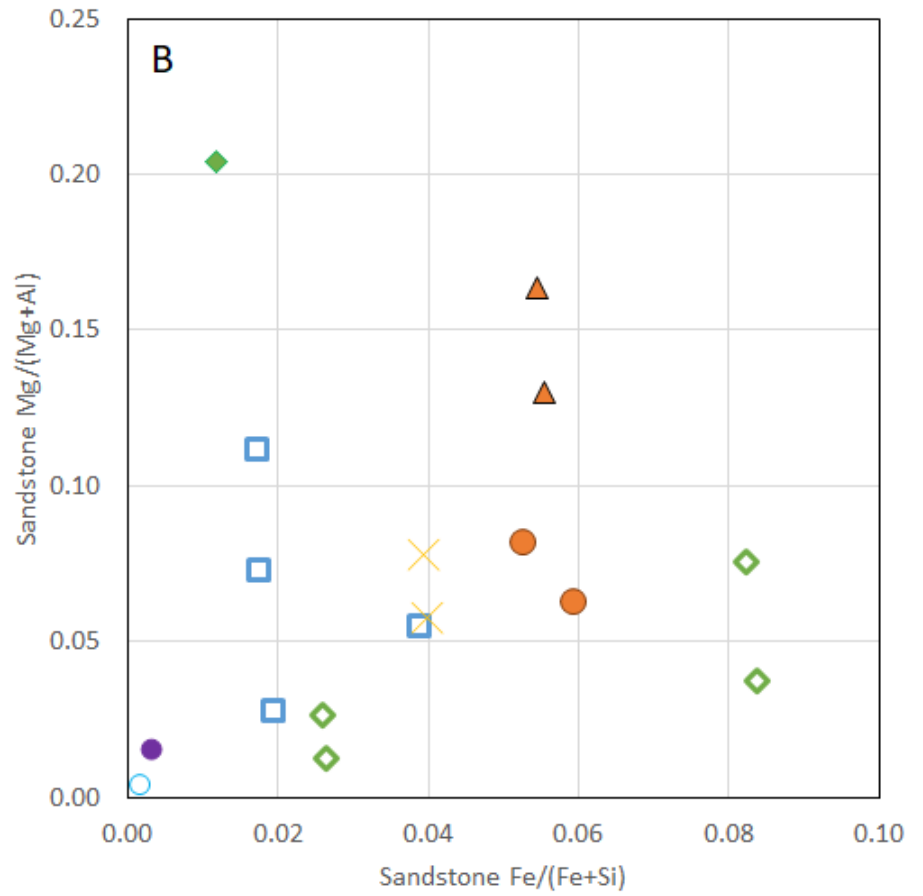
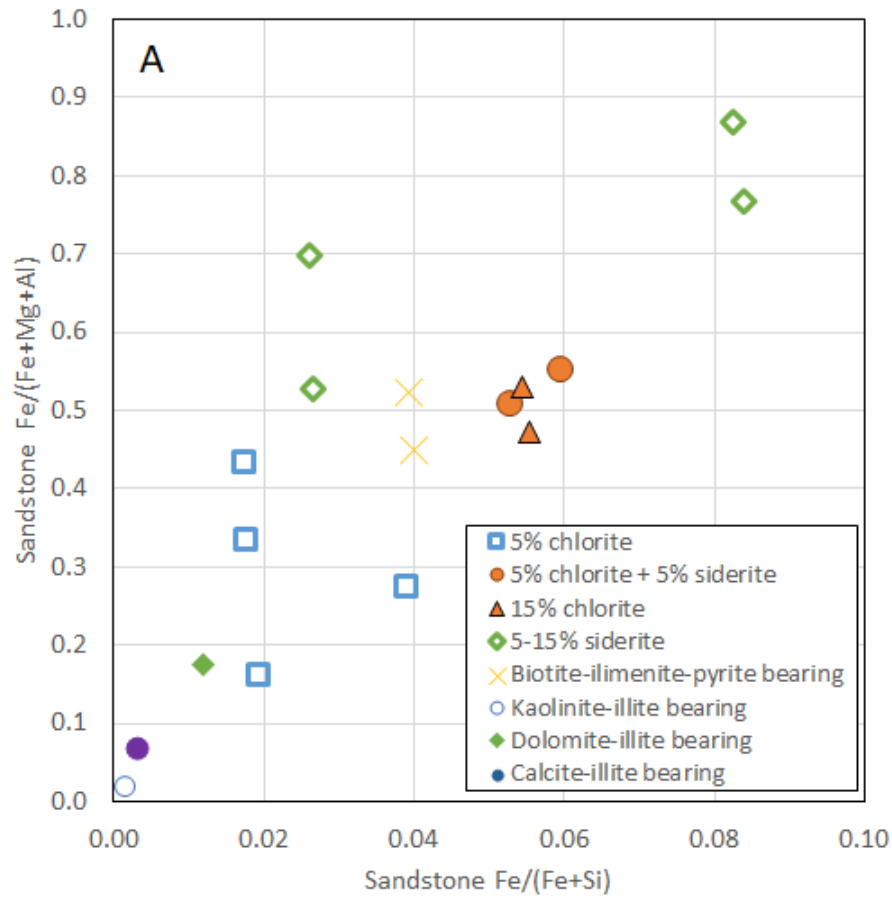
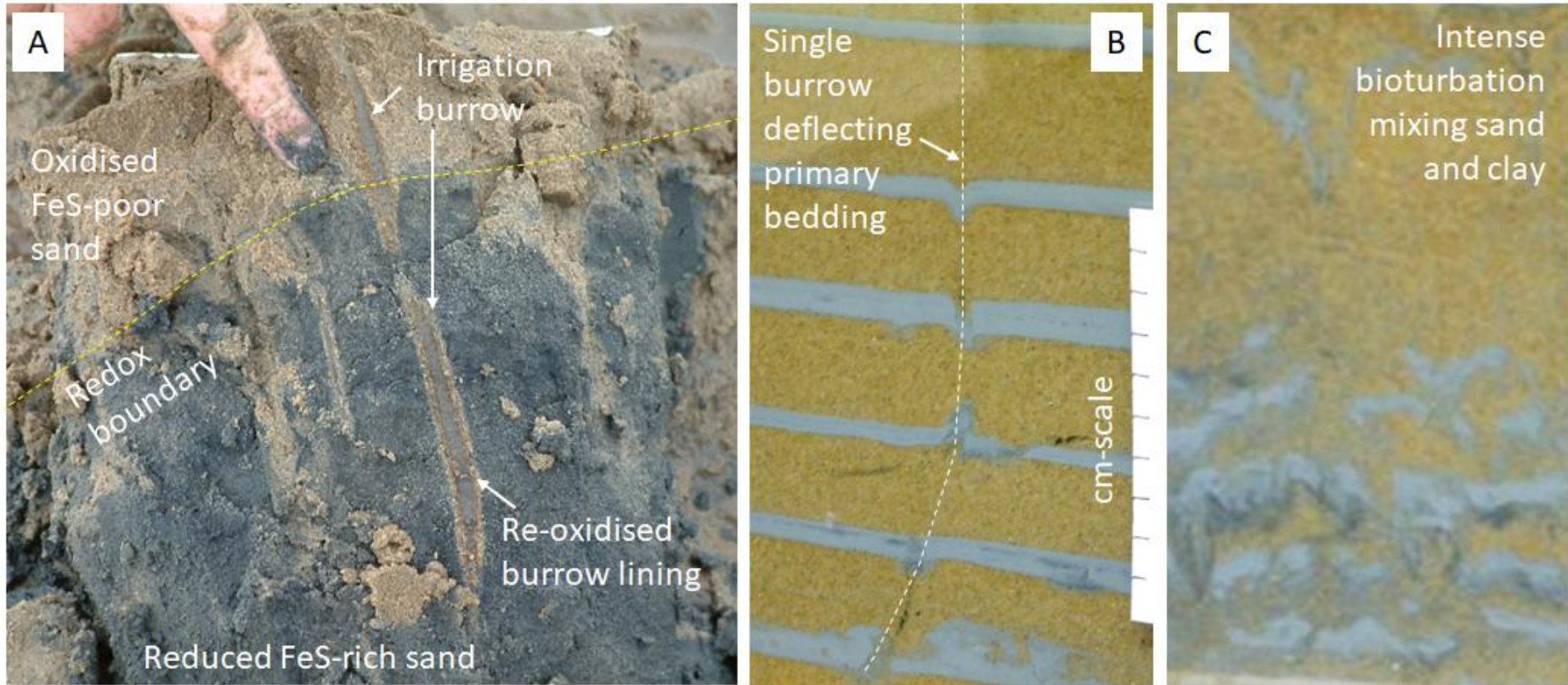
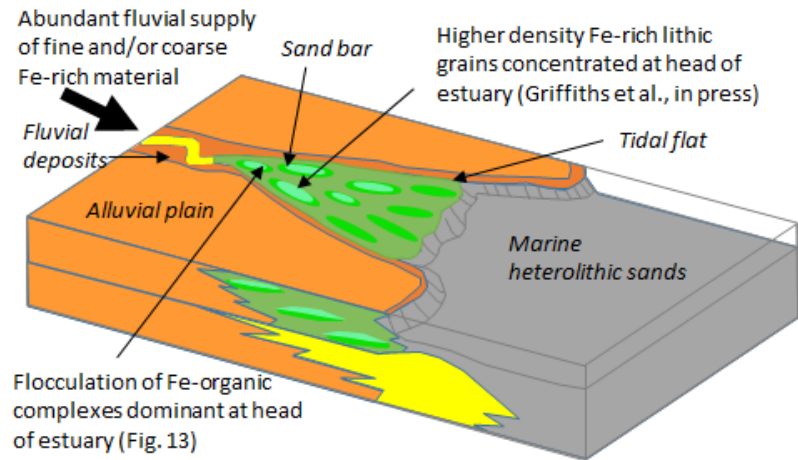


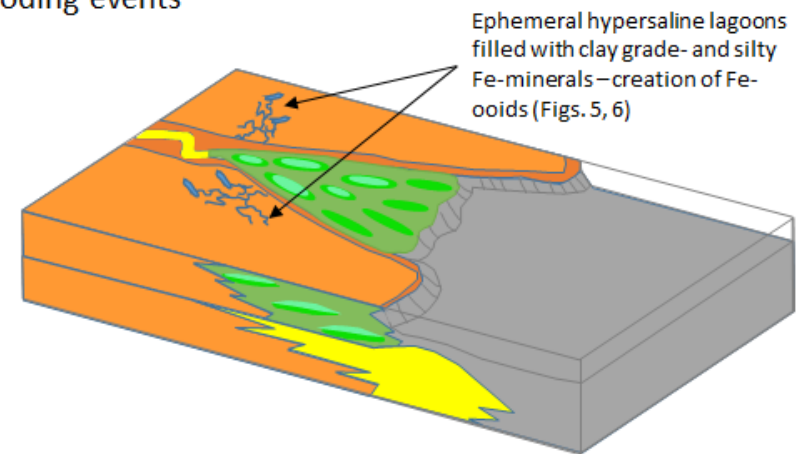
Figure 16



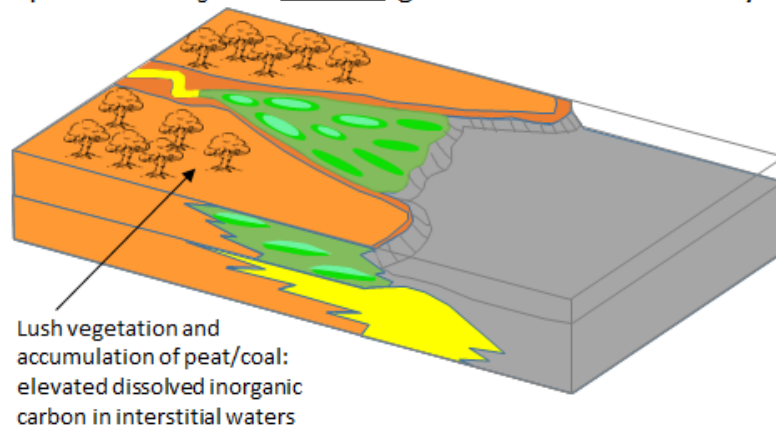
A: High chance of Fe-clay accumulation (and grain coats) in proximal bayhead delta sediments



B: Elevated chance of creation of Fe-oids in hypersaline lagoons, then Fe-oids flushed into estuary following flooding events



C: Elevated organic matter results in elevated aqueous  $\text{HCO}_3^-$  and siderite growth instead of Fe-clay



D: Greater interaction with  $\text{SO}_4$  leads to probability of elevated sulphide and Fe-sulphide growth instead of Fe-clay

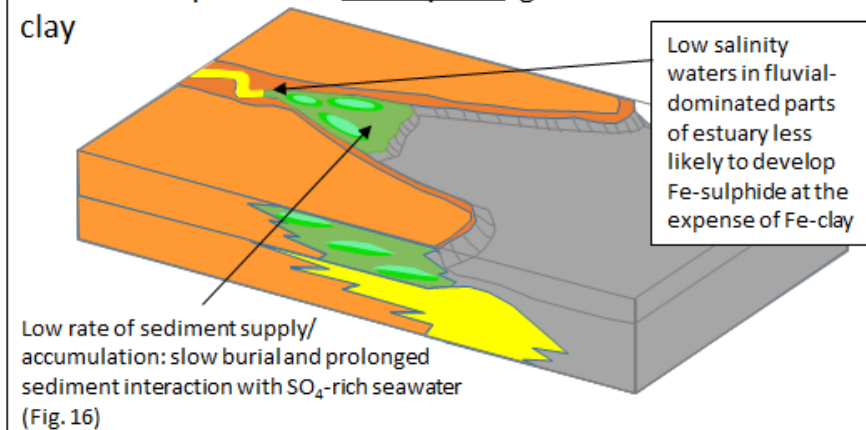


Figure 17

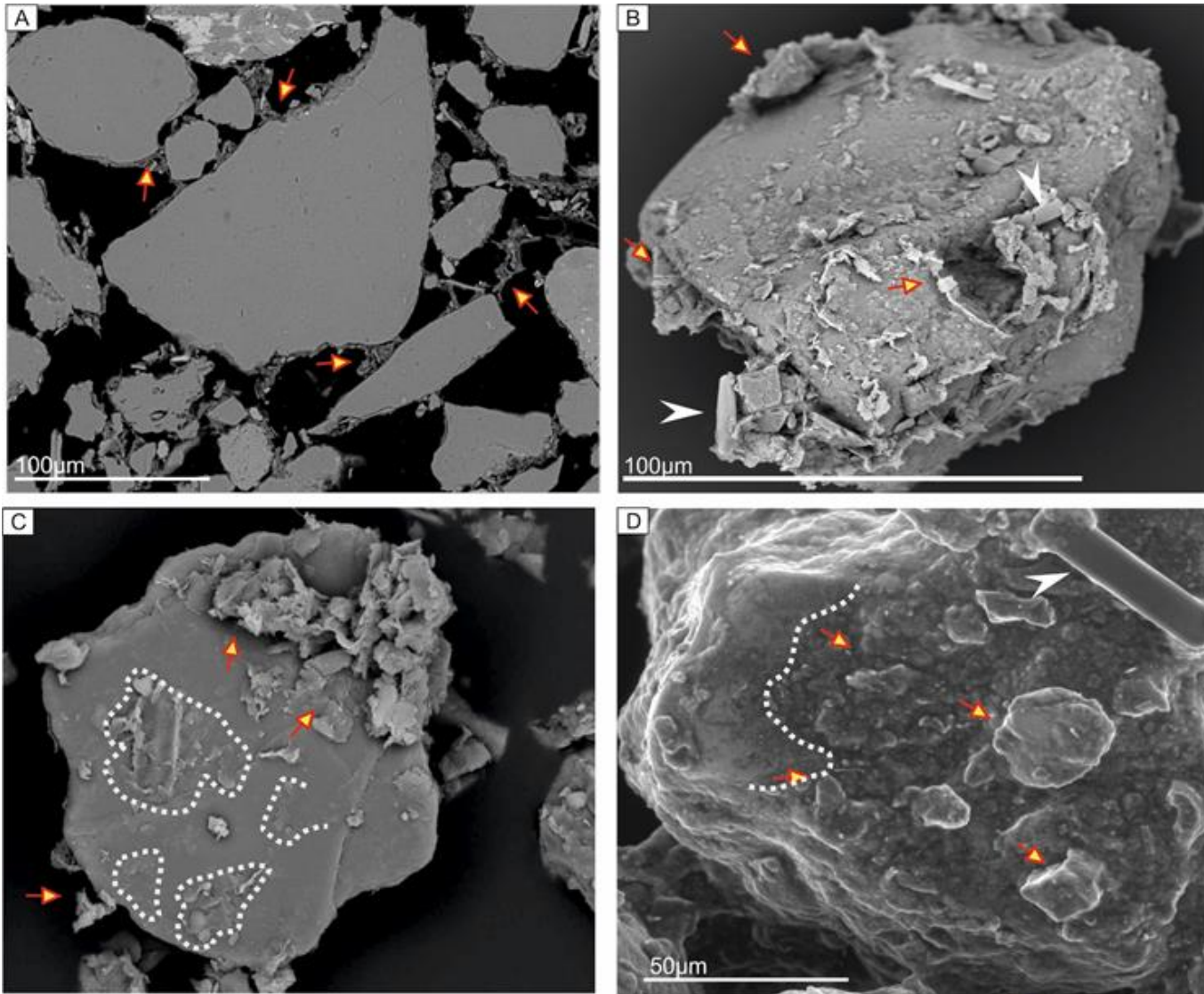


Figure 18

**Figure 19**

|  | list in main text | mechanism for incorporating chlorite precursor materials into sand | aeolian | alluvial | fluvial | deltaic | estuarine | paralic | shallow marine | fan/turbidite |
|--|-------------------|--|---------|----------|---------|---------|-----------|---------|----------------|---------------|
| Coarse grained chlorite-precursor        | i                 | clay grain coats   | ✓       | ✓        | ✓       | ✓       | ✓         | ✗       | ✗              | ✓             |
|  | ii                | lithic grains  | ✓       | ✓        | ✓       | ✓       | ✓         | ✓       | ✓              | ✓             |
|  | iiia              | Fe-ooids   | ✗       | ✗        | ✗       | ✓       | ✓         | ✓       | ✓              | ✗             |
|  | iiib              | clay intraclasts   | ✗       | ✓        | ✓       | ✓       | ✓         | ✗       | ✗              | ✓             |
| Fine grained chlorite-precursor minerals | iv                | bioturbation   | ✗       | ✗        | ✓       | ✓       | ✓         | ✗       | ✓              | ✗             |
|  | v                 | sediment ingestion and excretion                                   | ✗       | ✗        | ✓       | ✓       | ✓         | ✗       | ✓              | ✗             |
|  | vi                | soft sediment deformation  | ✓       | ✓        | ✓       | ✓       | ✓         | ✗       | ✗              | ✓             |
|  | vii               | infiltration   | ✓       | ✓        | ✓       | ✓       | ✓         | ✗       | ✗              | ✗             |

**Figure 20**

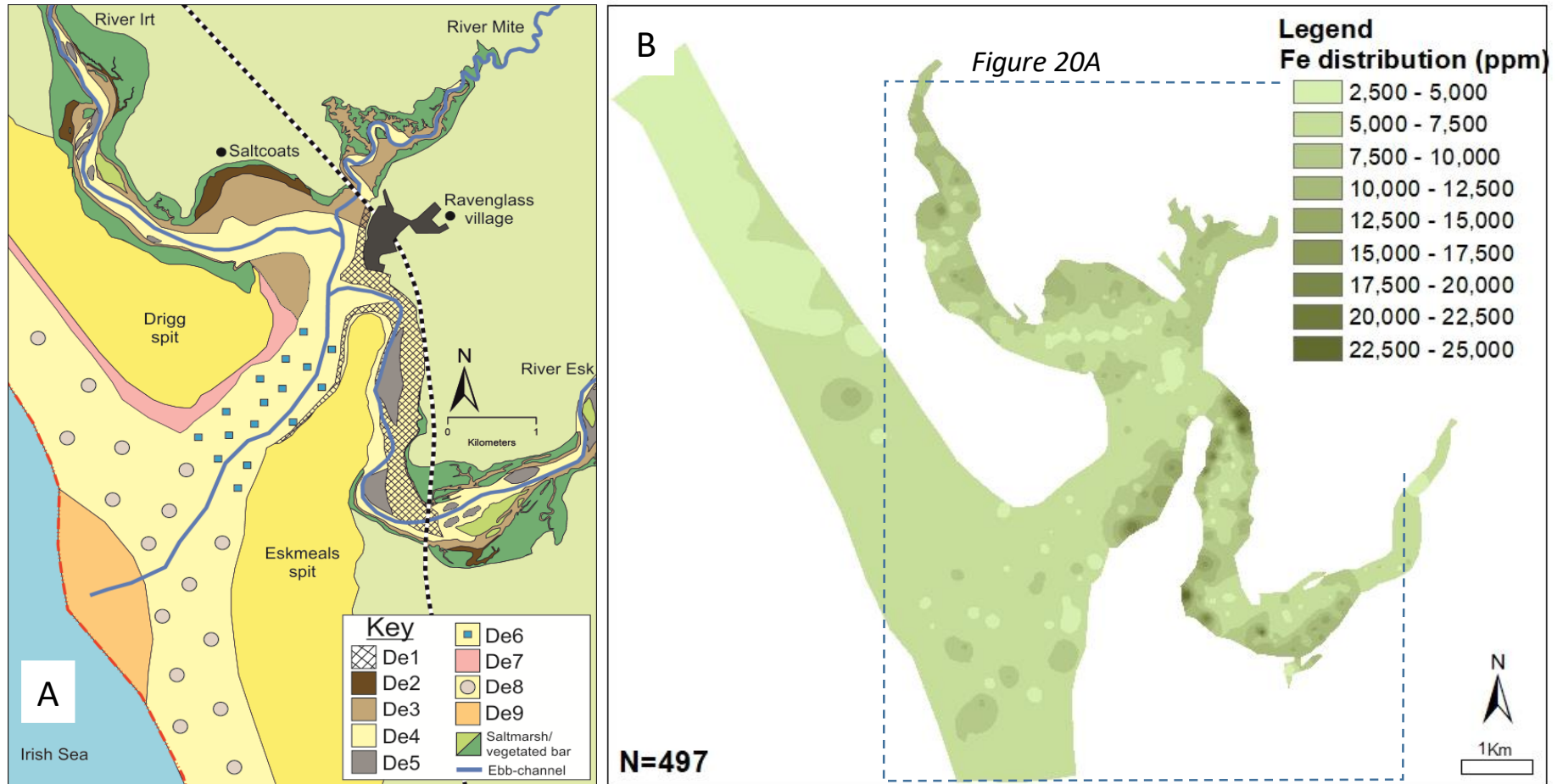
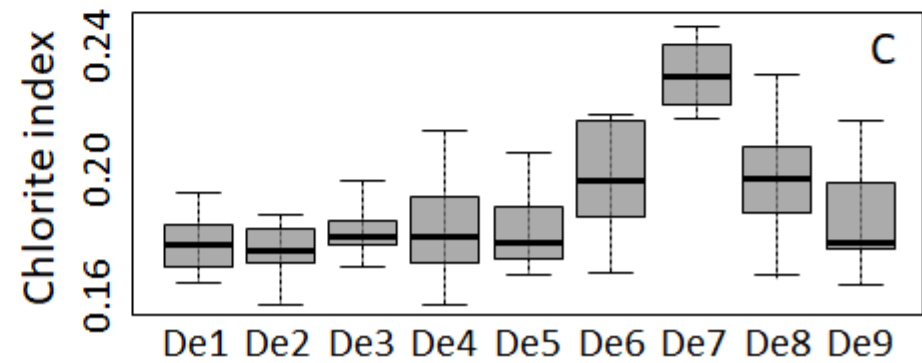
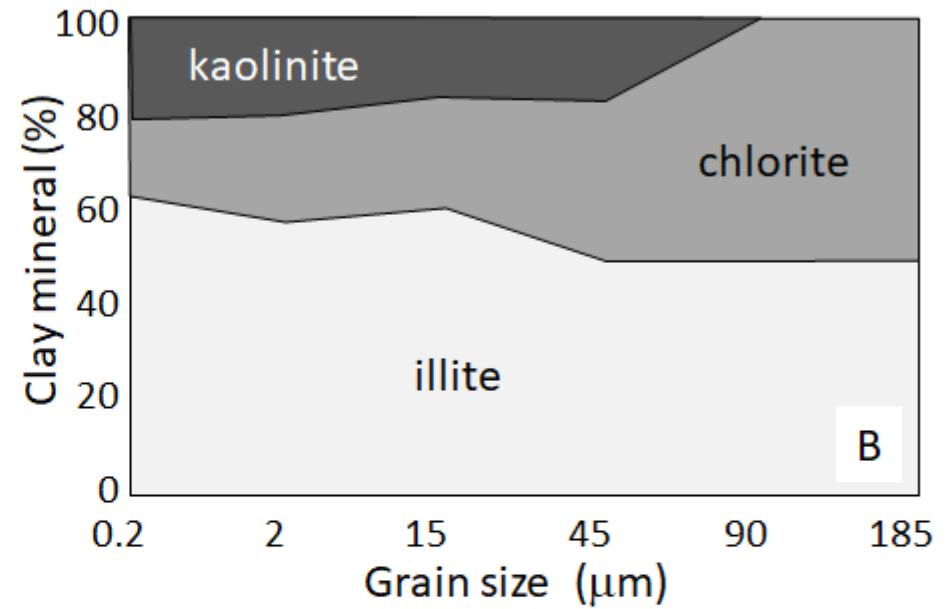
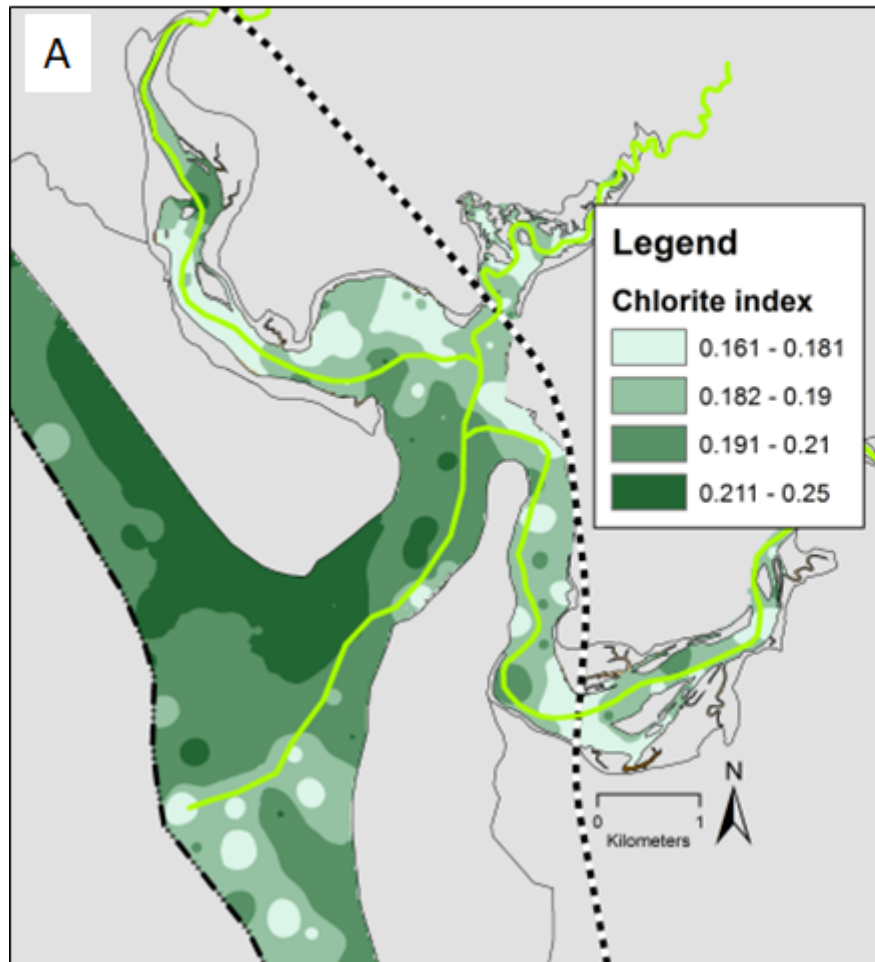




Figure 21



**Primary marginal marine sediment characteristics**

|                           |                           |                          |                        |
|---------------------------|---------------------------|--------------------------|------------------------|
| Environment of deposition | Foreshore and tidal inlet | Sandflats, tidal bars    | Mixed- and mud-flats   |
| Total clay                | Very low                  | Moderate                 | High                   |
| Detrital clay coats       | Absent/negligible         | Optimum coverage         | High                   |
| Detrital clay mineralogy  | Relatively chlorite-rich  | Relatively chlorite-rich | Relatively illite-rich |

**Diagenetic characteristics and deep (>>80-100°C) sandstone reservoir quality**

|                              |           |                       |          |
|------------------------------|-----------|-----------------------|----------|
| Degree of quartz cementation | High      | Low                   | Moderate |
| Predicted RQ                 | Very poor | Anomalously very good | Poor     |

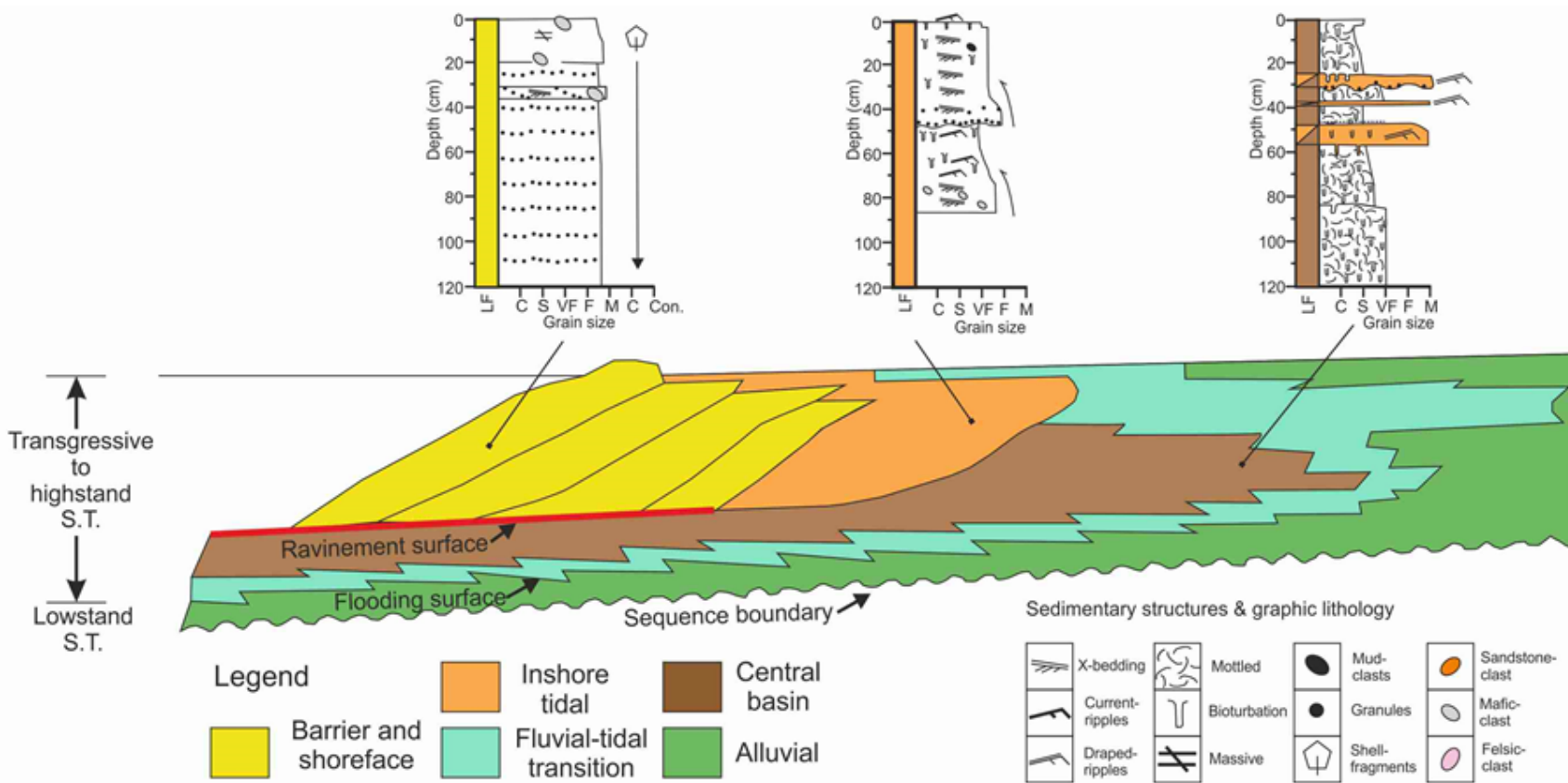


**Figure 22**

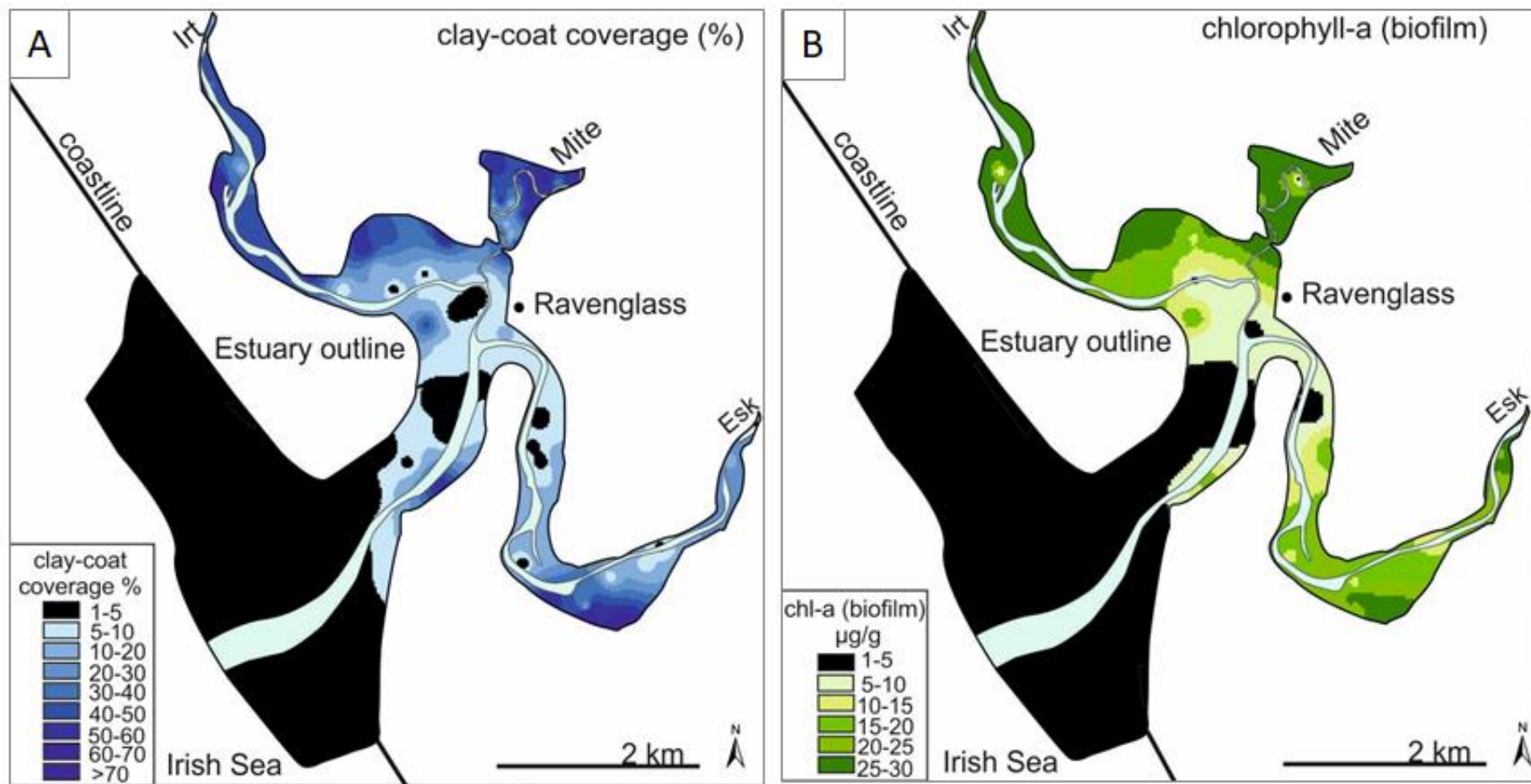


**Figure 23**

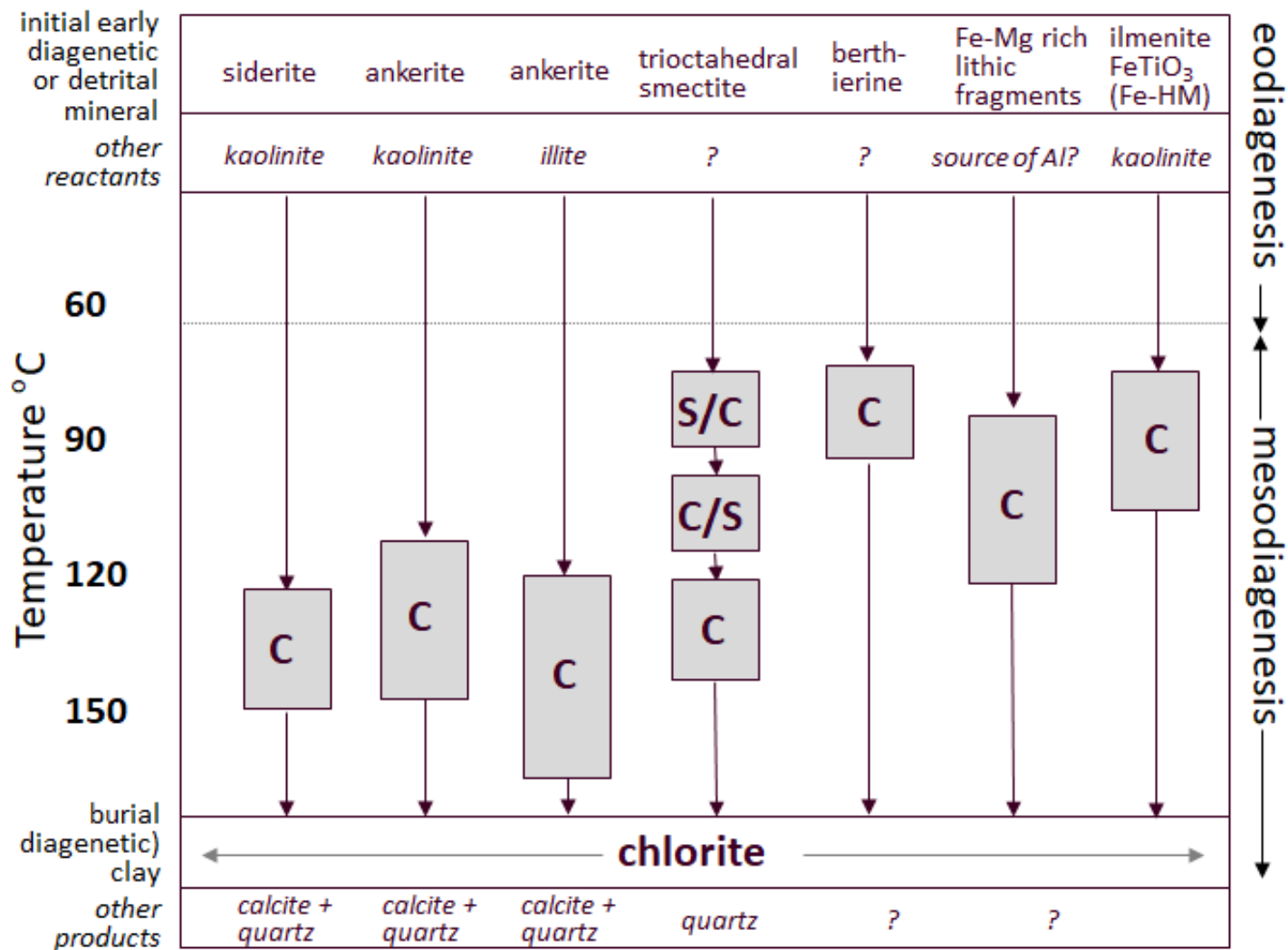


**Figure 24**

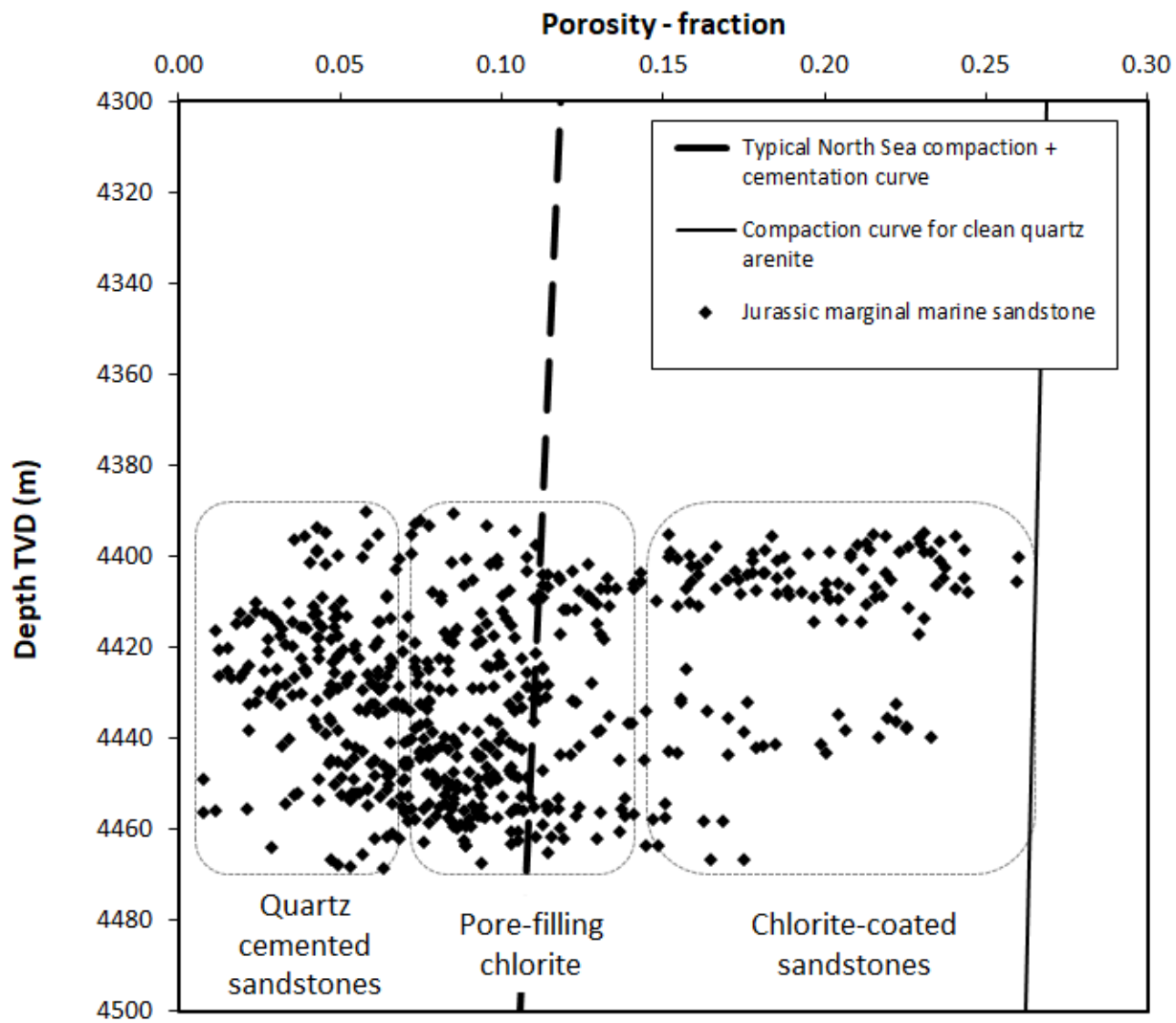
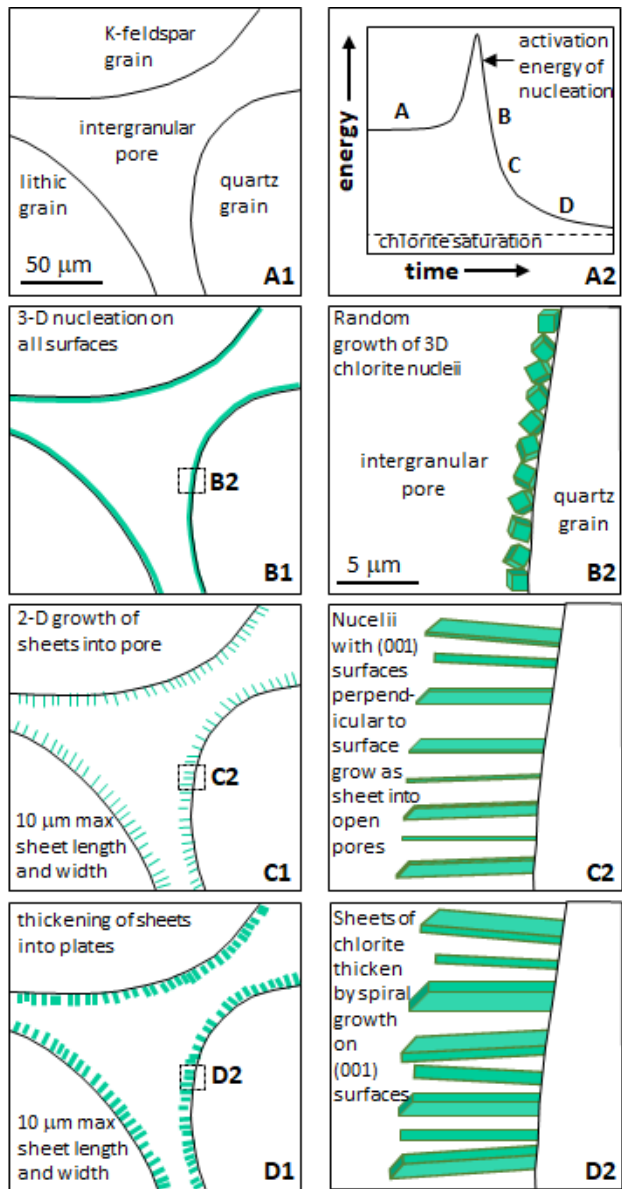
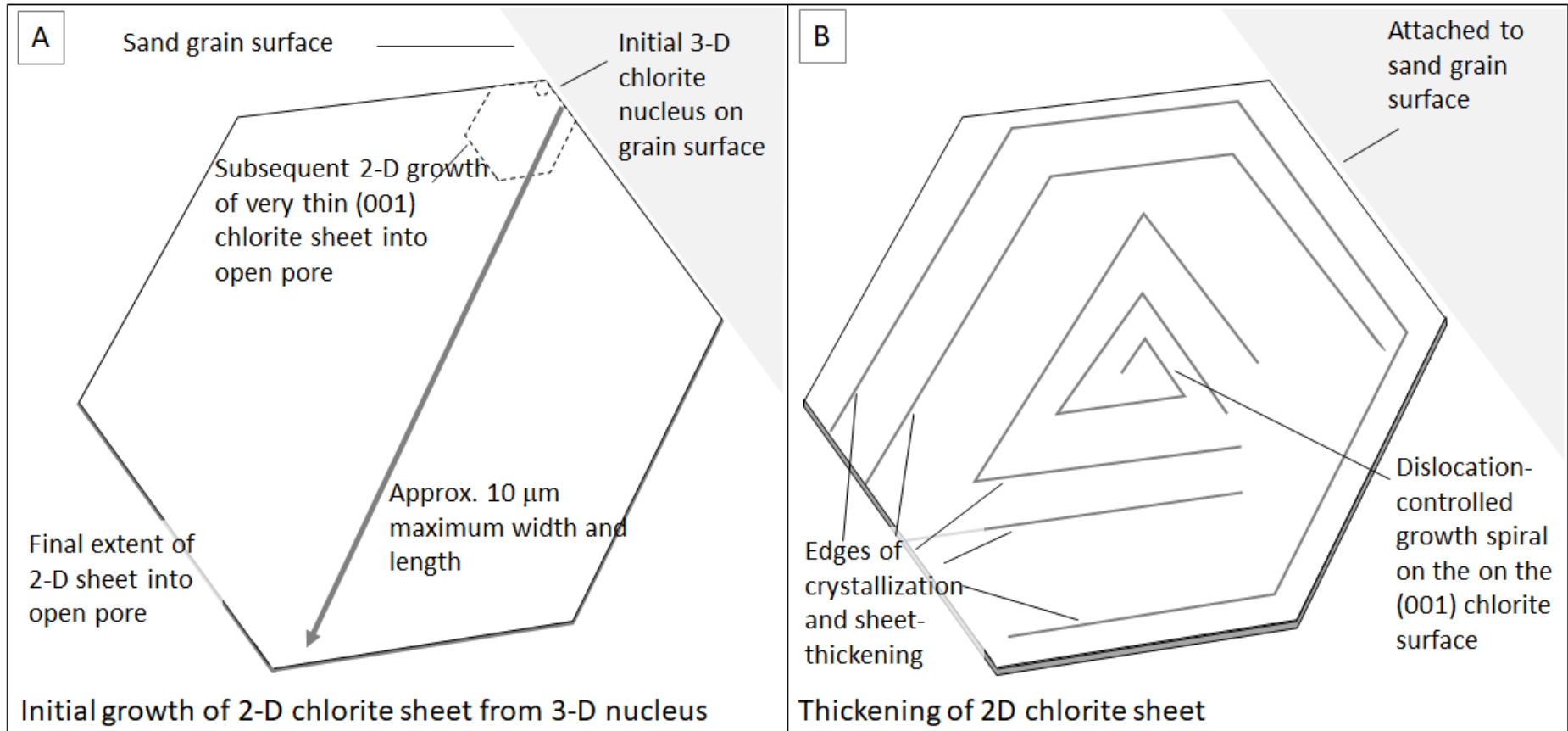


Figure 25



**Figure 26**

**Figure 27**



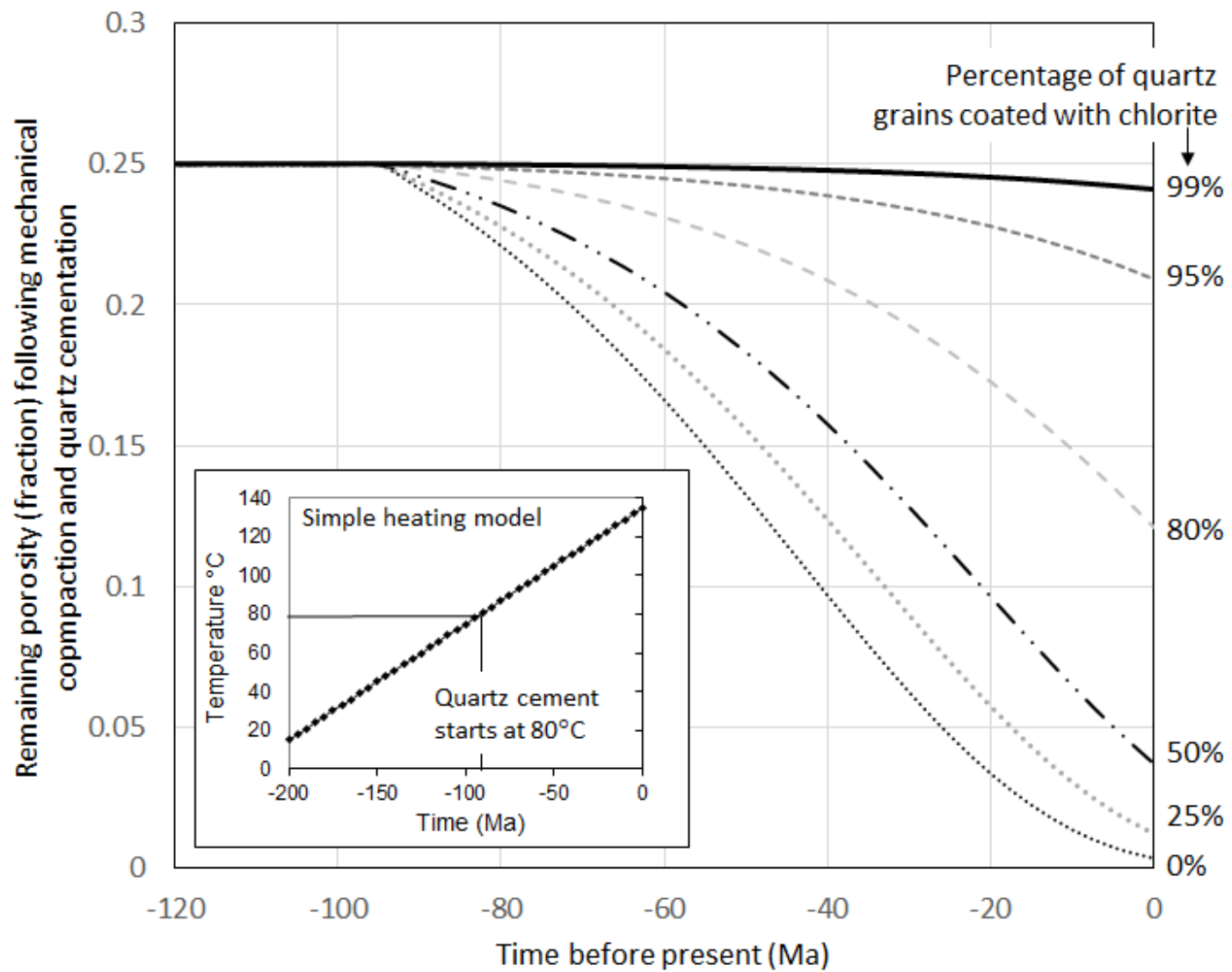


**Figure 28**



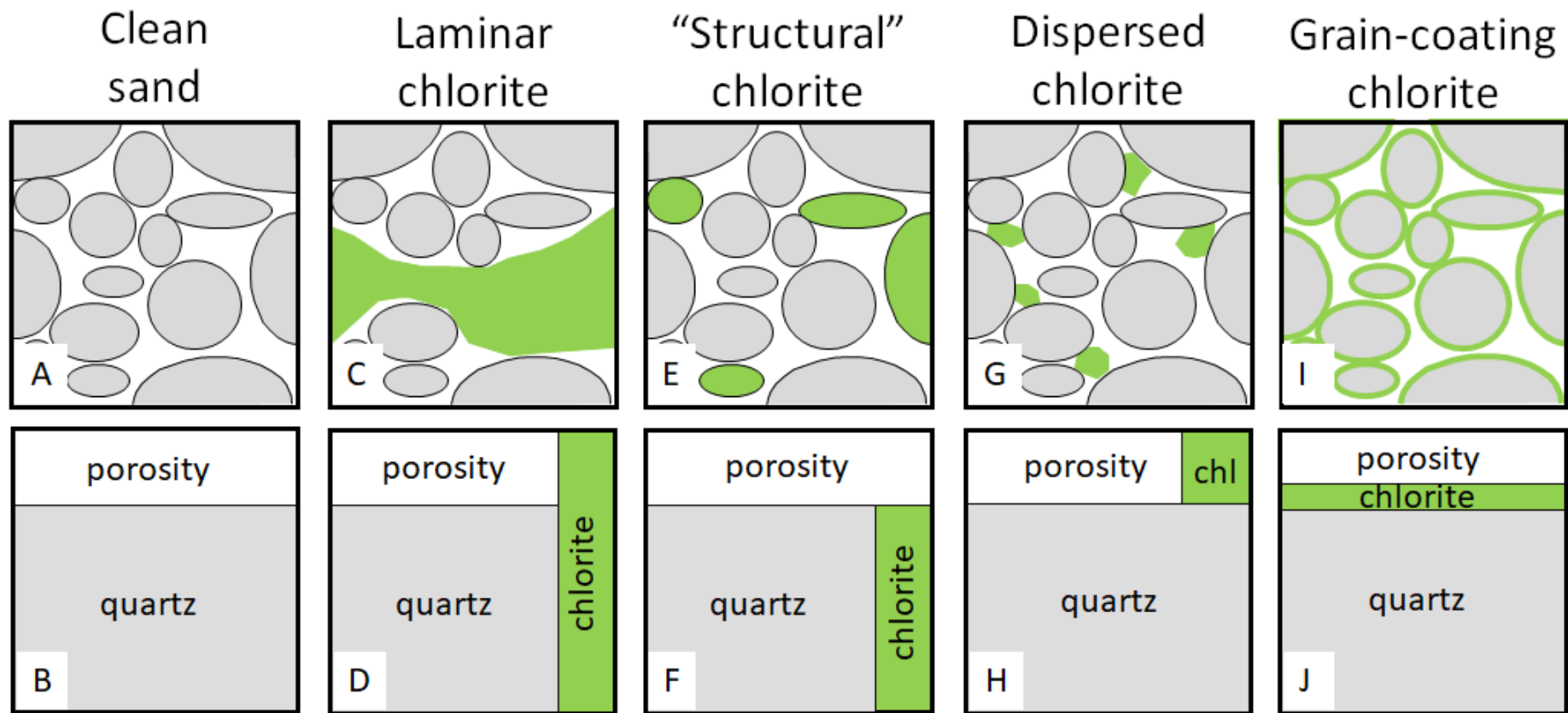
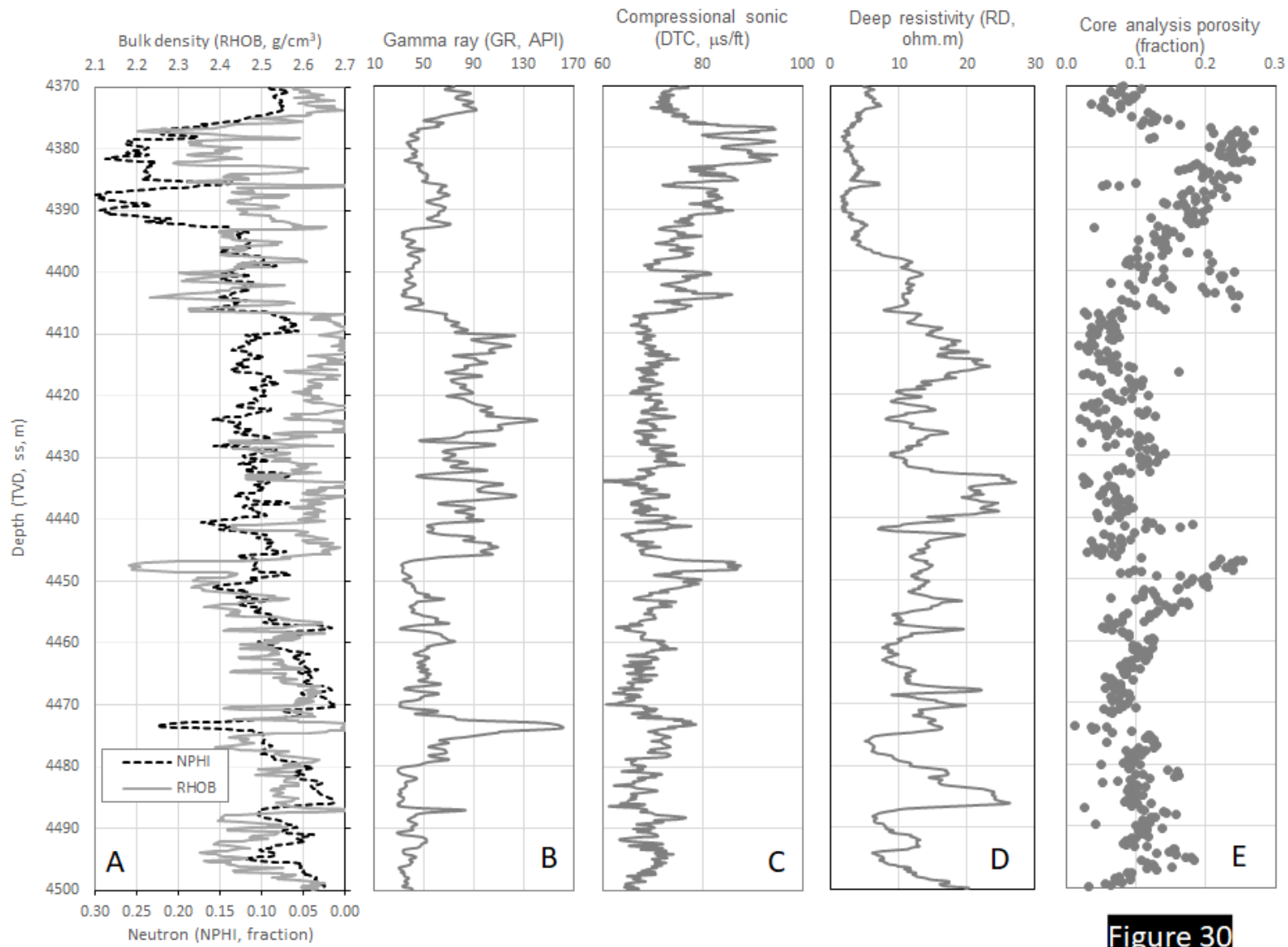
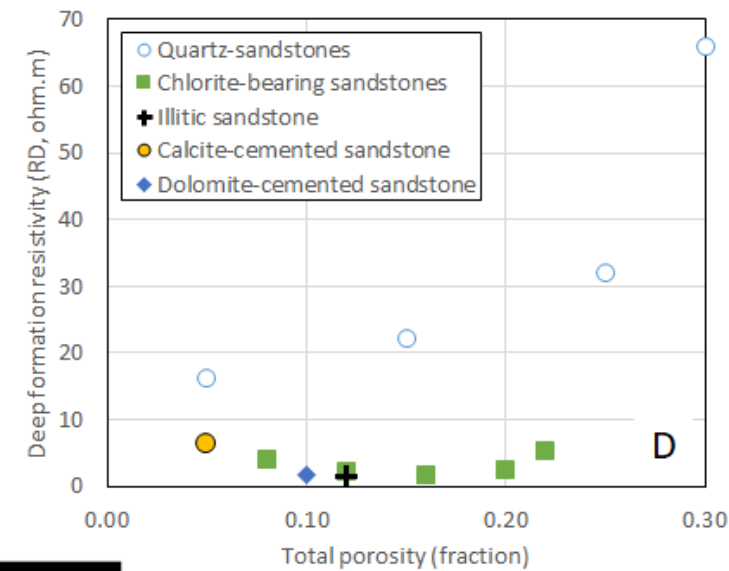
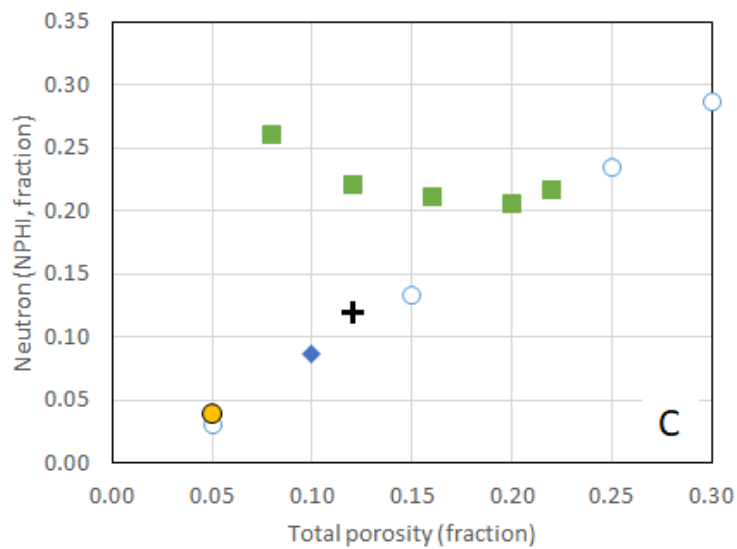
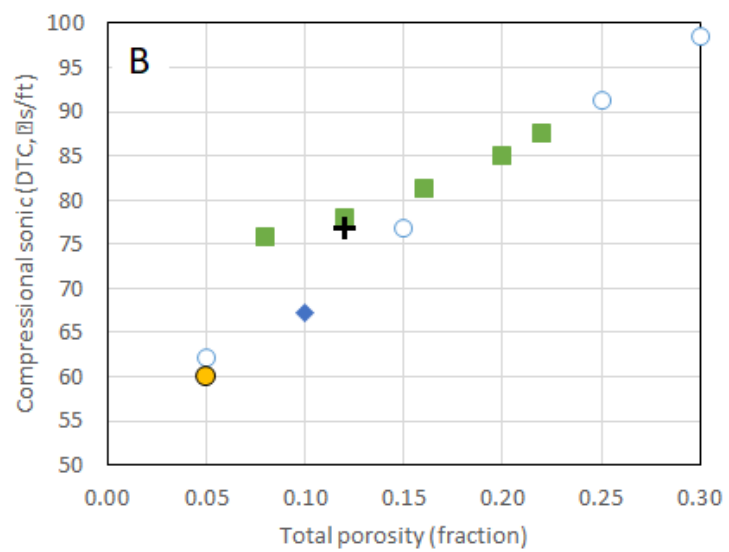
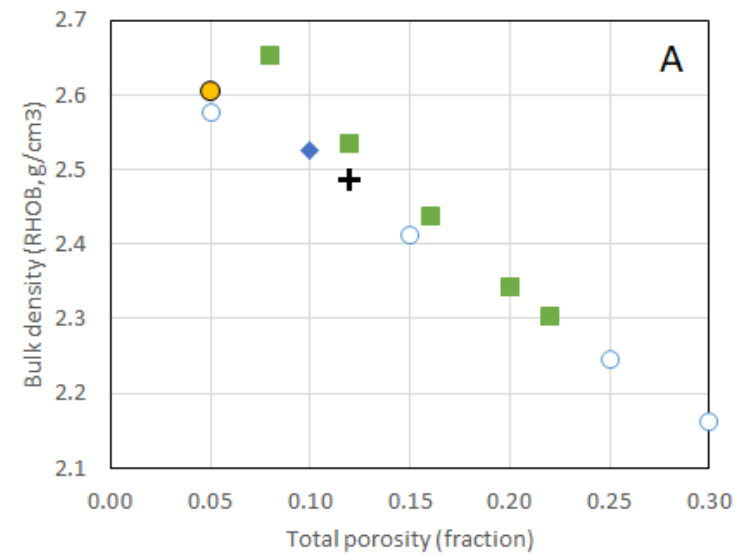


Figure 29



**Figure 30**



**Figure 31**

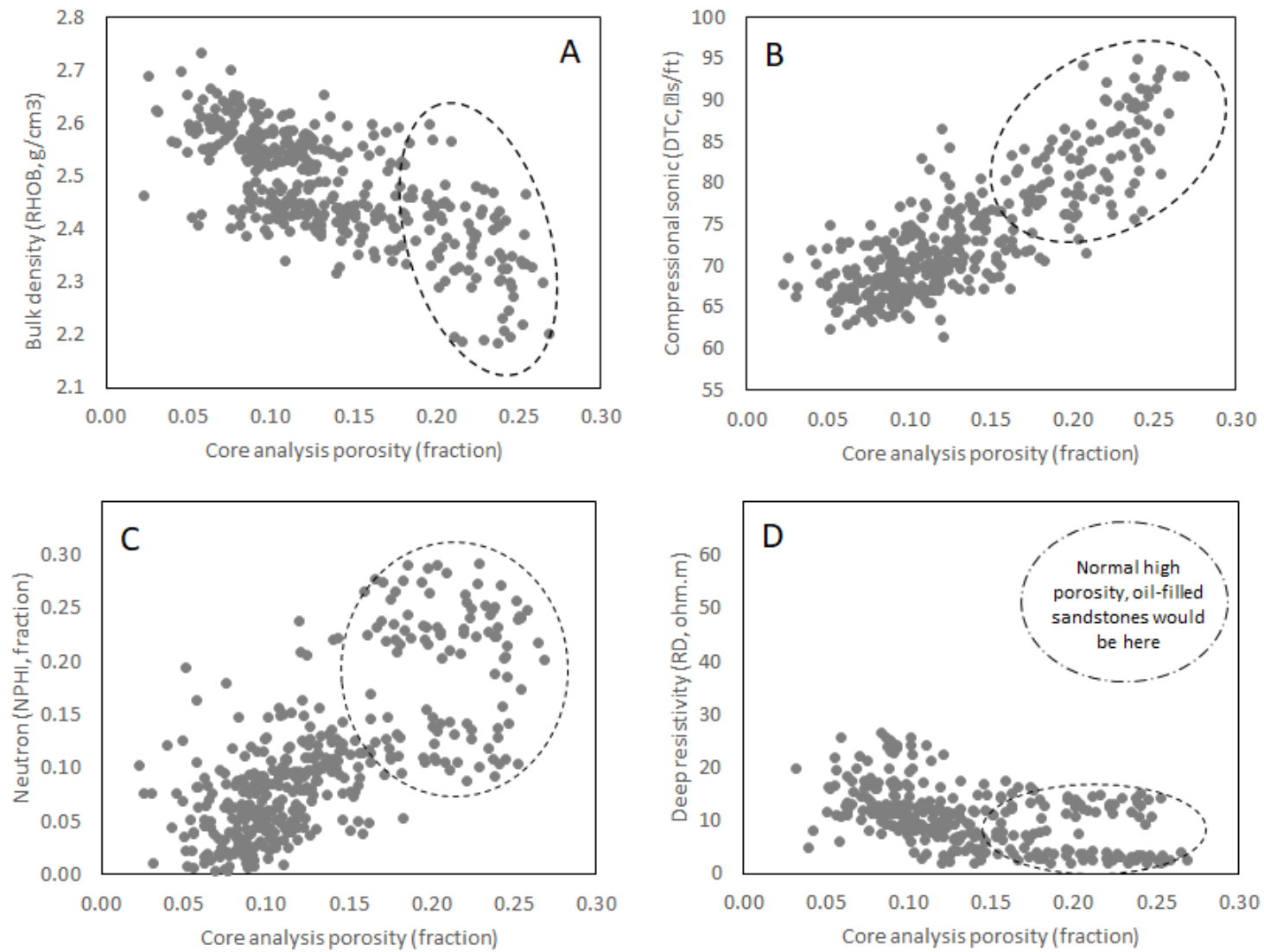


**Figure 32**